# NASA CR-134679

BOEING D180-18615-1

# EFFECT OF THERMAL PROFILE ON CYCLIC FLAW GROWTH IN ALUMINUM


by

W. L. Engstrom


January 1975


THE BOEING AEROSPACE COMPANY


Prepared For:

NATIONAL AERONAUTICS AND SPACE ADMINISTRATION

NASA-LEWIS RESEARCH CENTER
Contract NAS 3-17764
John A. Misencik - Project Manager


(NASA-CR-134679) EFFECT OF THERMAL PROFILE ON CYCLIC FLAW GROWTH IN ALUMINUM Contractor Report, Jun. 1973 - Sep. 1974 (Boeing Aerospace Co., Seattle, Wash.) 146 p HC $5.75 CSCL 11F G3/26

N75-18338

Unclas 12493



MAR 19

| 1 Report No. | 2 Government Accession No | 3 Recipient's Catalog No |
|---|---|---|
| NASA CR 134679 | | |

| 4. Title and Subtitle | 5 Report Date |
|---|---|
| EFFECT OF THERMAL PROFILE ON CYCLIC FLAW GROWTH IN ALUMINUM | JANUARY 1975 |
| | 6 Performing Organization Code |
| 7 Author(s) W.L. ENGSTROM | 8 Performing Organization Report No D180-18615-1 |
| | 10 Work Unit No |
| 9 Performing Organization Name and Address BOEING AEROSPACE COMPANY RESEARCH AND ENGINEERING DIVISION SEATTLE, WASHINGTON 98124 | 11 Contract or Grant No NAS 3-17764 |
| 12 Sponsoring Agency Name and Address NATIONAL AERONAUTICS AND SPACE ADMINISTRATION LEWIS RESEARCH CENTER 21000 BROOKPARK ROAD - CLEVELAND, OHIO 44135 | 13 Type of Report and Period Covered Contract Report June 1973 Through Sept. 1974 |
| | 14 Sponsoring Agency Code |

15 Supplementary Notes PROJECT MANAGER, JOHN A. MISENCIK
MATERIALS AND STRUCTURES DIVISION
NASA LEWIS RESEARCH CENTER - CLEVELAND, OHIO 44135

16 Abstract


Surface flawed and single edge notch tension specimens of 2219-T851 and -T87 aluminum were tested to determine static fracture characteristics and base line (constant amplitude, constant temperature) cyclic flaw growth behavior. Subsequent testing was then conducted in which flawed specimens were subjected to a thermal profile in which the applied stress was varied simultaneously with the temperature. The profile used represents a simplified Space Shuttle orbiter load/temperature flight cycle. Test temperatures included the range from 144K (-200°F) up to 450K (350°F). The measured flaw growth rates obtained from the thermal profile tests were then compared with rates predicted by assuming linear cumulative damage of base line rates.


| 17 Key Words (Suggested by Author(s)) | 18 Distribution Statement |
|---|---|
| • 2219-T851 Aluminum<br>• 2219-T87 Aluminum<br>• Cyclic Crack Growth Rates<br>• Surface Flaw Specimens<br>• Single Edge Notch Tension Specimens<br>• Fracture Characteristics<br>• Thermal Profile Spectrum | UNCLASSIFIED, UNLIMITED |

| 19 Security Classif (of this report) | 20 Security Classif (of this page) | 21 No of Pages | 22 Price* |
|---|---|---|---|
| UNCLASSIFIED | UNCLASSIFIED | 161 | $3.00 |

* For sale by the National Technical Information Service Springfield Virginia 22151



NASA-C-168 (Rev. 6-71)

## FOREWORD

This report describes an investigation of fracture characteristics and cyclic flaw growth behavior of 2219-T851 and -T87 aluminum alloys subjected to loading under a thermal profile. The work was performed by the Boeing Aerospace Company from June 1973 through September 1974 under Contract NAS3-17764. The work was administered by Mr. John A. Misencik of the NASA-Lewis Research Center.

Boeing personnel who participated in this investigation included J. N. Masters, Project Manager and W. L. Engstrom, Technical Leader. Test support was provided by A. A. Ottlyk. Metallurgical support was provided by M. V. Hyatt and M. H. Gramling. George Buehler prepared the art work and Eva Cornelius typed the manuscript.

The information contained in this report is also released as Boeing Document D180-18615-1.

PRECEDING PAGE BLANK NOT FILMED

TABLE OF CONTENTS


| | | | Page |
|---|---|---|---|
| ABSTRACT | | | 1 |
| SYMBOLS AND ACRONYMS | | | vii |
| SUMMARY | | | 1 |
| 1.0 | INTRODUCTION | | 3 |
| 2.0 | MATERIALS | | 5 |
| 3.0 | PROCEDURES | | 7 |
| | 3.1 | SPECIMEN FABRICATION | 7 |
| | | 3.1.1 Tensile Specimens | 7 |
| | | 3.1.2 Single Edge Notch Tension and Surface Flaw Specimens | 7 |
| | 3.2 | TEST SETUP | 8 |
| | 3.3 | EXPERIMENTAL APPROACH | 9 |
| | | 3.3.1 Mechanical Property Tests | 9 |
| | | 3.3.2 Static Fracture Tests | 10 |
| | | 3.3.3 Constant Amplitude, Constant Temperature Cyclic Base Line Tests | 11 |
| | | 3.3.4 Thermal Profile Tests | 13 |
| | 3.4 | STRESS INTENSITY SOLUTIONS | 14 |
| | | 3.4.1 Surface Flaw Specimens | 14 |
| | | 3.4.2 Single Edge Notch Tension Specimens | 14 |
| 4.0 | TEST RESULTS AND ANALYSIS | | 17 |
| | 4.1 | MECHANICAL PROPERTIES | 17 |
| | 4.2 | STATIC FRACTURE TESTS | 17 |
| | | 4.2.1 Surface Flaw Specimens | 17 |
| | | 4.2.2 Single Edge Notch Tension Specimens | 18 |
| | 4.3 | CONSTANT TEMPERATURE, CONSTANT AMPLITUDE CYCLIC BASE LINE TESTS | 20 |
| | | 4.3.1 Surface Flaw Specimens | 20 |
| | | 4.3.2 Single Edge Notch Tension Specimens | 22 |
| | 4.4 | THERMAL PROFILE TESTS | 26 |
| | | 4.4.1 Surface Flaw Specimens | 26 |
| | | 4.4.2 Single Edge Notch Tension Specimens | 27 |


PRECEDING PAGE BLANK NOT FILMED

TABLE OF CONTENTS (Cont'd)


| | Page |
|---|---|
| 4.4.3 Metallurgical Analysis | 30 |
| 5.0 CONCLUSIONS | 35 |
| REFERENCES | 39 |

## SYMBOLS AND ACRONYMS

| | |
|---|---|
| $a$ | Crack depth of semi-elliptical surface flaw in surface flaw specimen, length of through-the-thickness crack in single edge notch tension specimen. |
| $a_{cr}$ | Critical flaw size for single edge notch tension specimen. |
| $2c$ | Flaw length of semi-elliptical surface flaw. |
| C | Crack opening displacement constant. |
| COD | Crack opening displacement. |
| da/dN | Cyclic crack growth rate. |
| E | Young's Modulus. |
| ET | Elevated temperature (450K (350°F) unless noted otherwise). |
| EDM | Electrical discharge machine. |
| K | Single edge notch tension specimen stress intensity factor. |
| $K_{CN}$ | Single edge notch tension specimen stress intensity at failure-- calculated from $a_i$ and $\sigma_{max}$. |
| $K_{cr}$ | Critical single edge notch tension specimen stress intensity factor-- calculated from $a_{cr}$ and $\sigma_{cr}$. |
| $K_I$ | Irwin surface flaw stress intensity with deep flaw magnification. |
| $K_{IE}$ | Surface flaw critical stress intensity. |
| $K_{IMAX}$ | Maximum cyclic surface flaw stress intensity. |
| $K_{MAX}$ | Maximum cyclic single edge notch tension through-the-thickness flaw stress intensity. |
| $K_R$ | Crack growth resistance. |
| $\Delta K$ | Difference between maximum and minimum applied cyclic stress intensities. |
| $M_K$ | Deep flaw magnification factor from NASA CR 72606. |
| N | Number of fatigue cycles. |
| NA | Not available. |
| Q | Flaw shape parameter = $\Phi^2 - 0.212(\sigma/\sigma_y)^2$. |
| SENT | Single edge notch tension specimen. |
| SF | Surface flaw specimen. |
| $r_y$ | Half plastic zone size. |
| R | Cyclic stress ratio. |

## SYMBOLS AND ACRONYMS

| | |
|---|---|
| RT | Room temperature. |
| $t$ | Thickness of specimen at flaw plane. |
| $W$ | Width of specimen at flaw plane. |
| $Y$ | Polynomial function of $a$ and $W$ used to calculate stress intensity for single edge edge notch tension specimens. |
| $\delta$ | Crack opening displacement. |
| $\sigma, \sigma_A, \sigma_G$ | Applied gross stress. |
| $\sigma_{FAILURE}, \sigma_F$ | Stress level at which failure occurs. |
| $\sigma_{cr}$ | Critical stress level at which failure occurs. |
| $\sigma_{MAX}$ | Maximum cyclic stress level. |
| $\sigma_N$ | Net section stress. |
| $\sigma_{ys}, \sigma_y$ | Yield strength. |
| $\sigma_{ULT}$ | Ultimate strength. |
| $\mu$ | Poisson's ratio. |
| $\phi$ | Complete elliptical integral of the second kind corresponding to modulus $k = [(c^2 - a^2)/c^2]^{1/2}$. |

## SUBSCRIPTS

| | |
|---|---|
| f | Final condition. |
| i | Initial condition. |
| cr | Critical condition. |
| RT | Condition at room temperature |
| ET | Condition at elevated temperature (450K (350°F) unless noted otherwise). |

## LIST OF FIGURES


| Figure | | Page |
|---|---|---|
| 1 | Basic Load/Thermal Profile Spectrum | 41 |
| 2 | Tensile Specimen Configuration | 42 |
| 3 | Crack Propagation Directions | 43 |
| 4 | 450K (+350°F) SENT Fracture Specimens | 44 |
| 5 | Room Temperature SENT Fracture Specimens | 45 |
| 6 | 144K (-200°F) SENT Fracture Specimens and 450K (350°F) and RT Cyclic Specimens | 46 |
| 7 | SENT Cyclic Specimens | 47 |
| 8 | 6.35 mm (0.250 in.) Surface Flaw Specimen | 48 |
| 9 | 3.18 mm (0.125 in.) Surface Flaw Specimen | 49 |
| 10 | Surface Flaw Specimen Installed in Test Machine | 50 |
| 11 | SENT Specimen Subjected to Thermal Profile Loading | 51 |
| 12 | SENT Thermal Profile Test Setup | 52 |
| 13 | Crack Propagation Gage and Crack Opening Displacement Clip Gage Installed on SENT Specimen | 53 |
| 14 | Examples of Pressure Cups Used to Detect Flaw Breakthrough on Surface Flaw Tests | 54 |
| 15 | Flaw Opening Measurement of Surface Flawed Specimens | 55 |
| 16 | Load vs. Pressure, Specimen 851-SF-3 | 56 |
| 17 | Load vs. Crack Propagation Gage Output for Specimen 87-2 | 57 |
| 18 | Shape Parameter Curves for Surface and Internal Flaws | 58 |
| 19 | Deep Flaw Magnification Curves (Reference 2) | 59 |
| 20 | Y vs. a/w for Single Edge Notch Specimens | 60 |
| 21 | Plot of Variation of Strength with Temperature, 2219-T851 and 2219-T87 Aluminum Alloys | 61 |

LIST OF FIGURES (Cont'd)


| Figure | | Page |
|---|---|---|
| 22 | Plot of Failure Stress vs. Flaw Size for 6.35 mm (0.250 in.) 2219-T851 Surface Flaw Static Fracture Tests, TS Propagation Direction | 62 |
| 23 | Plot of Failure Stress vs. Flaw Size for 6.35 mm (0.250 in.) and 3.18 mm (0.125 in.) 2219-T87 Surface Flaw Static Fracture Tests, TS Propagation Direction | 63 |
| 24 | Plot of Stress Intensity and Crack Growth Resistance vs. Flaw Length, 2219-T87 Alloy, 6.35 mm (0.25 in.) | 64 |
| 25 | Plot of Stress Intensity Factor, $K_{CN}$, vs. Temperature for 2219 Aluminum Alloy Single Edge Notch Tension Static Fracture Tests, TL Propagation Direction | 65 |
| 26 | Plot of Critical Stress Intensity Factor, $K_{cr}$, vs. Temperature for 2219 Aluminum Alloy Single Edge Notch Tension Static Fracture Tests, TL Propagation Direction | 66 |
| 27 | Plot of Crack Growth Rate vs. $K_{Imax}$, 6.35 mm (0.25 in.) 2219-T851 SF Specimens Tested at Room Temperature, R = 0, Freq = 1 Hz (60 cpm), TS Propagation Direction | 67 |
| 28 | Plot of Crack Growth Rate vs. $K_{Imax}$, 6.35 mm (0.25 in.) 2219-T851 SF Specimens Tested at 450K (350°F), R = 0.5, Freq = 1 Hz (60 cpm), TS Propagation Direction | 68 |
| 29 | Plot of Crack Growth Rate vs. $K_{Imax}$, 6.35 mm (0.250 in.) and 3.18 mm (0.125 in.) 2219-T87 SF Specimens Tested at Room Temperature, R = 0, Freq = 1 Hz (60 cpm), TS Propagation Direction | 69 |
| 30 | Plot of Crack Growth Rate vs. $K_{Imax}$, 6.35 mm (0.250 in.) and 3.18 mm (0.125 in.) 2219-T87 SF Specimens Tested at 450K (350°F), R = 0.5, Freq = 1 Hz (60 cpm), TS Propagation Direction | 70 |
| 31 | Plot Showing Summary of Crack Growth Rate vs. $K_{Imax}$ for 2219 SF Specimens, Freq = 1 Hz (60 cpm), TS Propagation Direction | 71 |
| 32 | Plot Showing Comparison of Room Temperature SF Data Generated on this Program with Room Temperature SF Data Compiled in CR-115388 (Ref. 15) | 72 |

LIST OF FIGURES (Cont'd)


| Figure | | Page |
|---|---|---|
| 33 | Plot Showing Forman's Equation Fitted to Room Temperature 2219-T851 SF Crack Growth Data | 73 |
| 34 | Plot Showing Forman's Equation Fitted to Room Temperature 2219-T87 SF Crack Growth Data | 74 |
| 35 | Plot of Flaw Length vs. Cycles, 2219-T87 SENT Specimen 87-C16 Tested at Room Temperature | 75 |
| 36 | Plot of Flaw Length vs. Cycles, 2219-T87 SENT Specimen 87-C19 Tested at 450K (350°F) | 76 |
| 37 | Plot of Crack Growth Rate vs. $K_{max}$, 6.35 mm (0.25 in.) 2219-T851 SENT Specimens Tested at Room Temperature, R = 0, Freq = 1 Hz, TL Propagation Direction | 77 |
| 38 | Plot of Crack Growth Rate vs. $K_{max}$, 6.35 mm (0.25 in.) 2219-T851 SENT Specimens Tested at 450K (350°F), R = 0.5 & 0, Freq = 1 Hz (60 cpm), TL Propagation Direction | 78 |
| 39 | Plot of Crack Growth Rate vs. $K_{max}$, 6.35 mm (0.25 In.) 2219 T87 SENT Specimens Tested at Room Temperature, R = 0 & 0.5, Freq = 1 Hz (60 cpm), TL Propagation Direction | 79 |
| 40 | Plot of Crack Growth Rate vs. $K_{max}$, 6.35 mm (0.25 in.) 2219-T87 SENT Specimens Tested at 450K (350°F), R = 0.5, Freq = 1 Hz (60 cpm), TL Propagation Direction | 80 |
| 41 | Plot of Crack Growth Rate vs. $K_{max}$, 3.18 mm (0.125 in.) 2219-T87 SENT Specimens Tested at Room Temperature, R = 0, Freq = 1 Hz (60 cpm), TL Propagation Direction | 81 |
| 42 | Plot of Crack Growth Rate vs. $K_{max}$, 3.18 mm (0.125 in.) 2219-T87 SENT Specimens Tested at 450K (350°F), R = 0.5, Freq = 1 Hz (60 cpm), TL Propagation Direction | 82 |
| 43 | Plot Showing Summary of Crack Growth Rate vs. $K_{max}$ for 2219 SENT Specimens, Freq = 1 Hz (60 cpm), TL Propagation Direction | 83 |
| 44 | Plot Showing Effect of Varying Stress Ratio on 2219 SENT Cyclic Specimens Tested at Room Temperature, Freq = 1 Hz (60 cpm), TL Propagation Direction | 84 |

LIST OF FIGURES (Cont'd)


| Figure | | Page |
|---|---|---|
| 45 | Plot Showing Effect of Varying Stress Ratio on 6.35 mm (0.250 in.) 2219-T851 SENT Cyclic Specimens Tested at 450K (350°F), Freq = 1 Hz (60 cpm), TL Propagation Direction | 85 |
| 46 | Plot Showing Effect of Varying Test Temperature on 6.35 mm (0.250 in.) 2219-T851 SENT Cyclic Specimens Tested at R = 0, Freq = 1 Hz (60 cpm), TL Propagation Direction | 86 |
| 47 | Plot Showing Effect of Varying Test Temperature on 2219-T87 SENT Cyclic Specimens Tested at R = 0.5, Freq = 1 Hz (60 cpm), TL Propagation Direction | 87 |
| 48 | Plot Showing Effect of Suslic Loading on 2219 SENT Specimens Tested at 450K (350°F), R = 0.5, TL Propagation Direction | 88 |
| 49 | Plot Showing Comparison of Room Temperature SENT Data Generated on This Program with Room Temperature Data Generated by Grumman on Air Force Contract F33615-72-C-1744 (Ref. 19) | 89 |
| 50 | Plot Showing Forman's Equation Fitted to Room Temperature 2219-T851 SENT Crack Growth Data | 90 |
| 51 | Plot Showing Forman's Equation Fitted to 450K (350°F) 2219-T851 SENT Crack Growth Data | 91 |
| 52 | Plot Showing Forman's Equation Fitted to Room Temperature 2219-T87 SENT Crack Growth Data | 92 |
| 53 | Plot Showing Forman's Equation Fitted to 450K (350°F) 2219-T87 SENT Crack Growth Data | 93 |
| 54 | Plot of Crack Growth Rate vs. $K_{Imax}$ @ RT for 6.35 mm (0.250 in.) 2219-T851 SF Specimens Tested Under Thermal Profile Loading, TS Propagation Direction | 94 |
| 55 | Plot of Crack Growth Rate vs. $K_{Imax}$ @ RT for 6.35 mm (0.250 in.) and 3.18 mm (0.125 in.) 2219-T87 SF Specimens Tested Under Thermal Profile Loading, TS Propagation Direction | 95 |
| 56 | Plot of Crack Growth Rate vs $K_{max}$ @ RT for 6.35 mm (0.250 in.) 2219-T851 SENT Specimens Tested Under Thermal Profile Loading, RT Propagation Direction | 96 |

LIST OF FIGURES (Cont'd)


| Figure | | Page |
|---|---|---|
| 57 | Plot of Crack Growth Rate vs. $K_{max}$ for 6.35 mm (0.250 in.) 2219-T851 SENT Specimens Cycled at RT Showing RT Growth Rate Retardation in Specimen 851-C11 | 97 |
| 58 | Plot of Crack Growth Rate vs. $K_{max}$ @ RT for 6.35 mm (0.250 in.) and 3.18 mm (0.125 in.) 2219-T87 SENT Specimens Tested Under Thermal Profile, TL Propagation Direction | 98 |
| 59 | Plot of Crack Growth Rate vs. $K_{max}$ for 6.35 mm (0.250 in.) and 3.18 mm (0.125 in.) 2219-T87 SENT Specimens Cycled at RT Showing RT Crack Growth Rate Retardation in Specimens 87-C11 and 87-C22 | 99 |
| 60 | Plot of Crack Length vs. Cycles for SENT Specimen 87-C11 Cycled at Room Temperature, $\sigma$ = 40 MN/m$^2$ (5.8 ksi), R = 0 After Having Been Subjected to 58 Thermal Profile Flights | 100 |
| 61 | Plot of Crack Growth Rate vs. $K_{max}$ for 3.18 mm (0.125 in.) 2219-T87 SENT Specimens Cycled at ET Showing No ET Crack Growth Retardation in Specimen 87-C23 | 101 |
| 62 | Fracture Surface of 87-C11 and Locations from which Replicas were Taken | 102 |
| 63 | Fracture Surface of 87-SF-C6 and Location from which Replica was Taken | 103 |
| 64 | Typical Fatigue Striations in the Precrack Region of 87-C11 | 104 |
| 65 | Typical Area in the Thermal Profile Region of Specimen 87-C11. | 105 |
| 66 | Fractograph from the Thermal Profile Region of Specimen 87-C11 | 106 |
| 67 | Elongated Dimples Occasionally observed in the Thermal Profile Region of Specimen 87-C11 | 107 |
| 68 | Fatigue Striations Observed in the Constant Temperature, Constant Amplitude Region, Right After the Thermal Profile Region of Specimen 87-C11 | 108 |
| 69 | Fatigue Striations Observed in the Constant Temperature, Constant Amplitude Region of Specimen 87-C11, 0.64 mm (0.025 in.) Farther from Origin than Figure 68 | 109 |

LIST OF FIGURES (Cont'd)


| Figure | | Page |
|---|---|---|
| 70 | Typical Appearance of much of the Constant Temperature, Constant Amplitude Region of 87-C11, After the Thermal Profile Region | 110 |
| 71 | Fatigue Striations Farther Along in Constant Temperature, Constant Amplitude Region of Specimen 87-C11, where Crack Growth Retardation was Diminished | 111 |
| 72 | Thermal Profile Region on the Surface Flaw Specimen | 112 |
| 73 | Thermal Profile Region on Surface Flaw Specimen Showing Acicular Material Observed Throughout much of the Replica | 113 |

## LIST OF TABLES


| Table | | Page |
|---|---|---|
| 1 | Summary of Mechanical Property, Static Fracture and Constant Amplitude, Constant Temperature Cyclic Tests | 115 |
| 2 | Summary of Load/Thermal Profile Tests | 116 |
| 3 | Chemical Composition of Aluminum Alloys (% by Weight) As Determined by Boeing Aerospace Company Tests | 117 |
| 4 | Mechanical Properties of 6.35 mm (0.25 in.) 2219-T851 Aluminum Alloy | 118 |
| 5 | Mechanical Properties of 6.35 mm (0.25 in.) 2219-T87 Aluminum Alloy | 119 |
| 6 | Mechanical Properties of 3.18 mm (0.125 in.) 2219-T87 Aluminum Alloy | 120 |
| 7 | Static Fracture Data from Surface Flaw Tests, TS Propagation Direction | 121 |
| 8 | Static Fracture Data from Single Edge Notch Tension Tests of 6.35 mm (0.25 in.) 2219-T851 Aluminum Alloy, TL Propagation Direction | 122 |
| 9 | Static Fracture Data from Single Edge Notch Tension Tests of 6.35 mm (0.25 in.) 2219-T87 Aluminum Alloy, TL Propagation Direction | 123 |
| 10 | Static Fracture Data from Single Edge Notch Tension Tests of 3.18 mm (0.125 in.) 2219-T87 Aluminum Alloy, TL Propagation Direction | 124 |
| 11 | Cyclic Crack Growth Data, 6.35 mm (0.250 in.) 2219-T851 SF Specimens, Freq = 1 Hz (60 cpm), TS Propagation Direction, Constant Temperature | 125 |
| 12 | Cyclic Crack Growth Data, 6.25 mm (0.250 in.) 2219-T87 F Specimens. Freq = 1 Hz (60 cpm), TS Propagation Direction, Constant Temperature | 126 |
| 13 | Cyclic Crack Growth Data, 3.18 mm (0.125 in.) 2219-T87 SF Specimens. Freq = 1 Hz (60 cpm), TS Propagation Direction, Constant Temperature | 127 |
| 14 | Cyclic Crack Growth Data, 6.35 mm (0.250 in.) 2219-T851 SENT specimens, Freq = 1 Hz (60 cpm), TL Propagation Direction, Constant Temperature | 128 |

LIST OF TABLES (Cont'd)


| Table | | Page |
|---|---|---|
| 15 | Cyclic Crack Growth Data, 6.35 mm (0.250 in.) 2219-T87 SENT Specimens, Freq = 1 Hz (60 cpm), TL Propagation Direction, Constant Temperature | 129 |
| 16 | Cyclic Crack Growth Data, 3.18 mm (0.125 in.) 2219-T87 SENT Specimens, Freq = 1 Hz (60 cpm), TL Propagation Direction, Constant Temperature | 130 |
| 17 | Thermal Profile Cyclic Crack Growth Data, 6.35 mm (0.250 in.) 2219-T851 SF Specimens, TS Propagation Direction | 131 |
| 18 | Thermal Profile Cyclic Crack Growth Data, 6.35 mm (0.250 in.) and 3.18 mm (0.125 in.) 2219-T87 SF Specimens, TS Propagation Direction | 132 |
| 19 | Thermal Profile Cyclic Crack Growth Data, 6.35 mm (0.250 in.) 2219-T87 SENT Specimens, TL Propagation Direction | 133 |
| 20 | Thermal Profile Cyclic Crack Growth Data, 6.35 mm (0.250 in.) 2219-T851 SENT Specimens, TL Propagation Direction | 134 |
| 21 | Thermal Profile Cyclic Crack Growth Data, 3.18 mm (0.125 in.) 2219-T87 SENT Specimens, TL Propagation Direction | 135 |
| 22 | Thermal Profile Cyclic Crack Growth Data, Sustain Load at ET Followed by Constant Amplitude Cyclic Test at RT, 3.18 mm (0.125 in.) SENT Specimen, TL Propagation Direction | 136 |

## SUMMARY

This experimental program was undertaken to determine the behavior of 2219-T851 and -T87 aluminum alloys when subjected to a thermal profile spectrum in which applied stress levels are varied at the same time that the test temperature is varied over the range 144K (-200°F) up to 450K (350°F). Pursuant to the investigation of the above problem a number of other data were also generated including mechanical properties, static fracture characteristics and constant amplitude, constant temperature cyclic behavior. The -T851 temper was tested in a thickness of 6.35 mm (0.250 in.) and the -T87 temper was tested in thicknesses of 6.35 mm (0.250 in.) and 3.18 mm (0.125 in.). Flat tensile specimens and surface flaw and single edge notch tension fracture specimens were tested. Mechanical property and static fracture specimens were tested at 144K (-200°F), room temperature, and 450K (350°F). Cyclic specimens were tested at room temperature and 450K (350°F).

All surface flaw specimens tested exhibited failure stresses near the yield strengths of the materials. Single edge notch tension specimens produced $K_{cr}$ and $K_{CN}$ values which remained constant at 144K (-200°F) and room temperature. An increase in temperature to 450K (350°F) caused a substantial increase in $K_{cr}$ and $K_{CN}$ values.

Results of the constant amplitude, constant temperature cyclic crack growth tests indicate for both surface flaw and single edge notch tension specimens that 2219-T851 and -T87 have the same cyclic crack growth rates at room temperature. At 450K (350°F) the -T851 temper has slower crack growth rates than the -T87 temper. In addition, it has been shown that crack growth rates of each temper are approximately doubled by an increase of temperature to 450K (350°F) at low $K_{max}$ values (22 $MN/m^{3/2}$ (20 $ksi\sqrt{in}$)). At $K_{max}$ values above 44 $MN/m^{3/2}$ (40 $ksi\sqrt{in}$) growth rates at room temperature and elevated temperature are equal. Tests conducted on single edge notch tension specimens to evaluate the effect of hold time on crack growth rates have shown that holding at the maximum stress level for 2 minutes on each cycle increases crack growth rates substantially over those produced by sinusoidal loading at 1 Hz (60 cpm).

Results of thermal profile tests show that the flaw growth of surface flaw specimens can be successfully predicted by using a linear cumulative damage analysis. Crack growth rates of single edge notch specimens subjected to thermal profile loading are slower than those which would be predicted by a linear cumulative damage analysis. The crack growth rate retardation apparent in single edge notch tension specimens appears to be caused by the high temperature part of the thermal profile. Specimens subjected to subsequent room temperature exposure and cycling exhibit lower growth rates than would be expected from comparison with base line constant temperature, constant amplitude crack growth data. Additionally, there appears to be a specimen size and/or net section effect on single edge notch specimens subjected to thermal profile loading. Wide specimens subjected to net section stresses of 27% to 31% of $\sigma_{ys}$ display more retardation in flaw growth behavior than smaller specimens subjected to net section stresses of 42% to 84% of $\sigma_{ys}$. The surface flaw specimens, which did not show retardation, were subjected to net section stresses on the order of 53% to 97% of $\sigma_{ys}$.

## 1.0 INTRODUCTION

Experience has shown that large aerospace structures and pressure vessels often contain crack-like defects due to fabrication. Service life of these structures is dependent upon initial quality of the structure, the subcritical flaw growth characteristics of the materials in their respective service environments, and the critical flaw sizes at maximum operating stresses. Over the past few years, several research programs have been undertaken to investigate methods to prevent failure of aerospace structures and pressure vessels, and to provide test data which can be utilized in design (e.g., References 1 through 6). Most prior fracture experiments on 2219 aluminum have been performed at constant temperature. Several areas of the planned shuttle vehicle will be subjected to varying temperature profiles ranging from subzero temperatures to up to approximately +450K (+350°F) for aluminum components.

An earlier Boeing IR&D study investigated flaw growth of aluminum surface flawed specimens subjected to a simulated recoverable booster load/temperature profile. Loads were held relatively constant while temperature was varied between 78K (-320°F) and 450K (+350°F). Results indicated significantly higher growth rates than anticipated, with most of the damage occurring at elevated temperature.

The program reported herein was initiated to further explore the problem of flaw growth under load/temperature profiles simulating Space Shuttle orbiter primary structure. Materials selected for this investigation were 2219-T851 aluminum, 6.35 mm (0.250 in.) thick, and 2219-T87 aluminum, 6.35 mm (0.250 in.) and 3.18 mm (0.125 in.) thick. The fracture and flaw growth tests were performed using both surface flaw (SF) and single edge notch tension (SENT) specimen configurations.

The materials were characterized using mechanical property, static fracture and constant amplitude, constant temperature cyclic crack growth tests. A summary of tests performed are shown in Table 1. Tests in which the applied

stress and temperature were varied simultaneously were subsequently conducted. The load/thermal profile utilized for each flight was a simplified version of that which a shuttle structure might be subjected to during flight. It was kept as simple as possible to insure that the test results could be easily compared with the results of the constant amplitude, constant temperature cyclic tests. A schematic of the typical profile used for the tests is shown in Figure 1. A summary of the load/thermal profile tests is shown in Table 2.

The following sections of this report describe materials and procedures and include results and analysis, and conclusions.

## 2.0 MATERIALS

The material used in this program was 2219 aluminum in the -T851 and -T87 tempers in a plate thickness of 6.35 mm (0.250 in.). All material for each temper was from a single heat. The material was ordered per Boeing Specification BMS 7-105C (equivalent to Military Specification MIL-A-8920A). Chemical compositions of the two heats were determined by the Boeing Aerospace Company and are shown in Table 3. The cleanliness rating of both heats were better than classification "A" per ASTM E45-63.

# 3.0 PROCEDURES

## 3.1 SPECIMEN FABRICATION

### 3.1.1 Tensile Specimens

Tensile specimens were fabricated per Figure 2. The 2219-T851 specimens were tested in full thickness from 6.35 mm (0.250 in.) plate. 2219-T87 specimens were cut from the same heat of 6.35 mm (0.250 in.) plate and were tested in thicknesses of 6.35 mm (0.250 in.) and 3.18 mm (0.125 in.). Specimens were cut so that the loading axis was either parallel (longitudinal) or perpendicular (transverse) to the major rolling direction.

### 3.1.2 Single Edge Notch Tension and Surface Flaw Specimens

All single edge notch tension (SENT) and surface flaw (SF) specimens were fabricated so that the loading direction was perpendicular to the rolling direction. This produced a TL crack propagation direction for all SENT tests and a TS crack propagation direction for all SF tests. (See Figure 3 for a description of propagation directions.) Specimen configurations are shown in Figures 4 through 9. SENT static fracture specimens are shown in Figures 4, 5 and 6. The SENT configurations shown in Figures 6 and 7 were employed for the cyclic tests. The surface flaw specimens used for the static fracture and cyclic tests were fabricated per the configurations shown in both of Figures 8 and 9.

Flaws in the SENT specimens were introduced by cutting standard chevron shaped notches as shown in Figures 4 through 7. Flaws in the SF specimens were introduced by electric discharge machining (EDM). The chevron notches in the SENT specimens and the EDM notches in the SF specimens were extended by tension cycling at low stress levels. The maximum stress levels for the SENT specimens varied from 28 to 41 $MN/m^2$ (4 to 6 ksi). The SF specimens were precracked at 83 to 138 $MN/m^2$ (12 to 20 ksi). The number of cycles required was 10 to 453 thousand for SENT specimens and 2 to 30 thousand for SF specimens, depending on the initial flaw size and precracking stress. The cracks in SENT specimens were visually observed at the specimen surface with the aid of a magnifying glass, and the flaw periphery of SF specimens was visually observed with the aid of a microscope to determine when precracking was complete.

PRECEDING PAGE BLANK NOT FILMED

## 3.2 TEST SETUP

All tests were conducted in an environmentally controlled laboratory at the Boeing Space Center in Kent, Washington. Mechanical property and static fracture tests conducted at 144K (-200°F) were performed by enclosing the specimen in an insulated chamber and introducing gaseous nitrogen ($GN_2$) at low temperature. Several thermocouples were installed on each specimen and the temperature was maintained at 144K (-200°F) $\pm$3K (5°F) for at least ten minutes before each test. Tests conducted at 450K (350°F) were performed by installing electrical resistance contact heaters on the specimen. As with the cryogenic tests, the temperature was monitored with thermocouples and the specimen was allowed to soak at 450K (350°F) $\pm$3K (5°F) for at least ten minutes before each test. Thermal profile specimens which were tested at temperatures ranging from 144K (-200°F) up to 450K (350°F) were conducted by utilizing a combination of $GN_2$, $LN_2$ spray, and electrical resistance contact heaters.

Tensile specimens were tested in a 0.53 MN (120 kip) capacity Baldwin static test machine. The SENT and SF static fracture tests were tested in a Materials Testing System (MTS) machine with a 1.34 MN (300 kip) static capability and a 1.11 MN (250 kip) cyclic capability. The SF cyclic tests were conducted in either a 0.27 MN (60 kip) or a 0.67 MN (150 kip) capacity test machine of Boeing manufacture. A photo of a SF specimen installed in a test machine is shown in Figure 10. The SENT cyclic tests were conducted in the above mentioned 0.27 MN (60 kip) and 0.67 MN (150 kip) machines, and in the MTS machine. All SENT tests utilized pin loading. Thermal profile spectrum tests of the SF specimens were conducted in the MTS machine. Thermal profile spectrum SENT specimens were tested in the MTS machine and a 1.56 MN (350 kip) capacity resonant beam fatigue machine. During the thermal profile tests, the load was controlled by the use of a NOVA load programming system. The temperature profile was controlled with a programmable temperature control system using set points and timers. Control systems on the load and temperature programmers were interconnected to achieve the thermal/stress profiles required for the tests. A photo of a SENT specimen installed in a test machine and under test is shown in Figure 11. A closeup view is shown in Figure 12.

Crack propagation in SENT specimens was monitored with the use of crack propagation gages (CPG). These gages are manufactured by the Micro-Measurements Company under the catalog number TK-09-CPC03-003. They were applied in the same manner as standard strain gages. A photo of a specimen with a CPG installed is shown in Figure 13. Crack propagation was also measured by visual means during the cyclic tests.

For the SF static fracture tests, determination of flaw growth through the thickness (breakthrough) prior to ultimate failure was accomplished by employing pressure cups. The pressure cups were clamped to the specimens and a pressure differential of approximately 3.5 to 7 $KN/m^2$ (5 to 10 psi) was used. Helium gas was used as the pressurizing medium. Pressure transducers were employed on the front and/or back side to sense the pressure change associated with flaw breakthrough. Pressure cups were also utilized on SF cyclic tests to determine breakthrough. Examples of pressure cups are shown in Figure 14.

Crack opening displacement (COD) was monitored during static fracture and cyclic tests of both SENT and SF tests. A standard ASTM type clip gage (Reference 7) was used. The clip gage was attached to integrally machined knife edges on the SENT specimens. (See Figure 13 for an example of a clip gage installation.) For the SF specimens, it was necessary to spot weld knife edges to each specimen as shown in Figure 15.

## 3.3 EXPERIMENTAL APPROACH

Summaries of the types of tests conducted in this program are shown in Tables 1 and 2. Details of the experimental approach used are described below.

### 3.3.1 Mechanical Property Tests

Extensometers were used on all tensile specimens. Mechanical property tests were conducted at 144K (-200°F) in $GN_2$, in room temperature air, and in air at 450K (350°F). A strain rate of 0.005 mm/mm/minute was used on all specimens until the material yield stress was obtained. (Yield stress is defined at 0.2% offset in 50.8 mm (2.0 in.).) A strain rate of 0.10 mm/mm/minute was then used for the remaining portion of the loading until failure. A total of 36 specimens were tested.

### 3.3.2 Static Fracture Tests

Static fracture tests were conducted on 10 SF and 18 SENT specimens. Both types of fracture specimens were tested at 144K (-200°F) in $GN_2$, in room temperature air, and in air at 450K (350°F). Each specimen was loaded at a rate to cause failure in one to two minutes. The SF specimens were instrumented with pressure cups as described in Section 3.2 to determine if and when breakthrough occurred prior to failure. A typical plot of load vs. pressure is shown in Figure 16. Each SENT specimen was instrumented with crack propagation gages (CPG) described in Section 3.2. Data from these gages were used to determine the critical flaw size and critical failure load. A plot of load vs. CPG output is shown in Figure 17.

SF specimens were instrumented with a clip gage as shown in Figure 15 to determine crack opening displacements (COD). The clip gage was spring loaded against knife edges integrally machined into or spot welded to the specimen. An expression for the opening displacements of a completely embedded flaw has been provided by Green and Sneddon (Reference 8). Their study examined a flaw embedded in an elastic solid which was subjected to a uniform load normal to the crack surface at infinity. The maximum opening displacement occurs at the diametrical center of the crack and is expressed by the equation,

$$COD = \delta = \frac{4(1-\mu^2)}{E} \frac{\sigma a}{\Phi}$$

Although a rigorous solution is not available for flaw opening displacements for a semi-elliptical surface flaw, such displacements should also be proportional to $\sigma$ and $a/\Phi$ for elastic materials. By following Irwin's procedure (Reference 9) to account for the effect of plastic yielding, the COD for a surface flaw can be approximated by

$$\delta = C \frac{\sigma a}{\sqrt{Q}}$$

where C is a constant. COD measurements were not directly used in analysis of SF static fracture data, however, these measurements were made so that, if necessary, they could be used to supplement COD/flaw size correlations on the cyclic tests.

SENT specimens were also instrumented to determine LOD. These measurements were helpful in estimating the critical flaw size in tests where the sub-critical crack growth extended beyond the range of the CPG. The manner in which this was done is described in Section 4.2.2.

### 3.3.3 Constant Amplitude, Constant Temperature Cyclic Base Line Tests

Base line cyclic tests were conducted on 12 SF and 26 SENT specimens. These tests were conducted in order to produce crack growth rate data which could be correlated with crack growth rate data generated under the thermal/load spectrum. The tests were conducted in room temperature air at a stress ratio, R, of zero and in air at 450K (350°F) at R = 0.5 for all but two of the SENT specimens. These two tests were conducted in room temperature air at R = 0.5 and at 450K (350°F) at R = 0. A sinusoidal loading profile was used and the test frequency was 1 Hz (60 cpm) for all tests except for the suslic tests described in Section 4.3.2.

SF specimens were tested both in the low elastic range ($\sigma/\sigma_{ys}$ = 0.50) and near the plastic range ($\sigma/\sigma_{ys}$ = 0.85). Specimens were tested in a manner so that for each specimen tested at room temperature, there was a corresponding specimen tested at elevated temperature. The purpose of setting up tests in this manner was so that the results could be more easily correlated to the thermal profile tests. The cyclic stresses for room temperature and elevated temperature tests were such that the ratio $\sigma_{max}$ at elevated temperature/$\sigma_{max}$ at room temperature was constant for corresponding specimens of each temper. In most cases specimens were cycled until breakthrough occurred.

SENT specimen tests were planned in a manner similar to that of the SF tests. Because of net stress limitations, it was not possible to test at gross stress levels of 0.50 and 0.85 $\sigma_{ys}$. However, as in the SF tests, loads were chosen so that the ratio $\sigma_{max}$ at elevated temperature/$\sigma_{max}$ at room temperature was constant for corresponding specimens of each temper. Final crack lengths of each test were limited by the criterion that $\sigma_{net}/\sigma_{ys} \leq 0.8$.

SF specimens utilized pressure cups to determine breakthrough as in the static fracture tests. SENT specimens were instrumented with CPG's in order to monitor

crack growth during the tests. The crack length was also monitored visually on SENT tests at appropriate intervals.

SF cyclic specimens were instrumented with the clip gages described in Section 3.3.2 to determine COD during cycling tests. The COD measurements were used to calculate instantaneous growth rates by using the following approach. The crack opening displacement constant, C, can be determined at test initiation and termination from knowledge of the stress level, initial and final flaw sizes, and the corresponding flaw opening displacements as indicated belc

$$C_i = \frac{\delta i}{\sigma} \left( \frac{\sqrt{Q}}{a} \right)_i$$

$$C_f = \frac{\delta f}{\sigma} \left( \frac{\sqrt{Q}}{a} \right)_f$$

where the subscripts i and f refer to initial and final conditions, respectively. Tests have shown that for relatively deep flaws in the tougher materials the value of C tends to increase with increasing crack size, rather than remain constant. Crack growth rate calculations in this report were based on an assumed linear variation in C between the known initial and final values.

In order to relate the flaw parameter $(a/\sqrt{Q})$ to $\delta$ for values of $a/\sqrt{Q})$ between the initial and final values an assumption must be made as to the manner in which the flaw shape changes from

$$\frac{a - a_i}{a_f - a_i} = \frac{2c - (2c)_i}{(2c)_f - (2c)_i}$$

i.e., both flaw depth and width growth simultaneously reach the same percentage of their respective total growth from initial to final values. The flaw shape parameter, Q, can now be determined as a function of flaw depth and, in turn, COD can be related to crack depth. The number of cycles, N, corresponding to each selected flaw depth value can be determined from the test record and, consequently, the change in N for each increment of flaw depth is known. The crack growth rate da/dN can then be calculated.

SENT specimens were also instrumented to determine COD during cycling. These COD measurements were used to substantiate visual and CPG measurements.

### 3.3.4 Thermal Profile Tests

Thermal profile spectrum tests in which stress level changes were combined with variations in temperature were scheduled for 6 SF and 9 SENT specimens. In addition, one SENT specimen was sustain loaded for 2 hours at 450K (350°F) and subsequently cycled at RT. A diagram of the basic spectrum used for the thermal/load profile tests is shown in Figure 1. It is a simplified version of the thermal/load profile that a shuttle structure might see during a typical flight. The spectrum was kept as simple as possible to insure that the thermal profile tests could be easily compared with the constant temperature, constant amplitude cyclic tests.

The maximum cyclic loads at room temperature (RT) and at elevated temperature (ET) for most of the thermal profile tests were chosen so that the ratio

$$\frac{\sigma_{RT}}{\sigma_{ys}\ @\ RT} = \frac{\sigma_{ET}}{\sigma_{ys}\ @\ ET}$$

for each temper. For a given crack length, this kept the ratio $K/\sigma_{ys}$ constant. Since the calculated plastic yield zone size, $2r_y$, at the crack tip is a function of this ratio (e.g., see Reference 10), this was done in an attempt to remove $2r_y$ as another test variable.

For all but one thermal profile test, the room temperature cycles were applied at R = zero and the elevated temperature cycles were applied at R = 0.5 as in the constant temperature, constant amplitude base line tests. During these parts of the profile, the test frequency was 1 Hz (60 cpm) and the waveform was sinusoidal. One specimen was tested at R = zero during the high temperature part of the spectrum.

Because of the complexities of the heating and cooling apparatus, it was not possible to instrument the SF specimens with pressure cups. Nor was it possible to instrument the smaller SENT specimens with CPG's to monitor crack growth. Breakthrough on the SF specimens and crack length extension on the smaller SENT specimens were observed visually. The larger SENT specimens were equipped with CPG's.

SF thermal profile specimens were instrumented with clip gages to determine COD.

This data was used as described in Section 3.3.3 with the following exception. Because of large variations in the readings caused by large temperature changes, it was necessary to take COD measurements at the same arbitrary point in each spectrum. This method proved adequate in relating COD behavior to flaw growth.

SENT specimens were also instrumented for COD measurements. These data were helpful in supplementing visual and CPG measurements of crack growth.

## 3.4 STRESS INTENSITY SOLUTIONS

### 3.4.1 Surface Flaw Specimens

Where stress intensity values are reported, they were based on the Irwin equation (Reference 9) modified with the empirical deep flaw magnification factor developed in Reference 2. The resulting equation is as follows.

$$K_I = 1.95\ \sigma\left(\frac{\pi a}{Q}\right)^{1/2} M_K$$

where $K_I$ = surface flaw stress intensity

$\sigma$ = applied gross area stress

$a$ = flaw depth in a surface flaw specimen

$Q$ = shape parameter

$M_K$ = deep flaw magnification factor.

Values of Q and $M_K$ are shown in Figures 18 and 19, respectively.

### 3.4.2 Single Edge Notch Tension Specimens

Where stress intensity values are reported, they were calculated using the following solution from Reference 11:

$$K = \sigma a^{1/2}\left[1.99 - 0.41\left(\frac{a}{w}\right) + 18.70\left(\frac{a}{w}\right)^2 - 38.48\left(\frac{a}{w}\right)^3 + 53.85\left(\frac{a}{w}\right)^4\right]$$

or $K = \sigma a^{1/2} Y$

where $K$ = single edge notch tension stress intensity

$\sigma$ = applied gross area stress

$a$ = flaw length in a single edge notch specimen

$w$ = specimen width

$Y$ = polynomial function of a and w.

Values of Y are shown in Figure 20.

For static fracture tests two methods were used to calculate the stress intensity at fracture. The resultant values are referred to as $K_{CN}$ and $K_{cr}$. $K_{CN}$ values were calculated using the maximum applied stress, $\sigma_{max}$, and the initial flaw length, $a_i$. $K_{cr}$ values were calculated using the critical flaw size, $a_{cr}$, and the critical stress level, $\sigma_{cr}$. These latter values, $a_{cr}$ and $\sigma_{cr}$ were determined using resistance curve methods as described in References 12 and 13.

# 4.0 TEST RESULTS AND ANALYSIS

## 4.1 MECHANICAL PROPERTIES

Tensile properties of the two tempers of 2219 aluminum alloy used in the program are shown in Tables 4, 5 and 6. Tests of both tempers were conducted in gaseous nitrogen at 144K (-200°F), in room temperature air, and in air at 450K (350°F). Tests were conducted on the -T851 temper in the 6.35 mm (0.250 in.) thickness and on the -T87 temper in thicknesses of 6.35 mm (0.250 in.) and 3.18 mm (0.125 in.).

Room temperature strength levels were well above the values required by Military Specification MIL-A-8920A and the corresponding Boeing Specification BMS 7-105C. Strength levels are plotted as a function of temperature in Figure 21. The shapes of the curves connecting the datum points were determined by comparing the test data with strength vs. temperature curves in MIL-Handbook 5. As would be expected, strength levels of the -T87 temper are higher than those of the -T851 temper.

## 4.2 STATIC FRACTURE TESTS

### 4.2.1 Surface Flaw Specimens

Static fracture SF data are tabulated in Table 7. Plots of failure stress, $\sigma$, vs. flaw size, a/Q, are shown in Figures 22 and 23 for the -T851 and -T87 tempers, respectively. One point, from specimen 87-SF-3, did not appear to be truly representative of the material, so it is not shown in Figure 23. Instead, the datum point from a replicate test, 87-SF-7 is shown. All of the static fracture specimens failed before breakthrough occurred.

In Figures 22 and 23 straight line failure loci have been constructed connecting the test points to points at which unflawed specimens would exhibit ultimate tensile failure. Recently, Bixler has demonstrated that such a straight line relationship can be applied to data when the failure stress is above 90% of the yield stress (Reference 14). Bixler examined test results from aluminum, nickel base steel, and titanium alloys. The equation which describes this relationship is of the following form:

PRECEDING PAGE BLANK NOT FILMED

$$\sigma_{FAILURE} = \sigma_{ULT} - \frac{A}{t^m}(a/Q)$$

where $\sigma_{ULT}$ = ultimate tensile strength

$A$ = a constant dependent on material properties

$t$ = specimen thickness

$m$ = an exponent ranging from ≈0.6 to 0.76

$a$ = flaw depth

$Q$ = shape parameter

Examination of Figures 22 and 23 shows that the failure loci become more horizontal on the plots with an increase in temperature. Indeed, for the 3.18 mm (0.125 in.) -T87 specimen tested at 450K (350°F) the failure stress actually occurred at a stress level slightly above the average ultimate strength level determined in the mechanical properties tests. This type of behavior indicates that for the flaw sizes and high failure stresses experienced by these tests, the failure stress of the specimen becomes less sensitive to the existence of the flaw as the temperature increases.

Specimens of the -T851 temper failed at lower stress levels than did comparable specimens of the -T87 temper. Since the failure stress is a function of relative ultimate tensile strength, this type of behavior would be expected.

### 4.2.2 Single Edge Notch Tension Specimens

Data from the 6.35 mm (0.250 in.) 2219-T851 SENT tests are reported in Table 8. Data from the 6.35 mm (0.250 in.) and 3.18 mm (0.125 in.) 2219-T87 specimens are reported in Tables 9 and 10, respectively. Two stress intensity values are reported for each test, $K_{CN}$ and $K_{cr}$. $K_{CN}$ is defined as the stress intensity calculated using the maximum applied stress, $\sigma_{max}$, and the initial flaw length, $a_i$. The critical stress intensity, $K_{cr}$, was calculated from the critical stress level, $\sigma_{cr}$ and the corresponding critical crack length, $a_{cr}$. These values of $\sigma_{cr}$ and $a_{cr}$ were determined using resistance curve methods described in References 12 and 13.

Each SENT specimen was instrumented with crack propagation gages as described in Section 3.2. These gages provided a means of obtaining an output of applied load vs. estimated crack length for the specimens during the fracture tests. An example curve for specimen 87-2 is shown in Figure 17. Example crack growth resistance curves ($K_R$ vs. a) are plotted for the 6.35 mm (0.250 in.) 2219-T87 specimens in Figure 24. Stress intensity curves (K vs. a) for each test are plotted on the same figure. $K_{cr}$ is defined as the point at which the $K_R$ curve is tangent to a K curve.

Finding the tangency point of the K and $K_R$ curves requires the construction of K curves at several stress levels. However, a more simplified approach was found to be successful for these tests. Examination of the load vs. CPG curve in Figure 17 will show two points marked "A" and "B". These points correspond to the two points marked "A" and "B" on the $K_R$ curve in Figure 24. Point "A" is the point at which the maximum stress level is reached. Examination of Figure 24 and corresponding CPG curves shows that this relationship is also true for other tests plotted on Figure 24. This relationship was noted to hold for the other twelve tests also.

A critical crack length could not be determined for Specimen 851-4, tested at room temperature because the failure load was just beyond the maximum load range on the load vs. CPG curve. Specimens tested at 450K (350°F) exhibited subcritical flaw growth which extended further than the 39.6 mm (1.56 in.) gage length of the CPG's. Thus, for the first two specimens tested at this temperature (Specimens 851-6 and 87-6) critical crack lengths could not be determined directly from the CPG traces. However, critical flaw sizes were estimated from COD data. All other specimens subsequently tested at 450K (350°F) were instrumented with two CPG's in order to measure the large amount of subcritical flaw growth inherent in the tests at this higher temperature. Tables 8, 9 and 10 show values of $\sigma_{net}/\sigma_{ys}$ at $K_{CN}$ and at $K_{cr}$. The values of $\sigma_{net}/\sigma_{ys}$ at $K_{CN}$ were determined from the maximum applied stress level and the initial crack length, $a_i$. Values of $\sigma_{net}/\sigma_{ys}$ at $K_{cr}$ were calculated using the maximum applied stress level and the critical crack length, $a_{cr}$. Using the above methods, it was found that $\sigma_{net}/\sigma_{ys}$ exceeded 0.8 for all of the $K_{CN}$

values except the 144K (-200°F) and room temperature tests on the -T87 temper. For the $K_{cr}$ values $\sigma_{net}/\sigma_{ys}$ exceeded 0.8 for all tests.

$K_{CN}$ and $K_{cr}$ values are plotted vs. temperature in Figures 25 and 26, respectively. Average values are summarized in the table below:

| TEMPER | STRESS INTENSITY | TEST TEMPERATURE | | |
|---|---|---|---|---|
| | | 144 (-200°F) | RT | 450K (350°F) |
| -T851 | $K_{cr}$, $MN/m^{3/2}$ ($ksi\sqrt{in}$) | 126 (115) | 126 (115) | 199 (181) |
| | $K_{CN}$, $MN/m^{3/2}$ ($ksi\sqrt{in}$) | 97 (88) | 97 (88) | 121 (110) |
| -T87 | $K_{cr}$, $MN/m^{3/2}$ ($ksi\sqrt{in}$) | 106 (96) | 106 (96) | 184 (167) |
| | $K_{CN}$, $MN/m^{3/2}$ ($ksi\sqrt{in}$) | 86 (78) | 86 (78) | 110 (100) |

The -T87 temper did not appear to show any significant difference in stress intensity values for the two thicknesses (6.35 mm (0.250 in.) and 3.18 mm (0.125 in.)) which were tested. For both tempers, the $K_{cr}$ and $K_{CN}$ values remain constant at 144K (-200°F) and room temperature and increase as the temperature is raised to 450K (350°F). The higher toughness values exhibited by the lower strength -T851 temper (vs. those of the -T87 temper) demonstrate that the SENT fracture tests were toughness controlled regardless of the inherent high net section stresses.

## 4.3 CONSTANT TEMPERATURE, CONSTANT AMPLITUDE CYCLIC BASE LINE TESTS

### 4.3.1 Surface Flaw Specimens

Test parameters for the 2219-T851 SF tests are reported in Table 11. The 2219-T87 SF tests are reported in Tables 12 and 13. Maximum stress intensity vs. crack growth rate curves for the 2219-T851 room temperature and 450K (305°F) tests are plotted in Figures 27 and 28, respectively. Similar data for the 2219-T87 room temperature tests are plotted in Figure 29 and data for the elevated temperature tests are plotted in Figure 30. A summary plot of all SF tests is shown in Figure 31.

Figures 27 and 28 show fairly tight data bands for the -T851 temper. The -T87 data exhibits greater scatter, especially in the thicker gage specimens, as shown in Figures 29 and 30. There do not appear to be significant stress level effects, although, if such effects existed they may be masked by data scatter in the -T87 tests. Figure 31 shows that the room temperature crack growth rates are about the same for both tempers for a given thickness. Crack growth rates in the T87 temper appear to be slightly faster than those of the -T851 temper at elevated temperature. This difference is or the order of about twice as fast. It also can be seen that the 3.18 mm (0.125 in.) -T87 specimens appear to grow at a slightly faster crack growth rate than the 6.35 mm (0.250 in.) specimens at room temperature. Figure 32 shows the room temperature data generated on this program compared with an extensive body of 2219-T87 data compiled in Reference 15.

Forman, Kearney and Engle (Reference 16) have proposed a fatigue crack propagation model of the form:

$$da/dN = \frac{C(\Delta K)^n}{[(1 - R)K_{IE} - \Delta K]}$$

where:
- $da/dN$ = fatigue crack growth rate
- $\Delta K$ = cyclic stress intensity range
- $K_{IE}$ = critical stress intensity
- $R$ = stress ratio
- $C,n$ = empirically determined constants.

An attempt was made to fit this equation to the SF crack growth rate data generated on this program. Figures 33 and 34 show this equation fitted to room temperature SF 2219-T851 and 2219-T87 data, respectively. In Figure 33, $K_{IE}$ was estimated from the approximate stress intensity at failure of specimen 851-SF-C6 (this specimen was cycled to failure under thermal profile loading). In Figure 34, for the T87 temper, The $K_{IE}$ value was taken from Reference 15. Examination of these two figures shows that the equation of Forman et al, can be made to fit the data fairly well. No attempt was made to fit the equation to crack growth rate data generated at elevated temperature because of the lack of $K_{IE}$ data.

### 4.3.2 Single Edge Notch Tension Specimens

Test parameters for the 2219-T851 SENT tests are tabulated in Table 14. Data for the 2219-T87 tests are in Tables 15 and 16. Typical flaw length vs. cycles plots are shown in Figures 35 and 36 for a room temperature test and for a test at 450K (350°F), respectively. During cycling, crack length measurements were made visually and with the use of crack propagation gages as described in Section 3.2. Agreement between CPG measurements and visual measurements on room temperature tests was excellent as shown by the example in Figure 35. Agreement between CPG measurements and visual measurements on 450K (350°F) tests was not as good (see Figure 36), however, the CPG measurements still produced data which were more than adequate for determining crack growth rates.

Crack growth rates for the 2219-T851 SENT room temperature and 450K (350°F) tests are shown in Figures 37 and 38, respectively. Data from 6.35 mm (0.250 in.) 2219-T87 SENT room temperature and elevated temperature tests are shown in Figures 39 and 40. The 3.18 mm (0.125 in.) -T87 results are shown in Figures 41 and 42. Summary plots of all the data are shown in Figure 43.

Examination of Figures 37 through 42 shows that at a given stress intensity crack growth rate is not influenced by variations in maximum stress level and/or specimen size. Scatter bands on the summary plot of Figure 43 show that at room temperature and R = 0, the three temper/thickness combinations exhibit nearly equal growth rates. At elevated temperature and R = 0.5 there appears to be no thickness effect on the -T87 tests. However, a comparison between the two tempers shows that for most of the data, cracks in the -T87 temper grow at a rate about two times faster than those in the -T851 temper. This difference in crack growth rates at elevated temperature was also observed in the surface flaw tests.

All but one of the room temperature tests were conducted at a stress ratio, R, of zero. All but one of the elevated temperature tests were conducted at R = 0.5. In order to determine temperature effects at a given stress ratio (and likewise, stress ratio effects at a given temperature), one room temperature tests was conducted at R = 0.5 and one elevated temperature test was

conducted at R = zero. Additionally, three specimens were tested under a sustained load cyclic (suslic) loading profile. Effects of variations in stress ratio, test temperature and loading profile are discussed below. Illustrations are shown in Figures 44 through 48.

The effect of varying the stress ratio on crack growth rate at a constant test temperature is illustrated in Figures 44 and 45. Figure 44 shows scatter bands of crack growth rates for room temperature tests at R = 0 for the three temper/thickness combinations tested. For comparison, one specimen (87-C12) was tested at room temperature and R = 0.5. Datum points for this specimen are also shown in Figure 44. This figure shows that at room temperature the crack growth rate at R = 0 is on the order of 2 to 4 times as fast as the crack growth rate at R = 0.5 for the three temper/thickness combinations tested. Figure 45 shows the scatter band of crack growth rates for elevated temperature tests on the -T851 temper tested at R = 0.5. For comparison, one specimen (851-C12) was tested at elevated temperature and R = 0. Datum points for this specimen are also shown in Figure 45. This figure shows that at elevated temperature the crack growth rate at R = 0 is on the order of 3 to 10 times as fast as the crack growth rate at R = 0.5 for the -T851 temper.

The effect of varying the test temperature on crack growth rates at a constant stress ratio is illustrated in Figures 46 and 47. Figure 46 shows the scatter band of crack growth rates for room temperature tests on the -T851 temper at R = 0. The specimen (851-C12) tested at elevated temperature and R = 0 is also plotted for comparison. Figure 46 shows that for the 2219-T851 alloy tested at R = 0, raising the test temperature from room temperature to 450K (350°F) has the following effect on the cyclic growth rates:

1) at low stress intensities, 20 $MN/m^{3/2}$ (18 $ksi\sqrt{in}$) < $K_{max}$ < 33 $MN/m^{3/2}$ (30 $ksi\sqrt{in}$), crack growth rates at 450K (350°F) are about 2-3 times those at RT.

2) at intermediate stress intensities, 33 $MN/m^{3/2}$ (30 $ksi\sqrt{in}$) < $K_{max}$ < 44 $MN/m^{3/2}$ (40 $ksi\sqrt{in}$), crack growth rates at 450K (350°F) are up to twice the growth rates at RT.

3) at high stress intensity, $K_{max} > 44$ MN/m$^{3/2}$ (40 ksi$\sqrt{in}$), there appears to be no temperature effect on crack growth rates.

Figure 47 further illustrates the effect of test temperature on crack growth rates. Scatter bands of crack growth rates for elevated temperature tests on the -T87 temper tested at R = 0.5 are plotted in this figure. Datum points from the -T87 specimen (87-C12) tested at room temperature and R = 0.5 are also plotted in this figure for comparison. Figure 47 shows that for the 2219-T87 alloy tested at R = 0.5, raising the test temperature from room temperature to 450K (350°F) has the following effect on the cyclic crack growth rates:

1) at low stress intensities, 25 MN/m$^{3/2}$ (23 ksi$\sqrt{in}$) $< K_{max} <$ 33 MN/m$^{3/2}$ (30 ksi$\sqrt{in}$), growth rates at 450K (350°F) are about 1 1/2 to about 3 times those at RT.
2) at intermediate stress intensities, 33 MN/m$^{3/2}$ (30 ksi$\sqrt{in}$) $< K_{max} <$ 44 MN/m$^{3/2}$ (40 ksi$\sqrt{in}$), growth rates at 450K (350°F) are about the same as or as fast as 2 times those at RT.
3) at high stress intensity, $K_{max} > 44$ MN/m$^{3/2}$ (40 ksi$\sqrt{in}$), there appears to be no temperature effect on growth rates.

The small effects of elevated temperature on crack growth rates reported here have also been seen in other 2219 data (e.g , References 17 and 18).

Three specimens were subjected to suslic loading. These specimens, 851-C5 and -C7, and 87-C7 were reported in Figures 38 and 40. After being fatigue cycled in the normal manner with a sinusoidal loading profile at 1 Hz (60 cpm), each specimen was fatigue marked at a lower cyclic stress level in room temperature air. Each specimen was then subjected to 30 sustained load (suslic) cycles. This loading was conducted at a stress ratio of 0.5 and the specimens were held at the maximum load for 2 minutes during each cycle. Examination of crack opening displacement (COD) records indicates that crack growth probably occurred continuously during each hold time. After undergoing suslic loading, each specimen was fatigue marked at a lower stress in room temperature air and the original test was continued. Average crack growth rates were calculated for

these tests and they are plotted as solid points in Figure 48. Base line crack growth rate bands for the 1 Hz (60 cpm) sinusoidal loading profile are also reported in Figure 48. The limited amount of data shown here indicates that the suslic crack growth rates are 10 to 15 times the rates of the 1 Hz (60 cpm) data.

The room temperature SENT cyclic crack growth rate data from this program are compared with room temperature 2219-T851 through-the-thickness cyclic crack growth rate data generated by Grumman in the program in Reference 19. The Grumman data were generated at stress ratios of +0, +0.05 and +0.1. Figure 49 shows that the Boeing data compare very well with the data generated by Grumman.

Comparison of the summary plots on Figures 31 and 43 shows that at a given K value, a crack in a SENT specimen grows at a faster crack growth rate than does a crack in a SF specimen. (Note the shift in the abscissa between Figures 31 and 43.) This difference was also seen in Reference 6 and is attributed to the different propagation directions, TL for the SENT tests and TS for the SF tests.

An attempt was made to fit the equation of Forman, et al (Reference 16) to the SENT crack growth rate data generated on this program. $K_{CN}$ values used were determined from the SENT static fracture test results. Figures 50 and 51 show Forman's equation fitted to 2219-T851 crack growth rate data generated at room temperature and 450K (350°F), respectively. Figure 50 shows a very good fit for the 2219-T851 room temperature crack data generated at R = 0. In Figure 51, Forman's equation was fitted to the body of 2219-T851 SENT crack growth data generated at 450K (350°F) and R = 0.5. An R value of zero was substituted into the resulting equation and the locus of crack growth rates for this condition is also plotted. Data from specimen 851-C12, tested at 450K (350°F) and R = 0 are also plotted on Figure 51. Both sets of data, at R = 0.5 and R = 0, fit Forman's equation very well. Figures 52 and 53 show Forman's equation fitted to room temperature and 450K (350°F) 2219-T87 crack growth data. The room temperature 2219-T87 data generated at R = 0 also show a good fit to Forman's equation as shown in Figure 52. An R value of 0.5 was

also substituted into the equation for the room temperature -T87 data and it is plotted in Figure 52 along with data from specimen 87-C12 which was tested at R = 0.5. The data from specimen 87-C12 match the fitted curve of crack growth rates within a factor of two. The elevated temperature -T87 data matched the equation quite well as shown in Figure 53.

## 4.4 THERMAL PROFILE TESTS

Surface flaw and single edge notch tension specimens were subjected to a combination of changing loads and temperatures. The basic spectrum utilized for most tests is shown in Figure 1. Minor changes were made in this basic spectrum test for some of the tests. The results and discussions of all of the thermal profile tests are presented below.

### 4.4.1 Surface Flaw Specimens

All SF specimens were subjected to the basic spectrum shown in Figure 1. As described in Section 3.3.4, loads were chosen so that the ratio $\frac{K_{RT}}{\sigma_{ys}\ @\ RT} = \frac{K_{ET}}{\sigma_{ys}\ @\ ET}$ was utilized on each specimen.

Crack growth rate data from the 2219-T851 surface flaw tests are plotted in Figure 54 and listed in Table 17. Figure 54 shows the data presented in terms of the crack growth rate, da/d Flight, vs. the maximum applied stress intensity at the room temperature part of the flight, $K_{Imax}$ @ RT.

A predicted growth rate band is also shown in Figure 54. The prediction is based upon a linear cumulative damage approach, utilizing the base line data shown previously in Figure 31. Each flight contained 100 cycles at RT, 100 cycles at ET, a short period at zero load and cryogenic temperature and one sustained load cycle at ET of aoproximately two minutes duration. In the prediction, cyclic growth rates were taken at the appropriate $K_I$ values and the sustained load growth rate was taken to be 10 times the elevated teperature cyclic crack growth rate at the appropriate K value. The total relative damage which occurred was about 1-3% due to the elevated temperature sustained loading; about 10-25% due to the elevated temperature cyclic load; and the remainder due to the room temperature cyclic load. It was assumed that no damage

occurred during the cryogenic part of each flight. The growth rates were added to produce the scatter band in Figure 54. It can be seen that the experimental thermal profile crack growth rate data falls within this band.

Similar results were observed in the SF tests on the -T87 temper. Figure 55 shows a plot of da/dFlight vs. $K_{Imax}$ @ RT for both thicknesses (6.35 mm (0.250 in.) and 3.18 mm (0.125 in.)) of the -T87 temper. A scatter band of expected crack growth rates was constructed from base line data in Figure 31 in the same manner as was done from the -T851 base line data. The -T87 crack growth data in Figure 55 generally falls within this boundary. The -T87 crack growth data are listed in Table 18.

Net section stresses for the -T851 and -T87 specimens were on the order of 53% to 97% of yield strength.

### 4.4.2 Single Edge Notch Tension Specimens

Crack growth rate data from the 2219-T851 single edge notch tension tests are plotted in Figure 56 in terms of da/dFlight vs. $K_{max}$ @ RT. A scatter band of expected crack growth rates was constructed from base line da/dN rates found in Figure 43 in the same manner as described in Section 4.4.1. This scatter band is plotted in Figure 56 along with the data from the thermal profile tests. Two of the three -T851 specimens were tested under the basic thermal profile spectrum of Figure 1. The third specimen 851-C10, was subjected to thermal profile flights which differed in that the 100 cycles at elevated temperature on each flight were applied with a stress ratio of zero instead of 0.5. Examination of Figure 56 shows that all three of the specimens demonstrated some retardation in crack growth rates.

Specimen 851-C10 demonstrates retarded crack growth rates even though the high temperature cycles were applied at a lower stress ratio than that for which the scatter band was calculated. The highest amount of retardation occurred in Specimen 851-C11. This specimen was wider than the other two specimens (305 mm (12 in.) vs. 76 mm (3 in.)), and it was subjected to lower net section stresses than the other two specimens. ($\sigma_{net}/\sigma_{ys}$ = 0.29 to 0.31 vs. $\sigma_{net}/\sigma_{ys}$ = 0.44 to 0.84 as shown in Table 19.

After having been subjected to 73 thermal profile flights, specimen 851-C11 was cycled at RT and constant amplitude at R = 0. The maximum stress level used was the same as that applied during the RT portion of each thermal profile flight. Crack growth rate, da/dN, data from this test are compared with base line da/dN data in Figure 57. It can easily be seen that the room temperature cyclic growth rates were retarded by the previous thermal profile flights. This specimen was cycled under constant amplitude, constant temperature loading from a crack length of 80.8 mm (3.18 in.) to 95.8 mm (3.77 in.). Retardation occurred over this entire distance (15 mm (0.59 in.)) althrough, the amount of retardation decreased as the crack extended. The fact that retardation should be apparent over such a long distance is somewhat surprising especially since the estimated plastic zone size, $2r_y$, produced during the thermal profile test was on the order of 2.5 mm (0.10 in.). (This plastic zone size was calculated by the equation, $r_y = \frac{1}{2\pi} \left( \frac{K_{max}}{\sigma_{ys}} \right)^2$ suggested in Reference 10.)

The crack growth behavior of the -T87 temper was quite similar to that of the -T851 temper. The 6.35 mm (0.250 in.) and 3.18 mm (0.125 in.) -T87 data are listed in Tables 20 and 21, respectively. Crack growth data for both thicknesses are plotted in terms of da/dFlight vs. $K_{max}$ @ RT in Figure 58. The scatter band for predicted crack growth rates was generated from the base line da/dN data in Figure 43 as described above. This predicted band is also plotted on Figure 58 along with the actual thermal profile test datum points.

Three specimens were tested in each thickness for the -T87 temper. Two of the 6.35 mm (0.250 in.) specimens (87-C10 and 87-C11) and one of the 3.18 mm (0.125 in.) specimens (87-C23) were tested under the basic spectrum of Figure 1. The third 6.35 mm (0.250 in.) specimen (87-C9) was tested under the basic spectrum, but the maximum temperature used during the elevated temperature portion of the spectrum was 394K (250°F) rather than 450K (350°F). One of the remaining 3.18 mm (0.125 in.) specimens (87-C21) was subjected to a maximum temperature of 422K (300°F) during the elevated temperature portion of the spectrum. The third 3.18 mm (0.125 in.) specimen (87-C24) was subjected to a modified spectrum in which there was no sustained load at

elevated temperature and the maximum stress at elevated temperature was lowered so that $\sigma_{ET}/\sigma_{RT} = 0.5\ \sigma_{ys}$ @ ET/$\sigma_{ys}$ @ RT.

Figure 58 shows that all of the specimens tested exhibited at least some retardation in crack growth rates. There appears to be no thickness effect on growth rates. However, as in the -T851 tests, there does appear to be a specimen width and/or a net section stress effect. Specimens 87-C9, 87-C10 and 87-C21 were 76 mm (3 in.) wide and showed less retardation in their crack growth rates than did specimens 87-C11, 87-C23 and 87-C24 which were 305 mm (12 in.) wide. The 76 mm (3 in.) wide specimens were subjected to net section stresses on the order of 42% to 80% of the yield stress and the 305 mm (12 in.) wide specimens were subjected to net section stresses on the order of 27% to 31% of yield. Lowering the test temperature at the elevated temperature portion of the spectrum from 450K (350°F) to 394K (250°F) did not appear to have any substantial impact on the crack growth rates. Furthermore, removing the sustained portion of the spectrum at elevated temperature and lowering the maximum stress at elevated temperature did not appear to remove retardation effects. Lowering the stress level at elevated temperature would also slightly lower the crack growth rate, da/dFlight, however, not to the extent that was experienced by specimen 87-C24.

In order to further investigate the observations of retardation, additional testing was performed on several -T87 SENT specimens. Specimen 87-C11 was cycled at RT under constant amplitude at R = 0 after having been subjected to 58 thermal profile flights. The maximum stress level used in the RT test was the same as that applied during the RT portion of each thermal profile flight. The resultant crack growth data are shown on a da/dN vs. $K_{max}$ plot along with base line data in Figure 59. These crack growth data (shown as square points on the plot) demonstrate behavior similar to that shown by specimen 851-C11 discussed earlier. Retardation in the cyclic crack growth rate was very apparent at the beginning of the test, however, as the crack grew from a length of 82.6 mm (3.25 in.) to a length of 97.8 mm (3.85 in.) the growth rates eventually matched those of the base line tests. A further illustration of this retardation in crack growth rates is shown in Figure 60. This figure shows the crack length of specimen 87-C11 plotted as a function of numbers of cycles. Data from base line specimen 87-C3 are also shown for comparison.

Figure 59 also contains crack growth rate data points from specimen 87-C22. This specimen was sustain loaded at 450K (350°F) to a stress level comparable to that used for many of the thermal profile tests. The specimen was then cycled at RT and constant amplitude with R = 0. The maximum stress level for the RT cyclic test was chosen so that, $\frac{\sigma_{RT}}{\sigma_{ET}} = \frac{\sigma_{ys\ @\ RT}}{\sigma_{ys\ @\ ET}}$, as in the thermal profile spectrum tests. This specimen (87-C22) also exhibited subsequent retardation in crack growth rates. Test parameters for specimen 87-C22 are tabulated in Table 22.

For most of the thermal profile tests, the elevated temperature portion of each flight caused retardation of crack growth during the room temperature portion of the subsequent flights, (i.e., crack growth rates indicated that most of the cyclic crack growth occurred at elevated temperature during each flight). As a further check on this observation, one specimen (87-C23) was cycled at 450K (350°F) and constant amplitude with R = 0.5, after having been subjected to 46 thermal profile flights. The maximum stress level used was the same as that applied during the ET portion of each thermal profile flight. The data are shown on a da/dN vs. $K_{max}$ plot along with ET base line data in Figure 61. These data fall within the scatter band generated from the base line tests.

### 4.4.3 Metallurgical Analysis

The fracture faces of the base line cyclic and thermal profile specimens were examined after testing and the following observations were noted. Base line SF specimens generally exhibited flatter fracture faces than did the SENT specimen over the area where cyclic growth occurred. Room temperature and elevated temperature SF specimens were similar in appearance although the fracture faces of the ET specimens were slightly duller in appearance. SENT specimens tested at RT and ET also exhibited differences in fracture face brightness with most of the ET SENT specimen fracture faces being somewhat darker than the RT SENT specimen fracture faces. This darkness in the ET tests was probably due to rubbing and fretting on the fracture face. It was also noted that this apparent fretting on the RT SENT FRACTURE faces became visible at K levels around 27.5 $MN/m^{3/2}$ (25 $ksi\sqrt{in}$) and above. A very subtle difference between RT and ET SENT fracture face texture was also noted. SENT

specimens tested at ET exhibited more facets in their fracture faces than did those tested at RT.

Examination of the fracture faces of thermal profile specimens showed that the SF specimens exhibited flatter fracture faces than the SENT specimens. Additionally the SENT specimen fracture faces were not as bright as those of the SF specimens.

Two of the thermal profile specimens were also subjected to a closer examination under an electron microscope. One SENT specimen (87-C11) and one SF specimen (87-SF-C6) were examined. Figures 62 and 63 show the regions from where replicas were taken on thse two specimens to produce the fractographs shown in the following figures.

Figure 64 shows an electron fractograph from the precrack region of SENT specimen 87-C11. This region displayed typical fatigue striations.

Figures 65, 66 and 67 show electron fractographs from the thermal profile region of specimen 87-C11. In this region "tire tracks," typical in fatigue fractures, were frequently observed (Figure 65). Fretting was suspected in this area of having rubbed out most of the fatigue striations. However, a couple of very small areas containing striations were noted (Figure 66). Isolated areas of elongated dimples were also observed (Figure 67).

As described earlier, specimen 87-C11 was subjected to constant amplitude cycles at RT after having been subjected to 58 thermal profile flights. It was noted earlier in Section 4.4.2 that the constant amplitude growth rates demonstrated crack growth delay due to the previous thermal profile flights. Figures 68, 69 and 70 are from the constant temperature, constant amplitude region where crack growth delay was apparent. Close to the interface between the thermal profile and constant amplitude regions fatigue striations were observed (Figure 68). Farther out from this interface (~0.64 mm (0.025 in.) from Figure 68) striations were still observed, but the striation spacing was much smaller (Figure 69). Still farther from the interface (~0.94 mm (0.037 in.) from Figure 68) what might be extremely small striations were observed. Much of the rest of the constant temperature, constant amplitude region of specimen 87-C11 was covered with flat, featureless areas where no

striations were seen (Figure 70). This topography is characteristic of very low $\Delta K$ fatigue cycling in aluminum alloys where striation spacing is too small to be resolved. Figure 71 is a fractograph typical of the area farther along the constant temperature, constant amplitude region of specimen 87-C11, where crack growth retardation was diminishing.

The preceeding description of "normally" spaced striations at the beginning of the post thermal profile delay region, followed at some small distance by finer and finer striations, and finally by larger and larger striations is typical of fractographic observations of delay regions following peak overloads in fatigue spectra observed by others on through-the-thickness tests (e.g., References 20 and 21). While there was no peak overload in this case the last 100 cycles at 450K (350°F) prior to RT cycling has had a delay effect similar to that of a peak overload. It should be noted that the "normal" flaw growth rates at the beginning of the delay region could not be detected by actual surface measurements or by COD measurements during the test.

Figures 72 and 73 show fractographs from the thermal profile region of the surface flaw specimen, 87-SF-C6. (See Figure 63 for location.) Examination of the replica from this specimen revealed three principal differences between it and the replica from the thermal profile region of the SENT specimen, 87-C11.

1. Fatigue striations were visible throughout much of the thermal region on the surface flaw specimen (Figure 72). In the SENT specimen visible fatigue striations were extremely rare.

2. Areas of uninterrupted striations where more than 100 striations could be counted were observed. Separating these groups was a large growth increment (Figure 72) which probably occurred during the single load application and hold where temperature increased from 144K (-200°F) to 450K (350°F). (See spectrum in Figure 1). The fractograph in Figure 72 indicates that the growth increment for this single load application and hold was about 10 times as large as for each cycle of the other load applications applied at 1 Hz (60 cpm). In contrast, crack growth in the SENT specimen during the RT portion of the thermal spectrum was apparently very minimal (based on macroscopic measurement only).

3. There was an abundance of an acicular material in the thermal profile region of the surface flaw specimen (Figure 73). These particles were not observed in the thermal profile region of the SENT specimen.

## 5.0 CONCLUSIONS

The following conclusions are based on test results of surface flawed and single edge notch tension tests on 2219 aluminum alloy in T851 and T87 tempers.

Static Fracture Behavior

1. All surface flaw specimens tested exhibited failure stresses at or above the yield strengths of the materials.

2. For single edge notch tension specimens, the stress intensity values at failure, $K_{cr}$ and $K_{CN}$ remain constart as the temperature is increased from 144K (-200°F) to room temperature. As the temperature is increased further up to 450K (350°F), $K_{cr}$ and $K_{CN}$ values increase substantially.

Constant Temperature, Constant Amplitude Cyclic Flaw Growth Behavior

1. At room temperature, 2219-T851 and 2219-T87 aluminum alloys exhibit the same cyclic crack growth rates at a given maximum cyclic stress intensity value for both surface flaw and single edge notch tension specimens.

2. At 450K (350°F), 2219-T851 aluminum alloy has a slower cyclic crack growth rate at a given maximum cyclic stress intensity value than does 2219-T87 aluminum alloy for both surface flaw and single edge notch tension specimens.

3. Surface flaw 2219-T851 and -T87 specimens (tested in the TS propagation direction) have slower cyclic crack growth rates than single edge notch tension specimens (tested in TL propagation direction).

4. Cyclic crack growth rates of 2219-T851 and -T87 surface flaw and single edge notch specimens, tested under the stresses and with the configurations used in this program are not affected by the maximum cyclic stress level. (i.e., They are K dependent.)

5. Cyclic crack growth rates of single edge notch tension specimens are not affected by specimen size in the configurations tested in this program.

PRECEDING PAGE BLANK NOT FILMED

6. For all three temper/thickness combinations tested in the SENT configurations at room temperature, the crack growth rate at R = 0 is about 2 to 4 times the growth rate at R = 0.5.

7. For the -T851 temper, tested in the SENT configuration at 450K (350°F), the crack growth rate at R = 0 is on the order of 3 to 10 times the crack growth rate at R = 0.5.

8. For the -T851 temper tested in the SENT configuration at R = 0, varying the temperature from RT to 450K (350°F) has the following effect on cyclic crack growth rates.

| $K_{max}$ | EFFECT ON GROWTH RATES |
|---|---|
| 20 $MN/m^{3/2}$ (18 $ksi\sqrt{in}$) to 33 $MN/m^{3/2}$ (30 $ksi\sqrt{in}$) | 2 to 3 times RT rates |
| 33 $MN/m^{3/2}$ (30 $ksi\sqrt{in}$) to 44 $MN/m^{3/2}$ (40 $ksi\sqrt{in}$) | same as to 2 times RT rates |
| Greater than 44 $MN/m^{3/2}$ (40 $ksi\sqrt{in}$) | same as RT rates |

9. For the -T87 temper tested in the SENT configuration at R = 0.5, varying the temperature from RT to 450K (350°F) has the following effect on cyclic crack growth rates.

| $K_{max}$ | EFFECT ON GROWTH RATES |
|---|---|
| 25 $MN/m^{3/2}$ (23 $ksi\sqrt{in}$) to 33 $MN/m^{3/2}$ (30 $ksi\sqrt{in}$) | 1-1/2 to 3 times RT rates |
| 33 $MN/m^{3/2}$ (30 $ksi\sqrt{in}$) to 44 $MN/m^{3/2}$ (40 $ksi\sqrt{in}$) | same as to 2 times RT rates |
| Greater than 44 $MN/m^{3/2}$ (40 $ksi\sqrt{in}$) | same as RT rates |

10. For both the -T851 and -T87 tempers tested at 450K (350°F) and R = 0.5, holding the maximum stress for 2 minutes on each cycle produces growth rates on the order of 10 to 15 times those produced by 1.0 Hz (60 cpm) sinusoidal loading.

Thermal Profile Flaw Growth Behavior

1. The flaw growth behavior of surface flaw specimens can be successfully predicted by a cumulative damage approach.

2. The flaw growth rates of single edge notch tension specimens were usually much slower than those which would be predicted by a cumulative damage approach. Crack growth retardation was

most pronounced for ET levels of 450K (350°F) but was still apparent for ET levels of 394K (250°F).

3. The flaw growth behavior of single edge notch tension specimens appears to be affected by specimen size and/or net section stress, with wider specimens subjected to net section stresses on the order of 27% to 31% of $\sigma_{ys}$ displaying more retardation in flaw growth behavior than smaller specimens subjected to net section stresses on the order of 42% to 84% of $\sigma_{ys}$. Note that these test variables did not affect constant temperature, constant amplitude cyclic flaw growth rates.

## REFERENCES


1. C. F. Tiffany, "Fracture Control of Metallic Pressure Vessels," NASA SP-8040, 1970.

2. J. N. Masters, W. P. Haese and R. W. Finger, "Investigation of Deep Flaws in Thin Walled Tanks," NASA CR-72606, December 1969.

3. J. N. Masters, W. D. Bixler and R. W. Finger, "Fracture Characteristics of Structural Aerospace Alloys Containing Deep Surface Flaws," NASA CR-134587, December 1973.

4. J. N. Masters, W. L. Engstrom and W. D. Bixler, "Deep Flaws in Weldments of Aluminum and Titanium," NASA CR-134649, April 1974.

5. Ramesh C. Shah, "Effects of Proof Loads and Combined Mode Loadings on Fracture and Flaw Growth Characteristics of Aerospace Alloys," NASA CR 134611, March 1974.

6. L. R. Hall and W. D. Bixler, "Subcritical Crack Growth of Selected Aerospace Pressure Vessel Materials," NASA CR-120834, December 1972.

7. Anon., "Standard Method of Test for Plane-Strain Fracture Toughness of Metallic Materials," American Society for Testing and Materials, Designation E399-72.

8. A. E. Green and I. N. Sneddon, "The Distribution of Stress in the Neighborhood of a Flat Elliptical Crack in an Elastic Solid," Proc. Cambridge Phil. Soc., 46, 1959 (1950).

9. G. R. Irwin, "Crack Extension Force for a Part-Through Crack in a Plate," J. of Applied Mechanics, Vol. 29, Trans. ASME, Vol. 84, Series E, December 1962.

10. F. A. McClintock and G. R. Irwin, "Plasticity Aspects of Fracture Mechanics," pp. 84-113, ASTM STP 381, 1965.

11. W. F. Brown, Jr. and J. E. Srawley, Plane Strain Crack Toughness Testing of High Strength Metallic Materials, p. 12, ASTM STP 410, 1967.

12. J. E Srawley and W. F. Brown, Jr., "Fracture Toughness Testing Methods," pp. 133-198, ASTM STP 381, 1965.

13. D. E. McCabe, Fracture Toughness Evaluation by R-Curve Methods, ASTM STP 527, 1973.

14. W. D. Bixler, "Composite Tanks With Load Sharing Liners," NASA Contract NAS3-14380, Monthly Progress Report No. 13, July 1 through July 31, 1974, Boeing Aerospace Company.


PRECEDING PAGE BLANK NOT FILMED

15. W. L. Engstom, "Determination of Design Allowable Properties, Fracture of 2219-T87 Aluminum Alloy," NASA CR-115388, March 1972.

16. R. G. Forman, V. E. Kearney and R. M. Engle, "Numerical Analysis of Crack Propagation in Cyclic-Loaded Structures," J. of Basic Engineering, Vol. 89, No. 3, September 1967.

17. R. G. Forman, "Fatigue Flaw Growth Behavior of 2219-T87 Aluminum at Cryogenic, Room and Elevated Temperatures," NASA MSC, Materials Technology Branch Report 71-ES5-1, September 2, 1971

18. W. E. Witzell, "Crack Growth Behavior of 2219-T87 Aluminum Alloy from 20K (-423°F) to 422K (300°F)," NASA CR 134047, August 1973.

19. "Crack Growth Analysis for Arbitrary Spectrum Loading," Air Force Contract No. F33615-72-C-1744, Grumman Aerospace Corporation.

20. E. F. J. von Euw, R. W. Hertzberg and R. Roberts, "Delay Effects in Fatigue Crack Propagation," pp. 230-259, ASTM STP 513, 1972.

21. V. W. Trebules, Jr., R. Roberts and R. W. Hertzberg, "Effect of Multiple Overloads on Fatigue Crack Propagation in 2024-T3 Aluminum Alloy," pp. 115-146, ASTM STP 536, 1973.

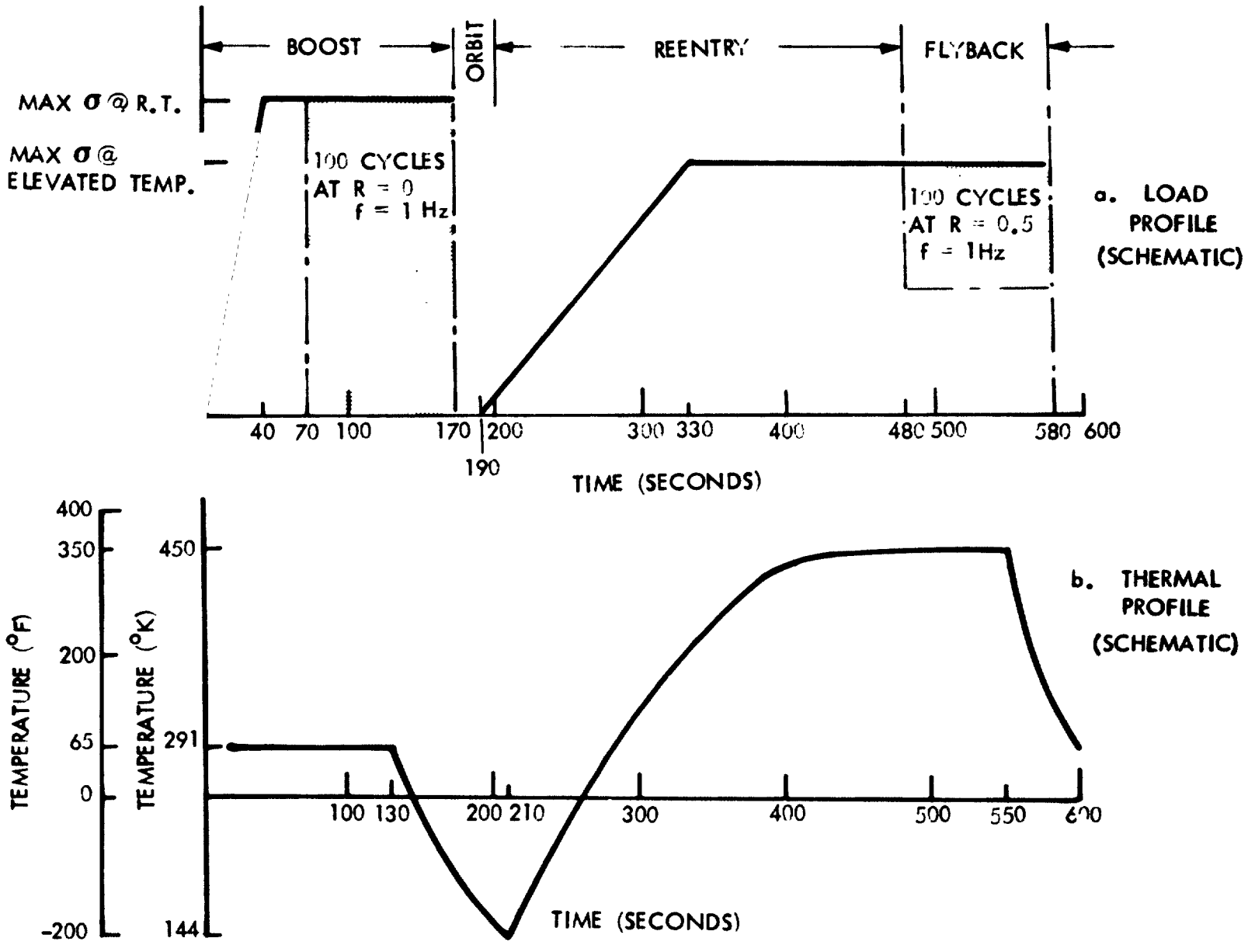


FIGURE 1: BASIC LOAD / THERMAL PROFILE SPECTRUM

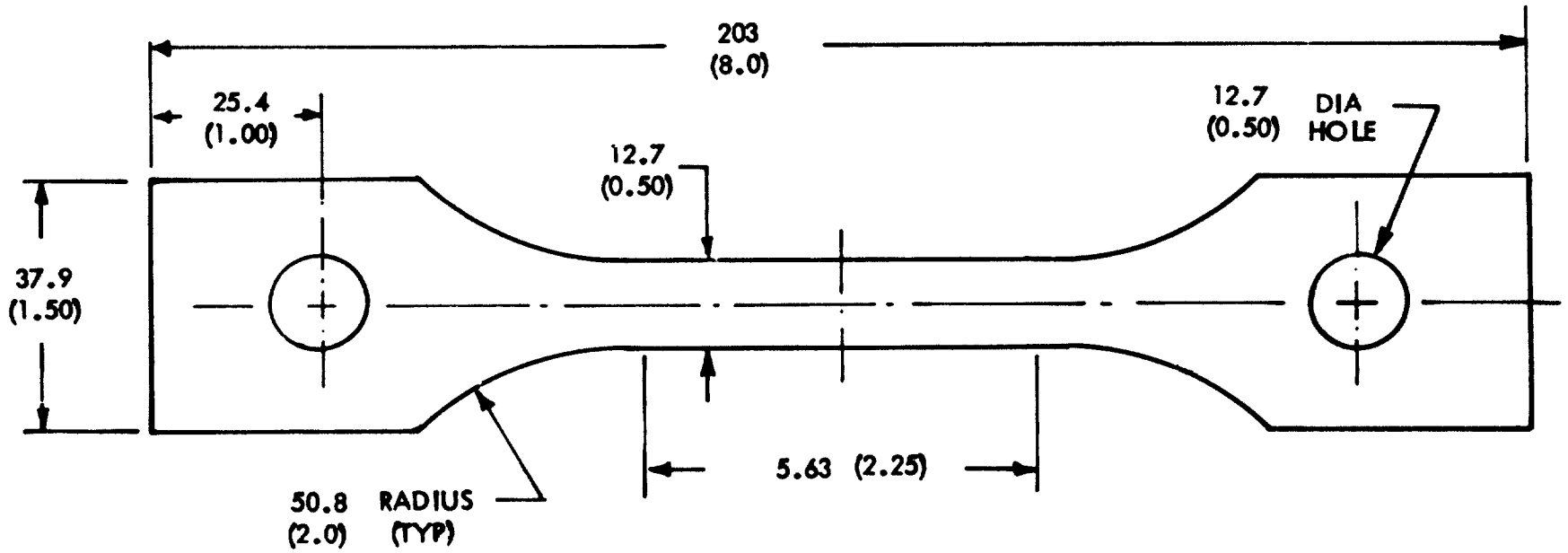


NOTE: DIMENSIONS GIVEN IN mm (INCHES)

FIGURE 2: TENSILE SPECIMEN CONFIGURATION

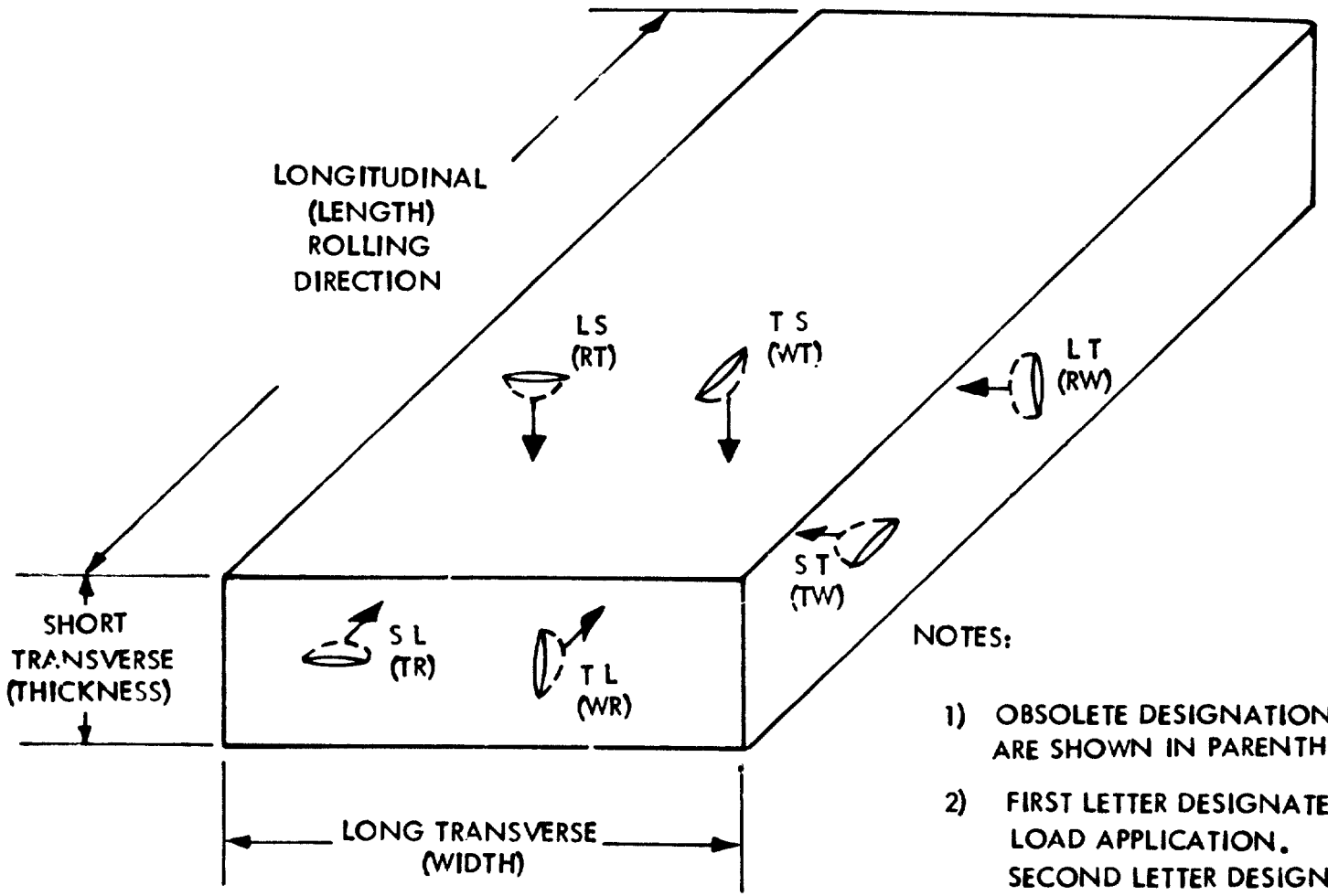


NOTES:

1) OBSOLETE DESIGNATIONS ARE SHOWN IN PARENTHESES.

2) FIRST LETTER DESIGNATES LOAD APPLICATION. SECOND LETTER DESIGNATES CRACK PROPAGATION DIRECTION.

FIGURE 3: CRACK PROPAGATION DIRECTIONS

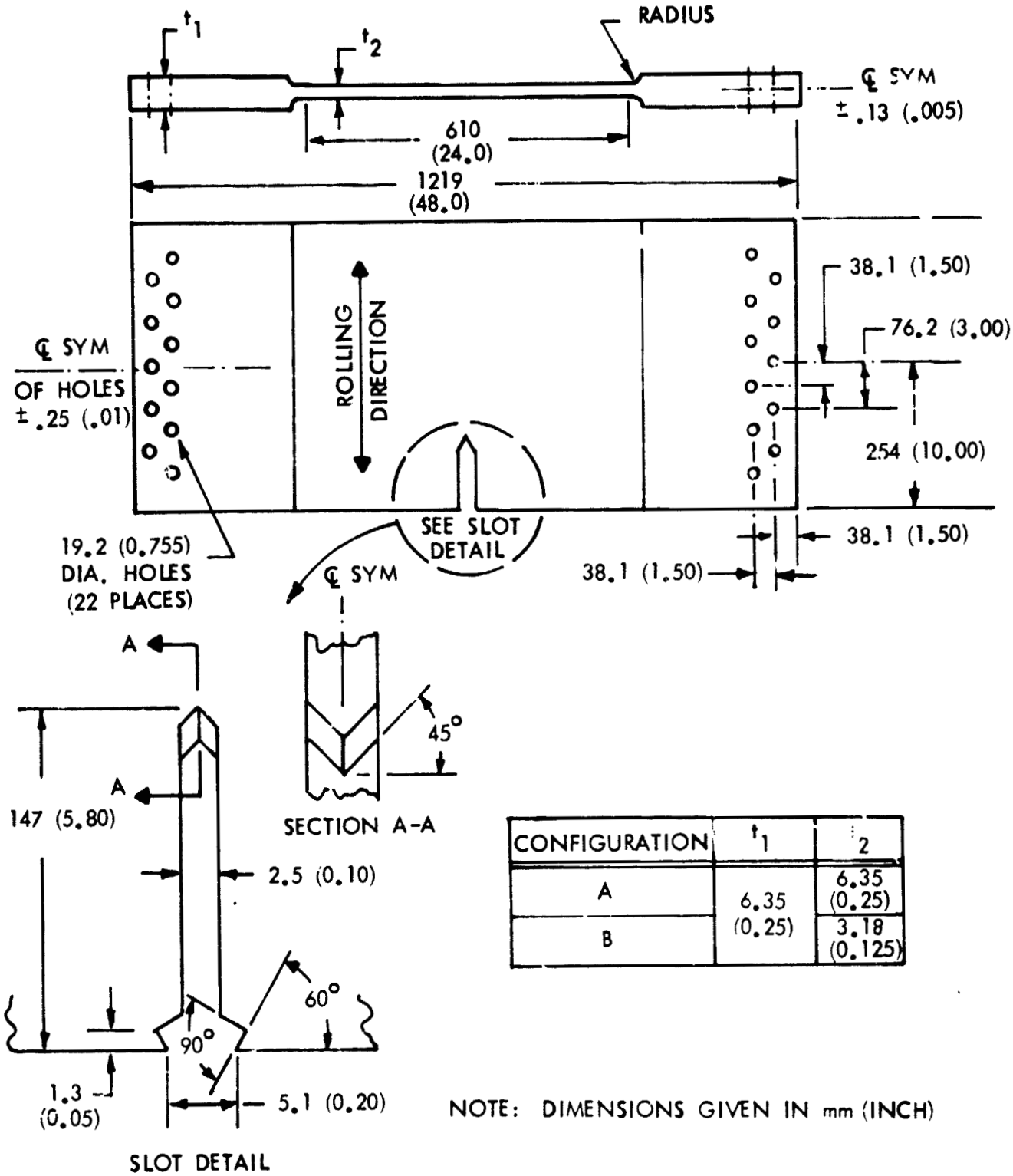


| CONFIGURATION | $t_1$ | $t_2$ |
|---|---|---|
| A | 6.35 (0.25) | 6.35 (0.25) |
| B | | 3.18 (0.125) |

FIGURE 4: 450K (+350F) SENT FRACTURE SPECIMENS

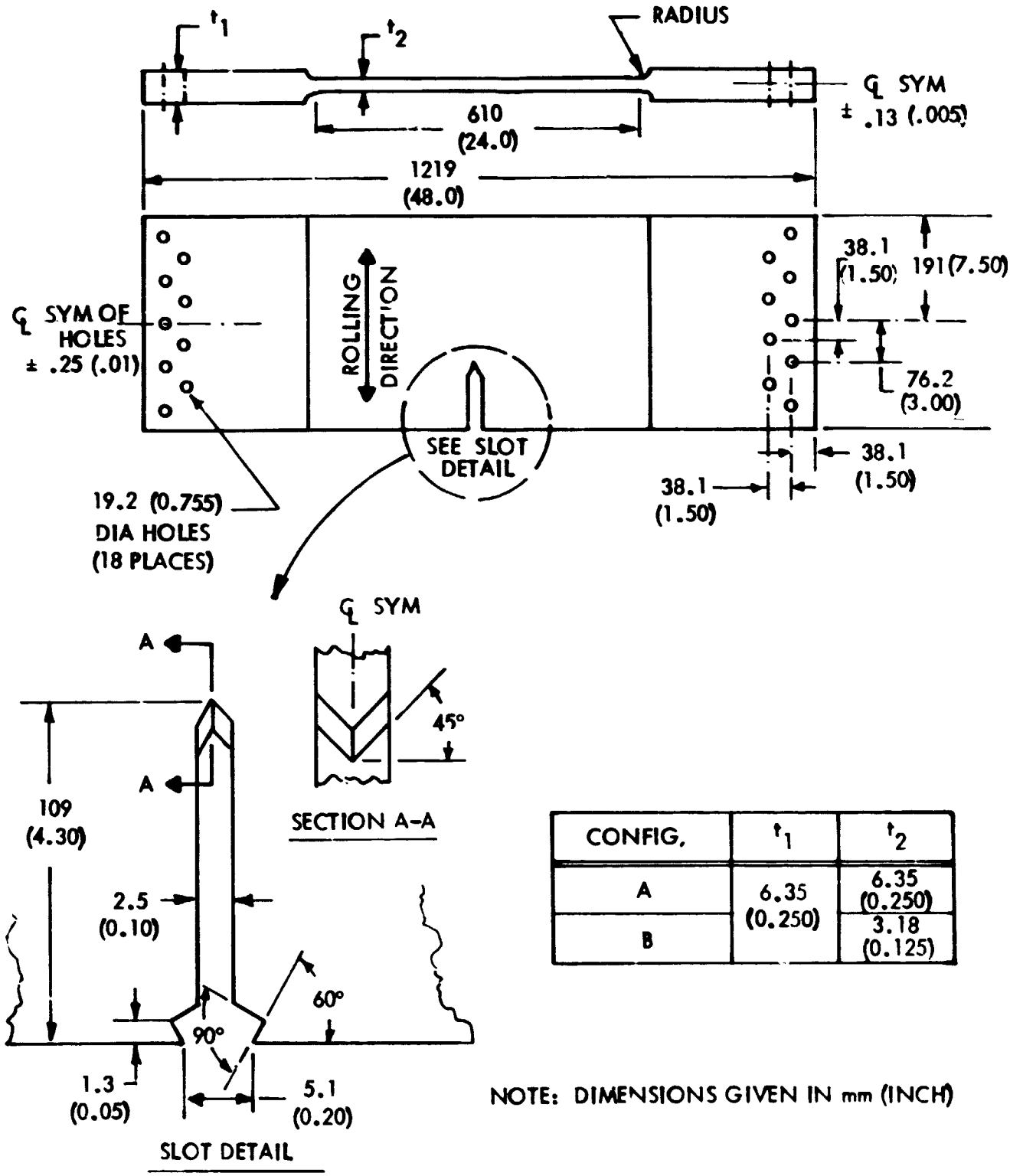


| CONFIG. | $t_1$ | $t_2$ |
|---|---|---|
| A | 6.35 (0.250) | 6.35 (0.250) |
| B | | 3.18 (0.125) |

NOTE: DIMENSIONS GIVEN IN mm (INCH)

FIGURE 5: ROOM TEMPERATURE SENT FRACTURE SPECIMENS

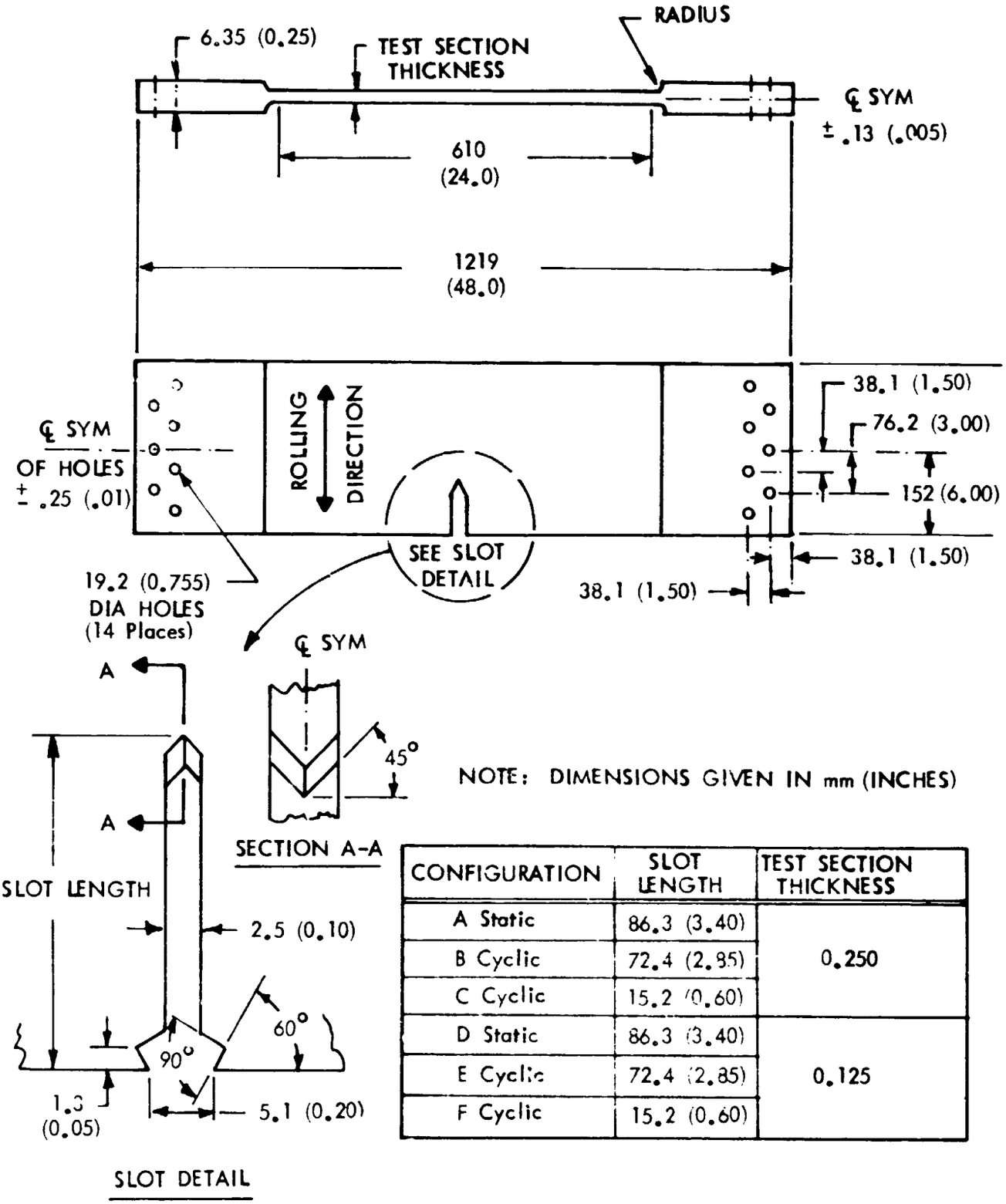


NOTE: DIMENSIONS GIVEN IN mm (INCHES)

| CONFIGURATION | SLOT LENGTH | TEST SECTION THICKNESS |
|---|---|---|
| A Static | 86.3 (3.40) | 0.250 |
| B Cyclic | 72.4 (2.85) | |
| C Cyclic | 15.2 (0.60) | |
| D Static | 86.3 (3.40) | 0.125 |
| E Cyclic | 72.4 (2.85) | |
| F Cyclic | 15.2 (0.60) | |

FIGURE 6: 144K (-200F) SENT FRACTURE SPECIMENS AND 450°K (350°F) AND RT CYCLIC SPECIMENS

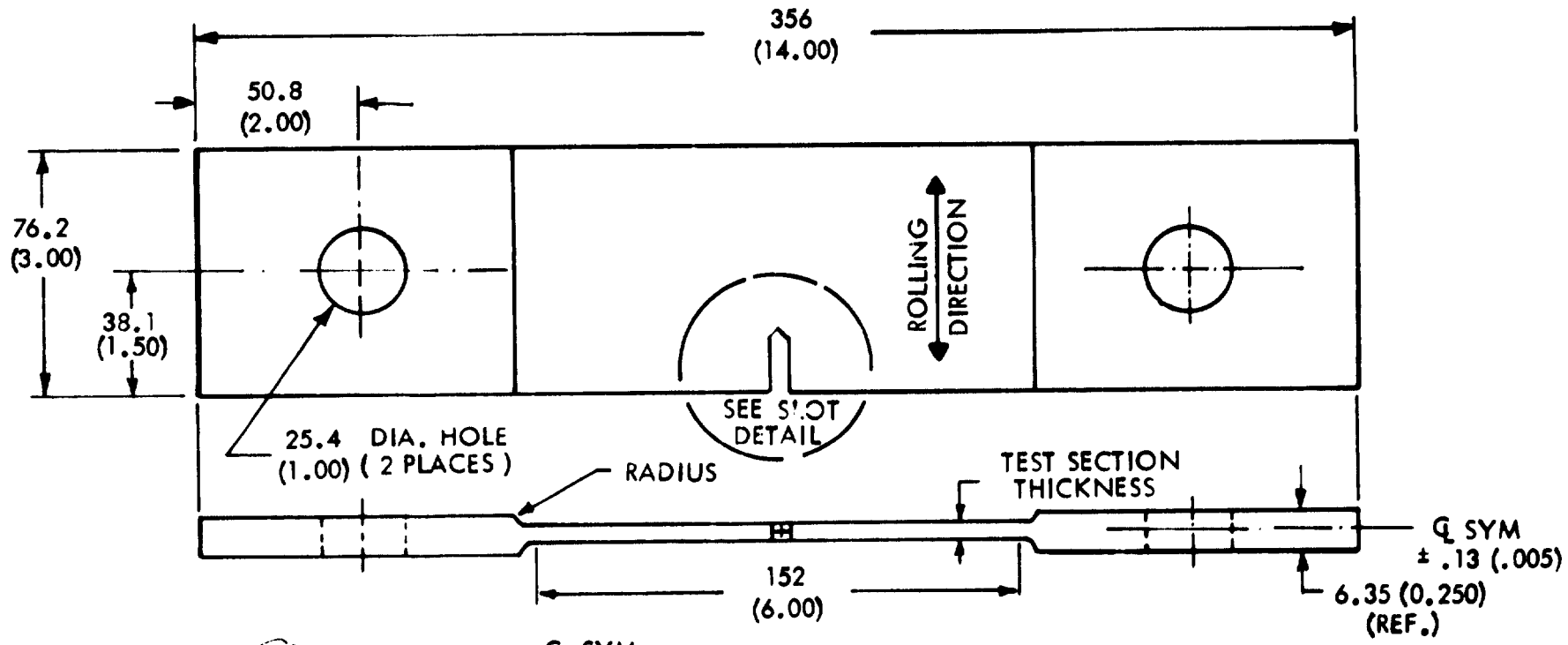


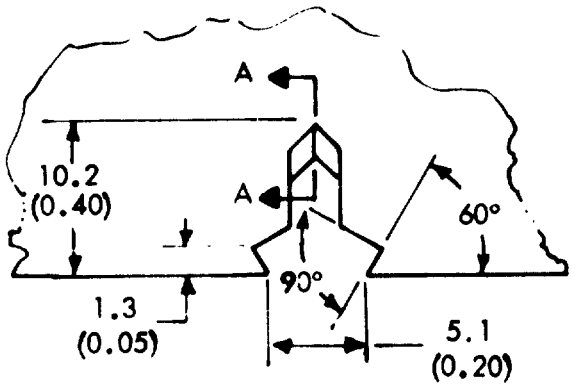


SLOT DETAIL

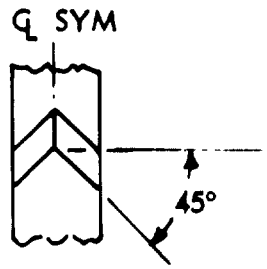


SECTION A - A

| CONFIGURATION | TEST SECTION THICKNESS |
|---|---|
| A | 6.35 (0.250) |
| B | 3.18 (0.125) |

NOTE: DIMENSIONS GIVEN IN mm (INCHES)

FIGURE 7: SENT CYCLIC SPECIMENS

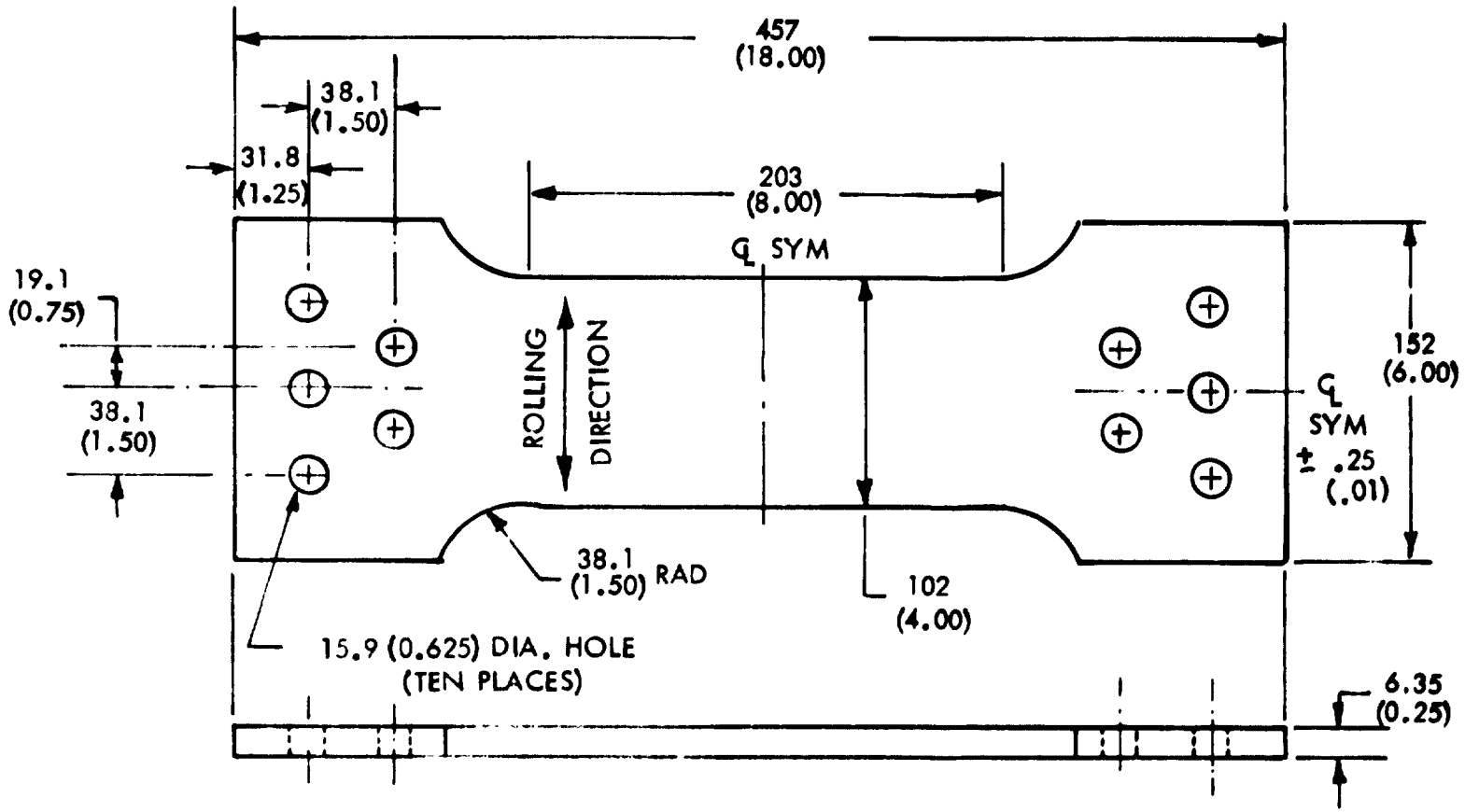


NOTE: DIMENSIONS GIVEN IN mm (INCHES)

FIGURE 8: 6.35 mm (0.250 INCH) SURFACE FLAW SPECIMEN

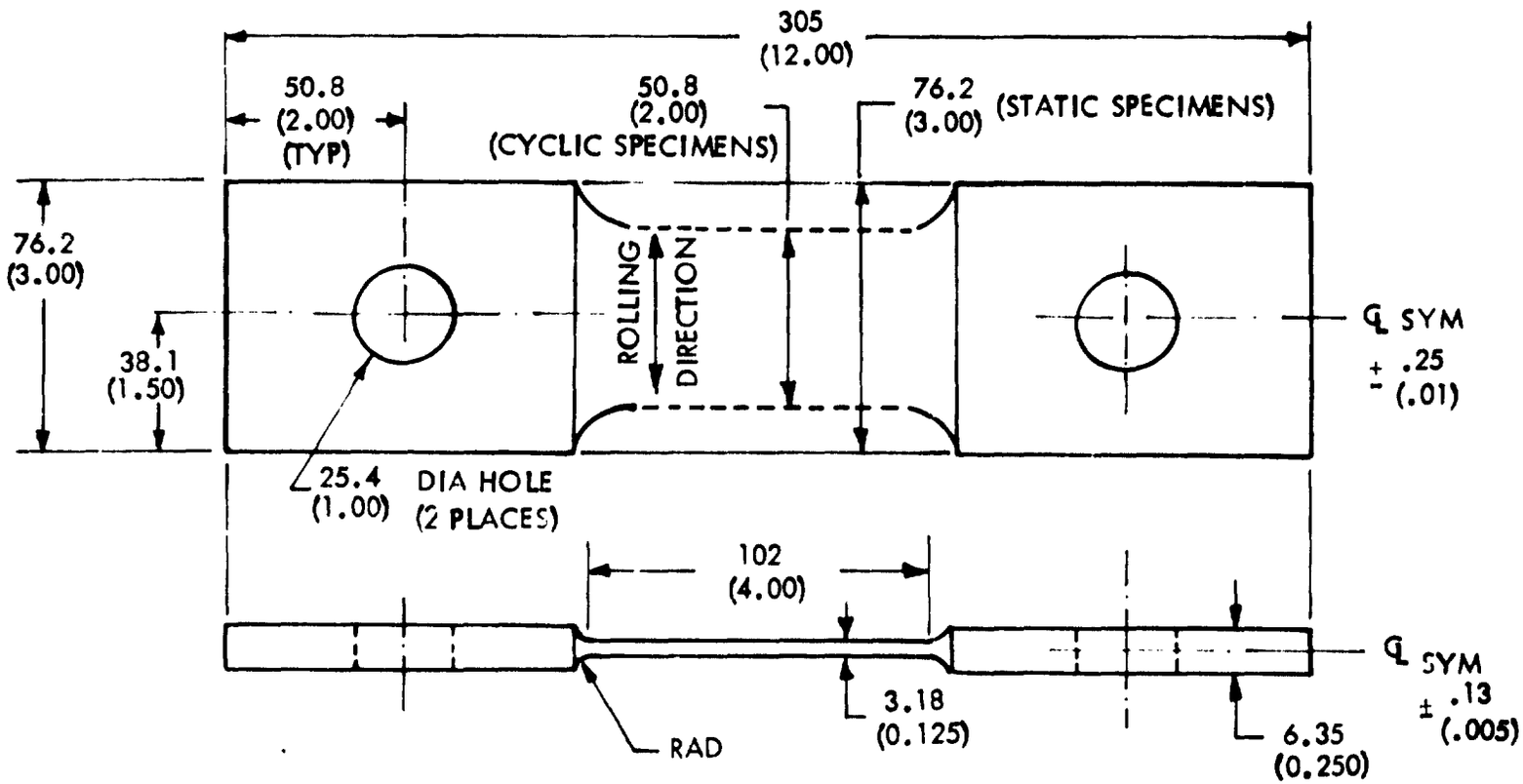


NOTE: DIMENSIONS GIVEN IN mm (INCHES)

FIGURE 9: 3.18 mm (0.125 INCH) SURFACE FLAW SPECIMEN

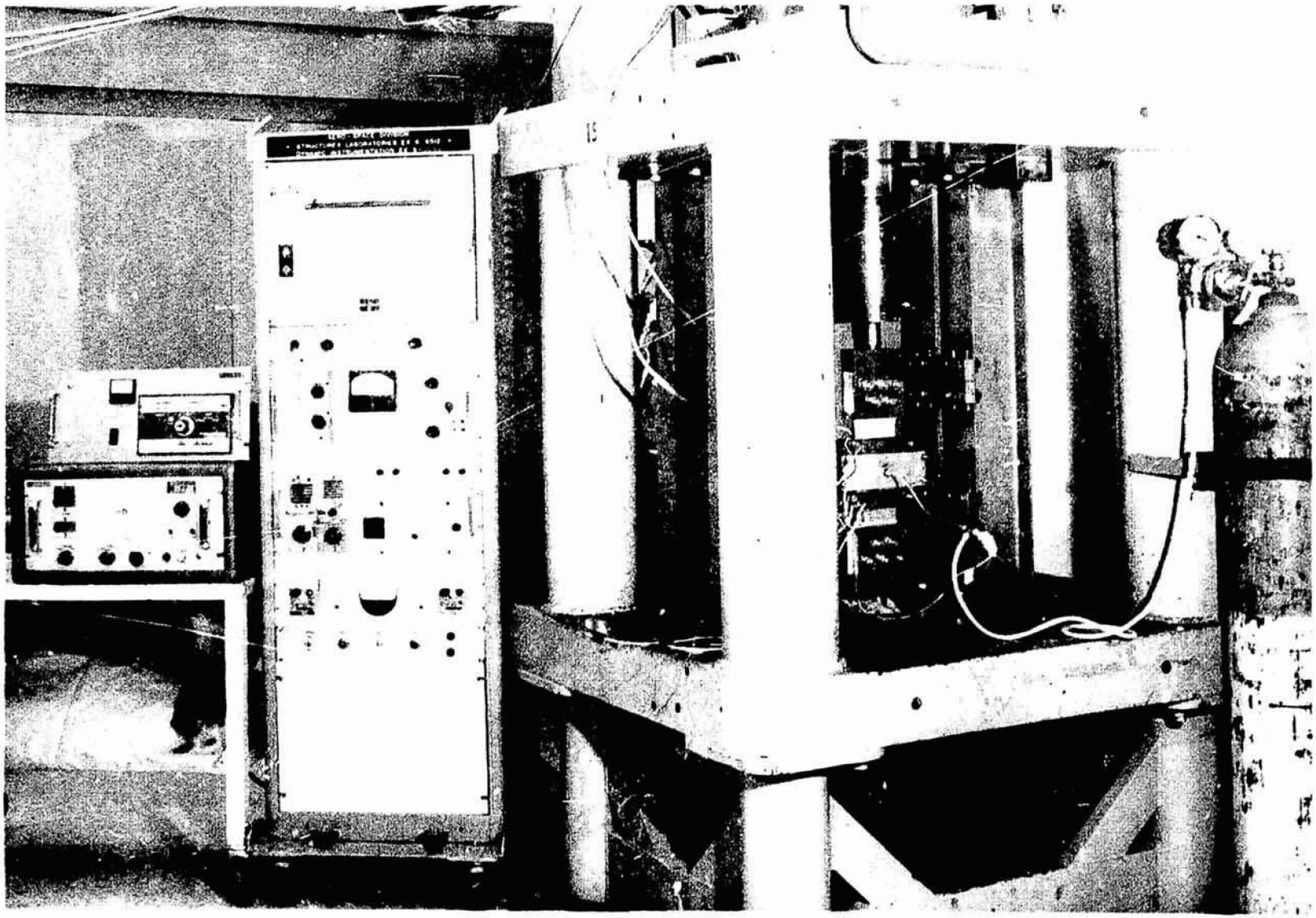

FIGURE 10: SURFACE FLAW SPECIMEN INSTALLED IN TEST MACHINE

ORIGINAL PAGE IS
OF POOR QUALITY

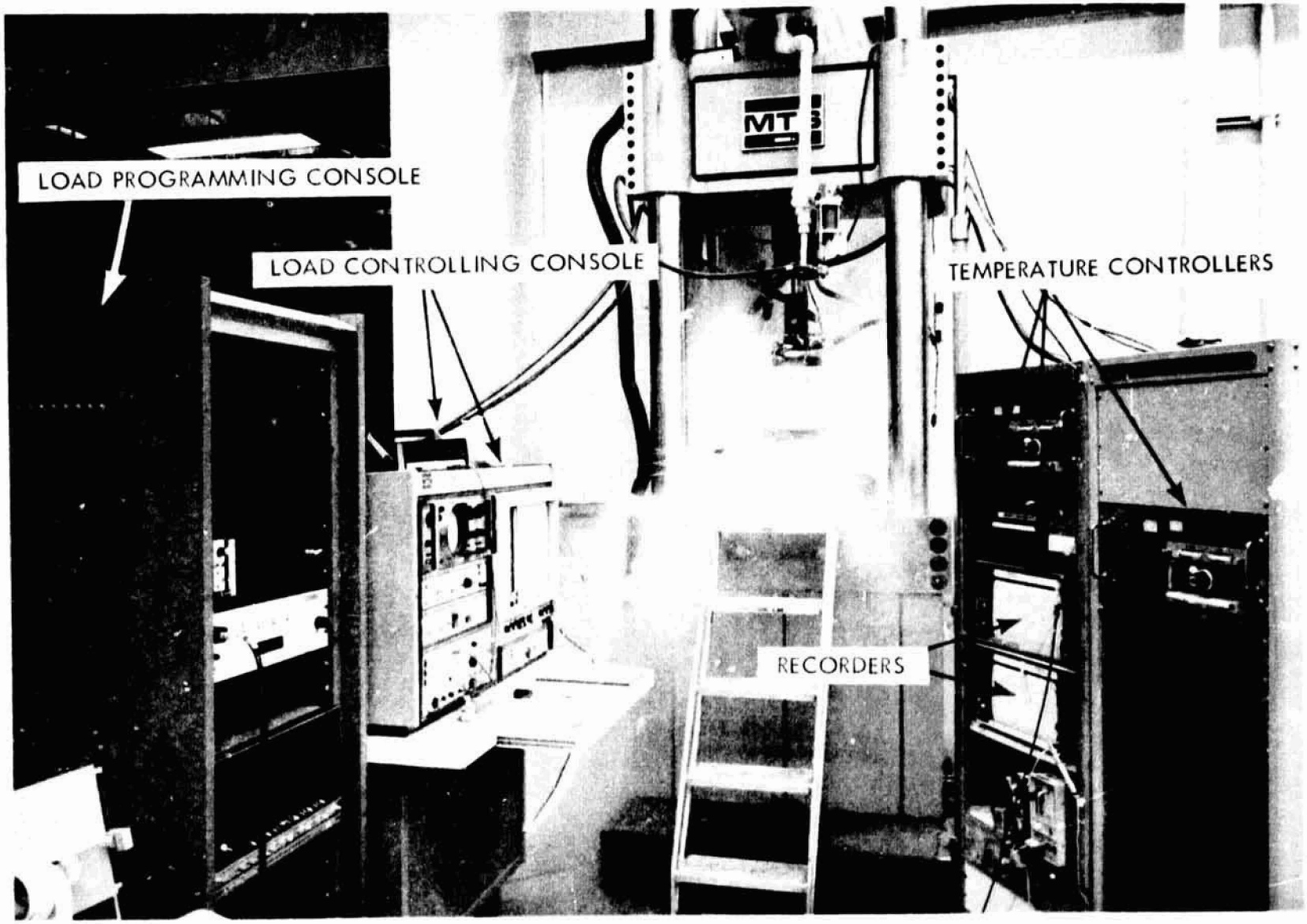


FIGURE 11: SENT SPECIMEN SUBJECTED TO THERMAL PROFILE LOADING

ORIGINAL PAGE IS
OF POOR QUALITY

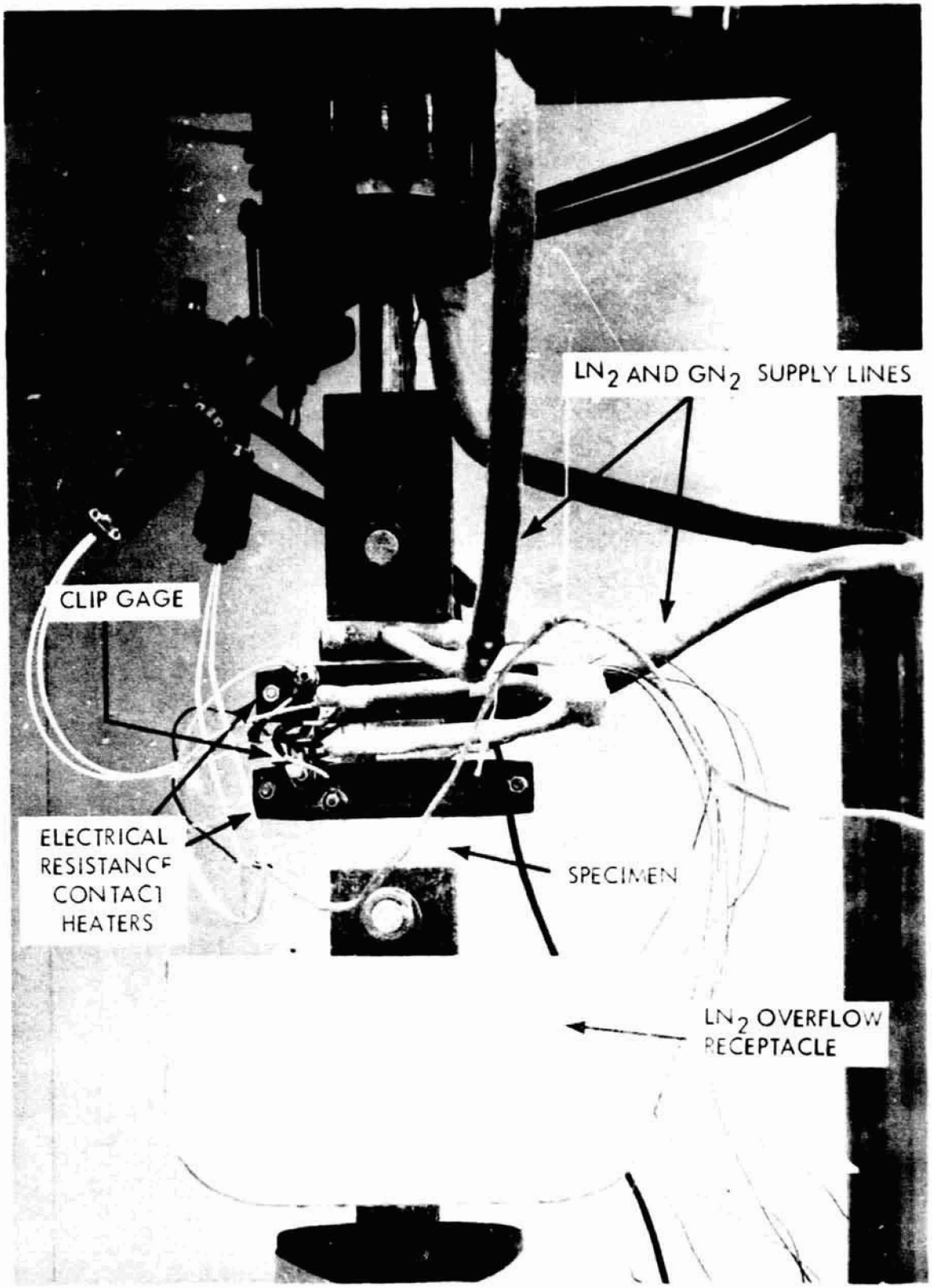


FIGURE 12: SENT THERMAL PROFILE TEST SETUP

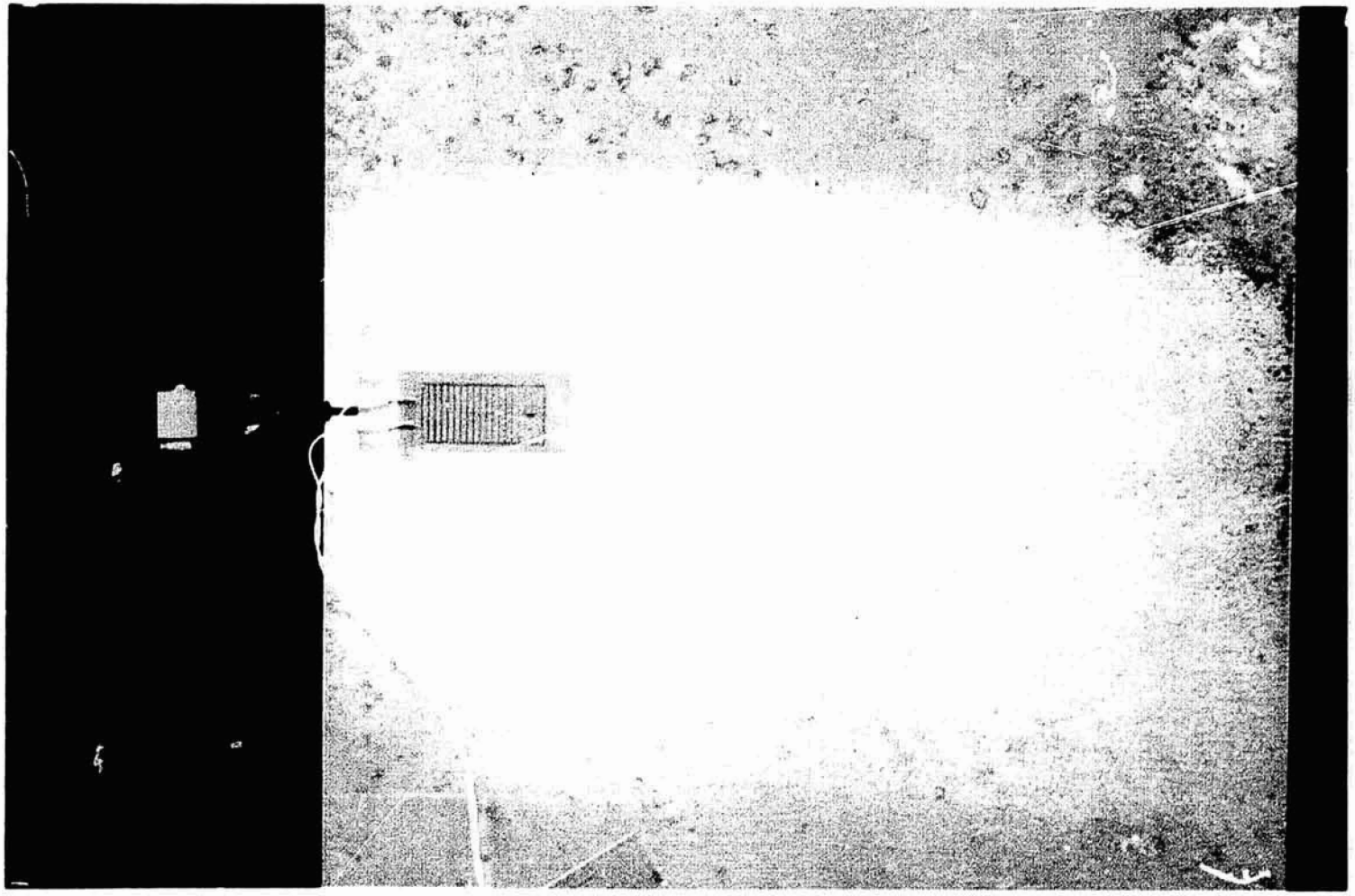

FIGURE 13: CRACK PROPAGATION GAGE AND CRACK OPENING DISPLACEMENT CLIP GAGE INSTALLED ON SENT SPECIMEN

ORIGINAL PAGE IS
OF POOR QUALITY

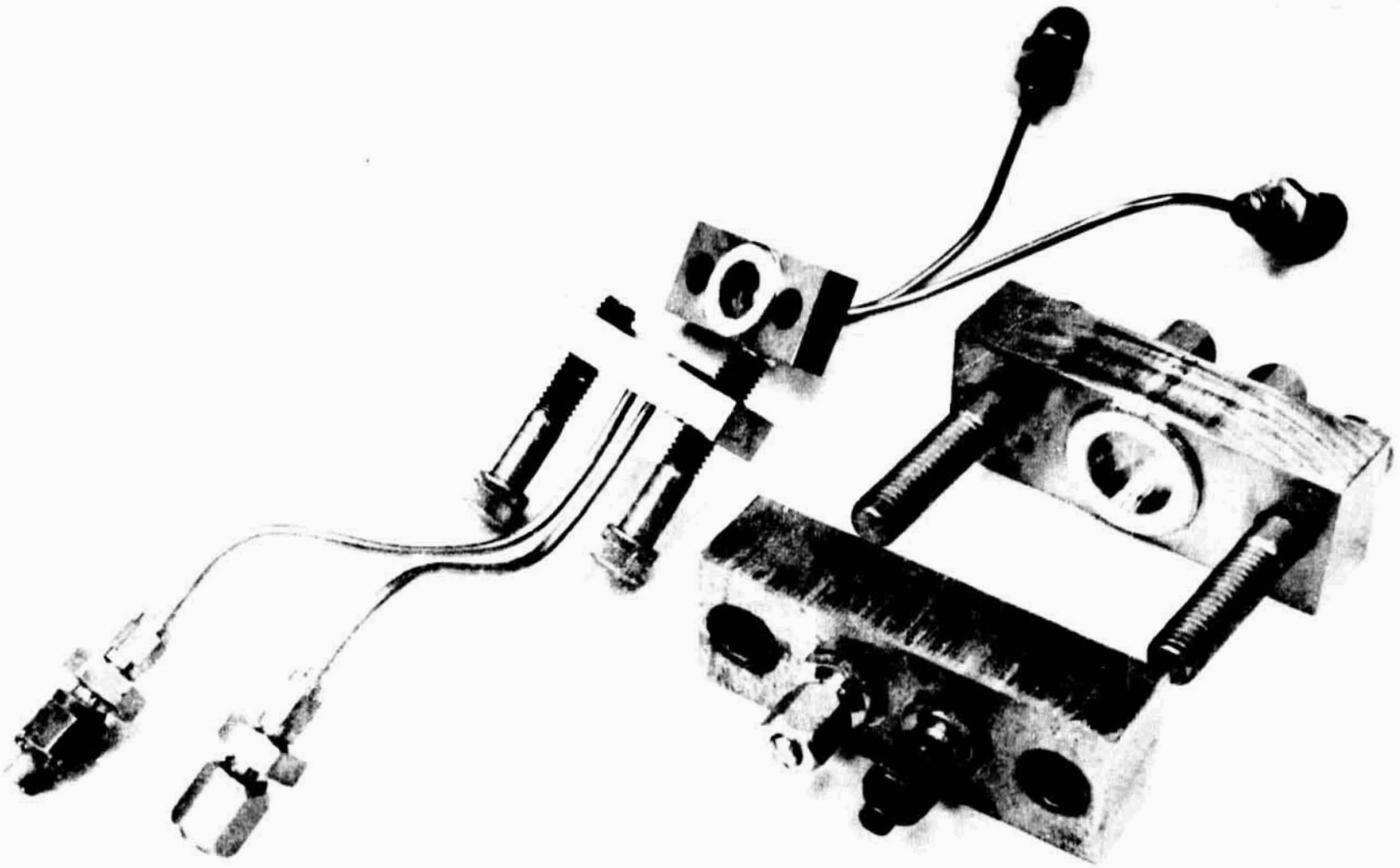

FIGURE 14: EXAMPLES OF PRESSURE CUPS USED TO DETECT FLAW BREAKTHROUGH ON SURFACE FLAW TESTS

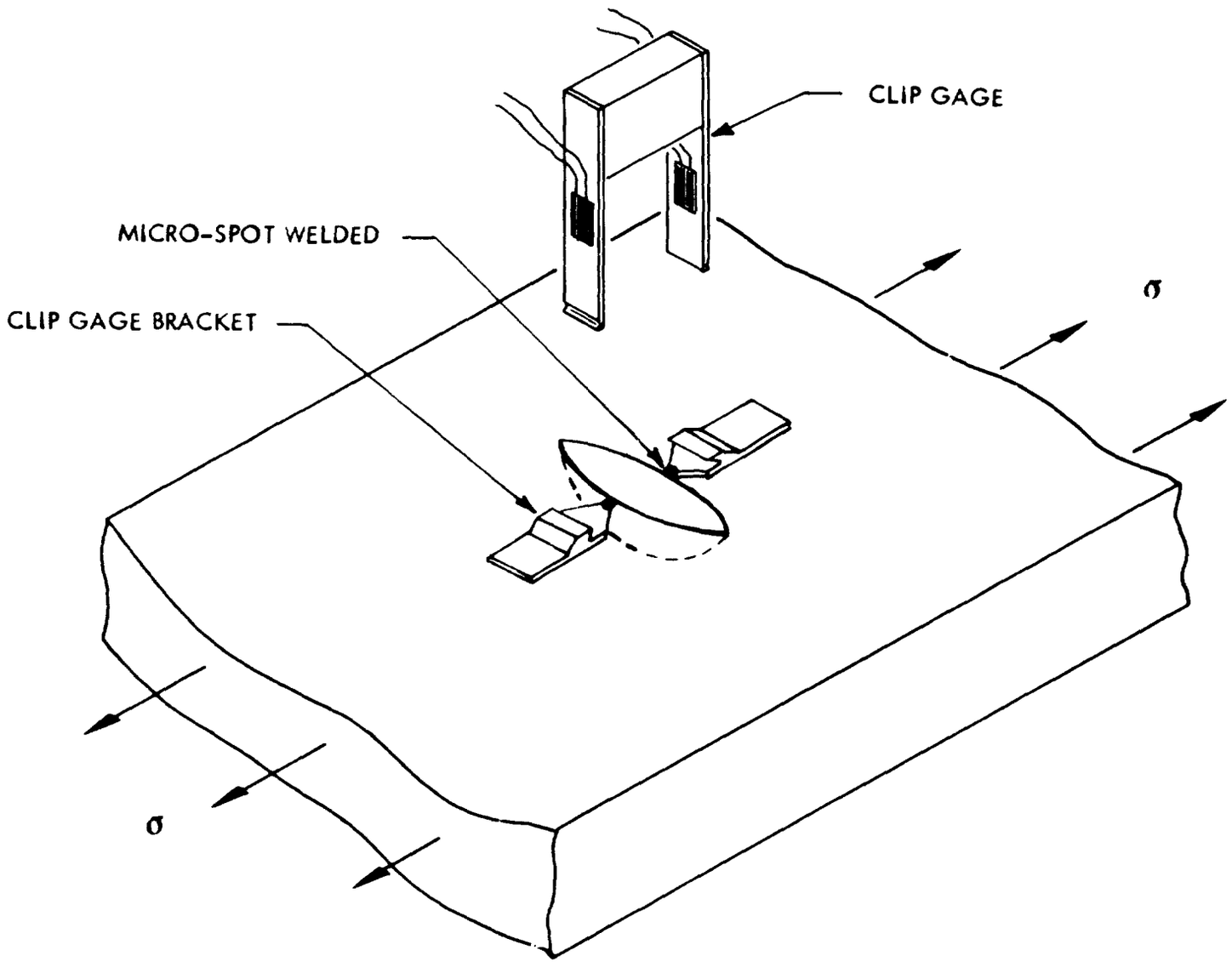


FIGURE 15: FLAW OPENING MEASUREMENT OF SURFACE FLAWED SPECIMENS

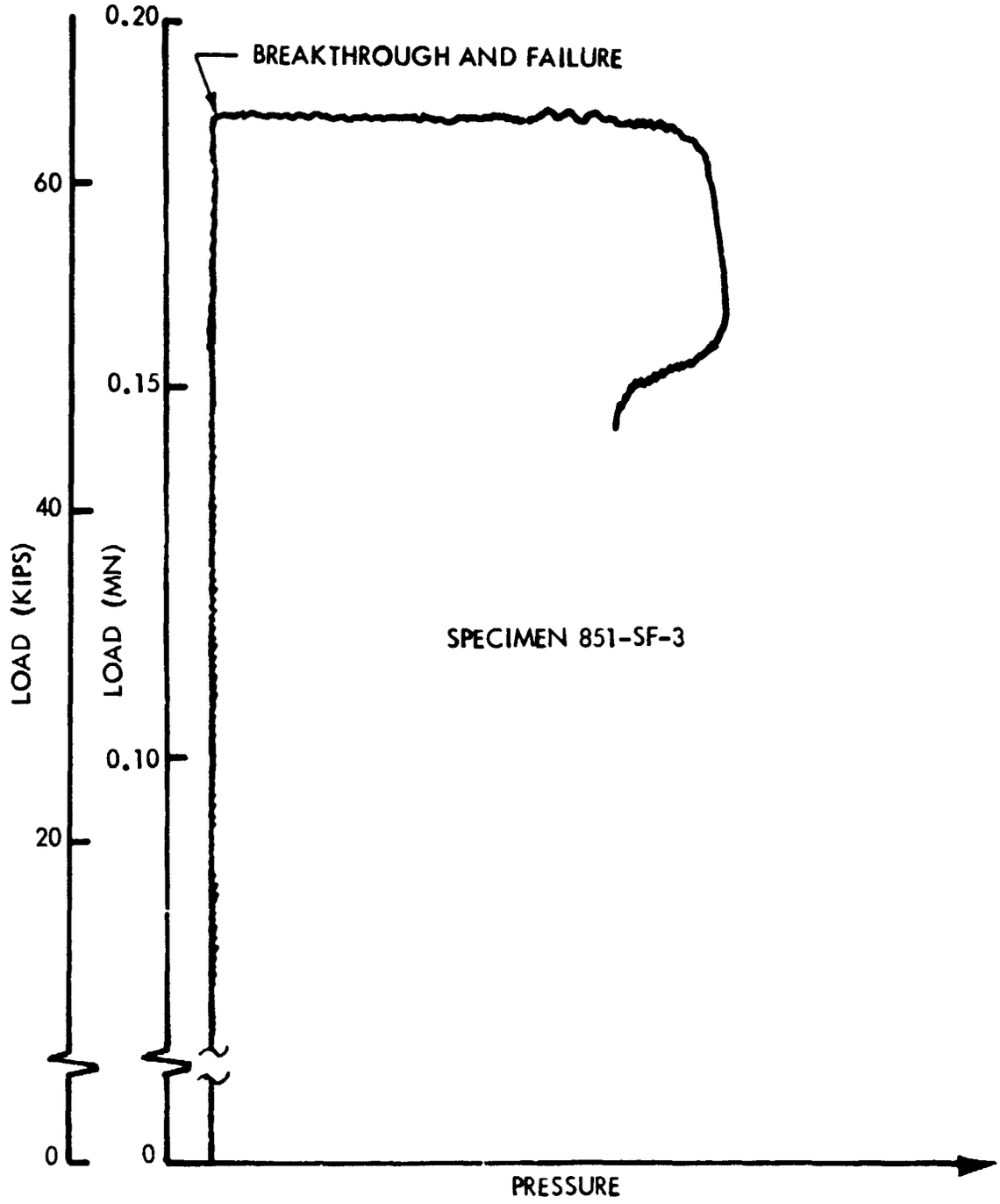


FIGURE 16: LOAD VS. PRESSURE, SPECIMEN 851-SF-3

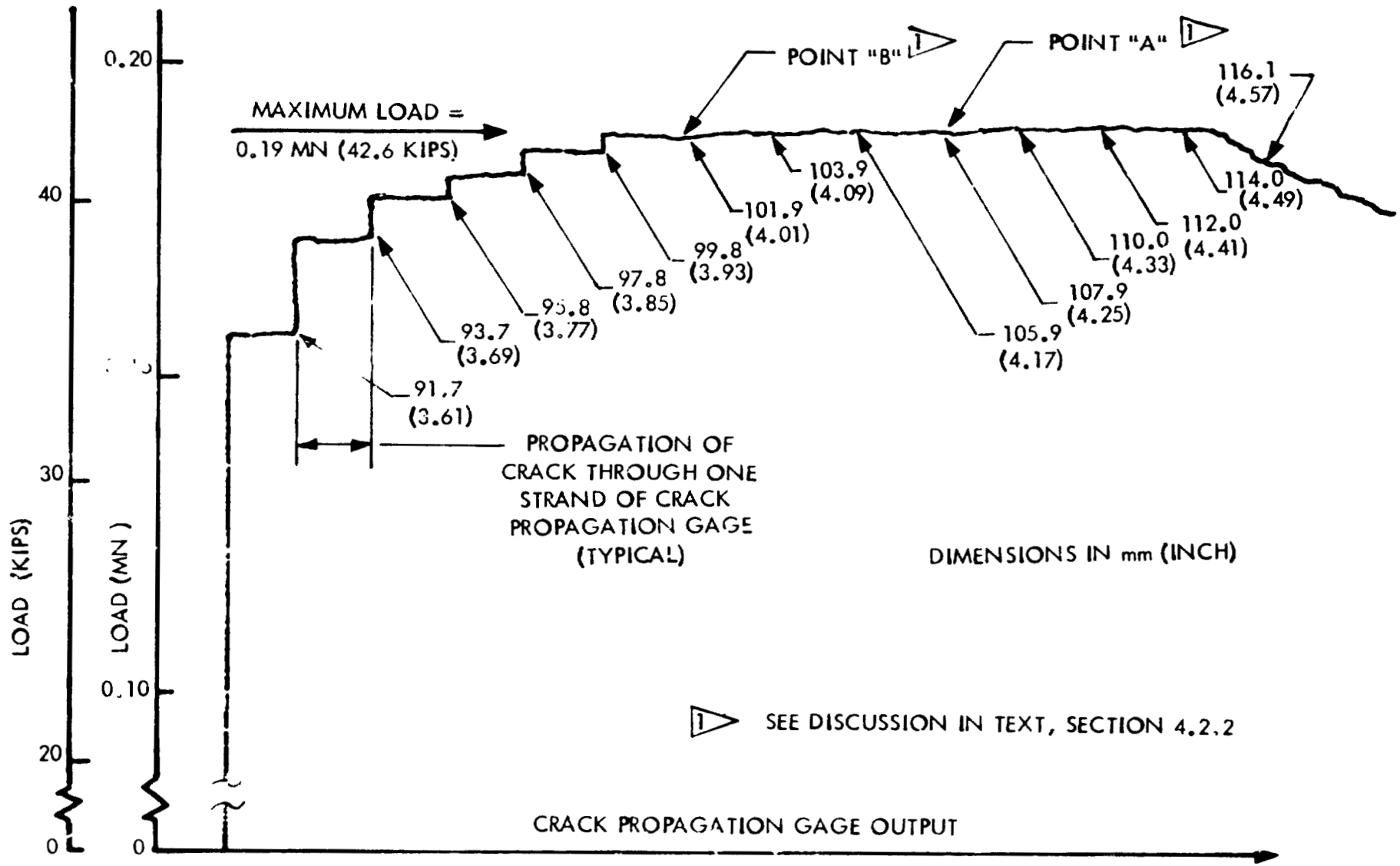


FIGURE 17: LOAD VS. CRACK PROPAGATION GAGE OUTPUT FOR SPECIMEN 87-2

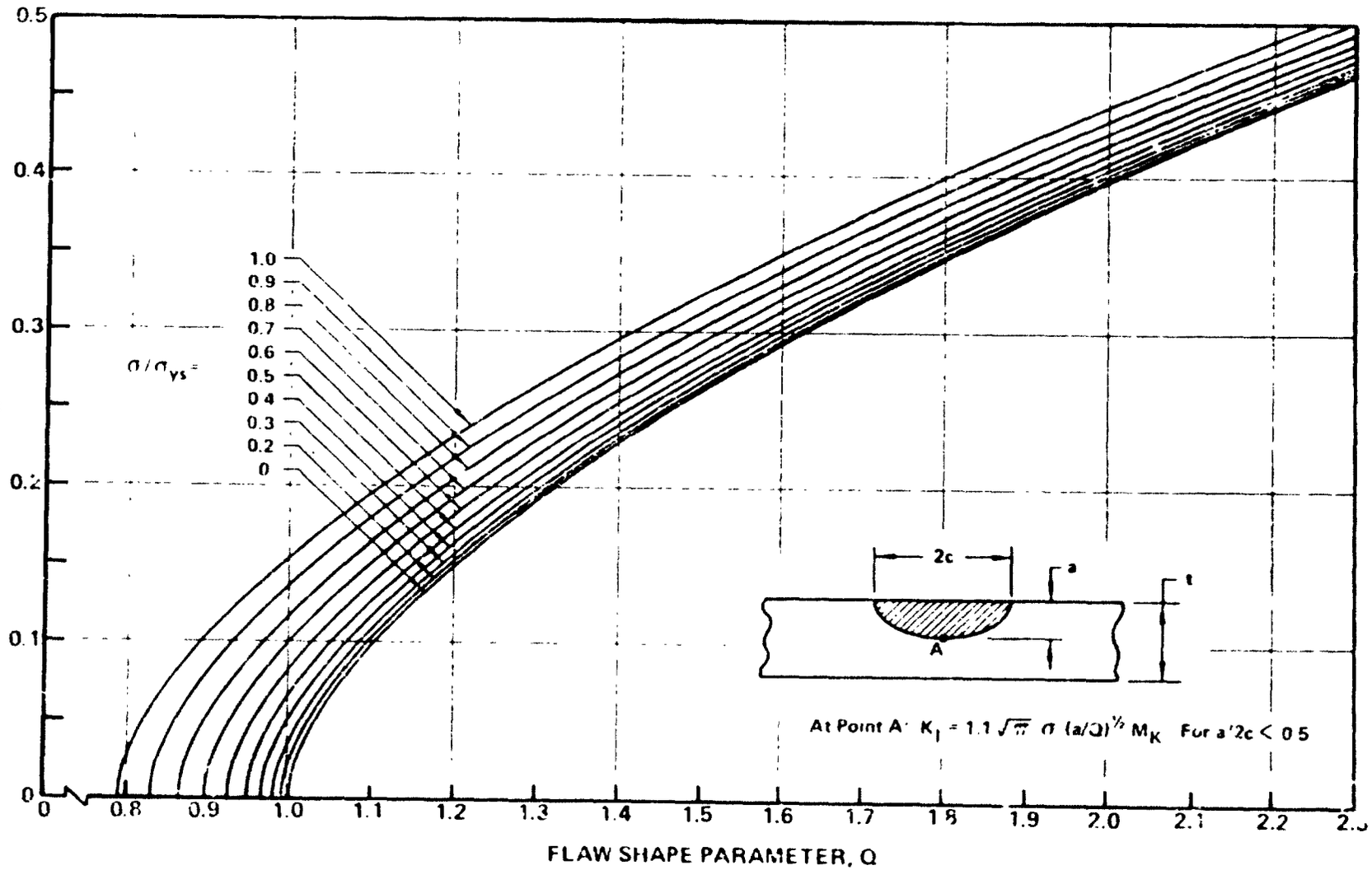


**FIGURE 18: SHAPE PARAMETER CURVES FOR SURFACE AND INTERNAL FLAWS**

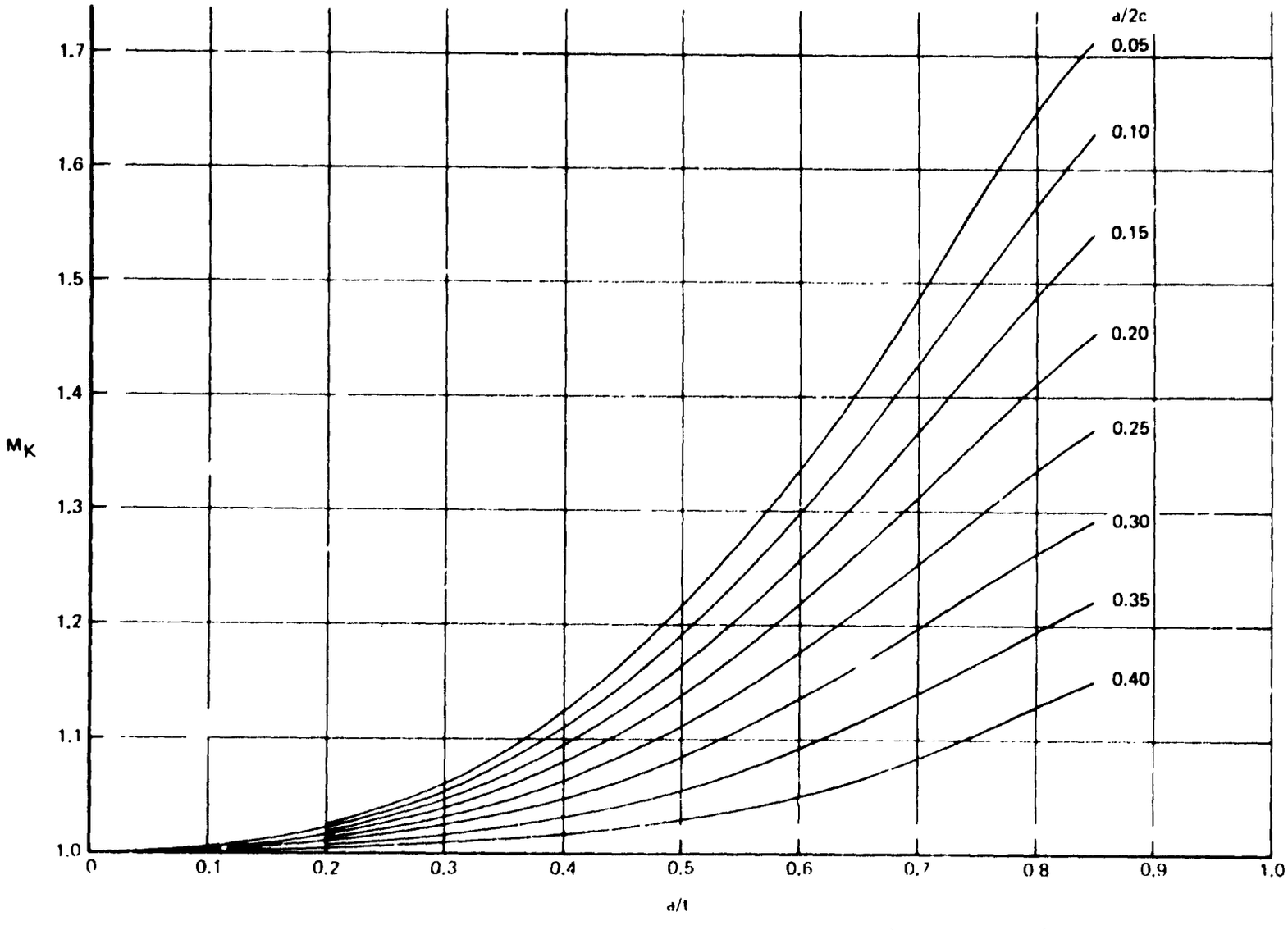


FIGURE 19: DEEP FLAW MAGNIFICATION CURVES (REFERENCE 2)

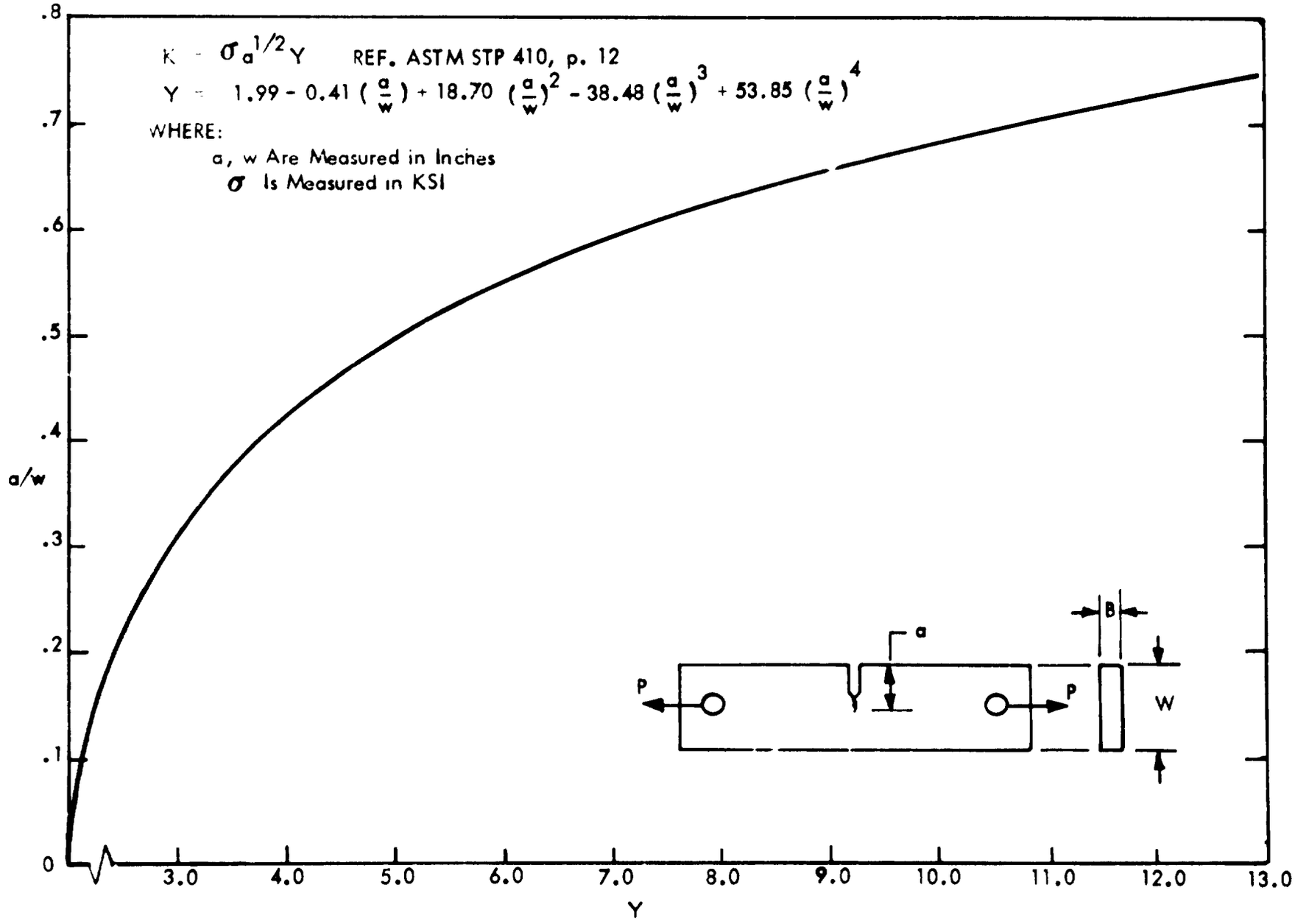


FIGURE 20: Y VS. a/w FOR SINGLE EDGE NOTCH SPECIMENS

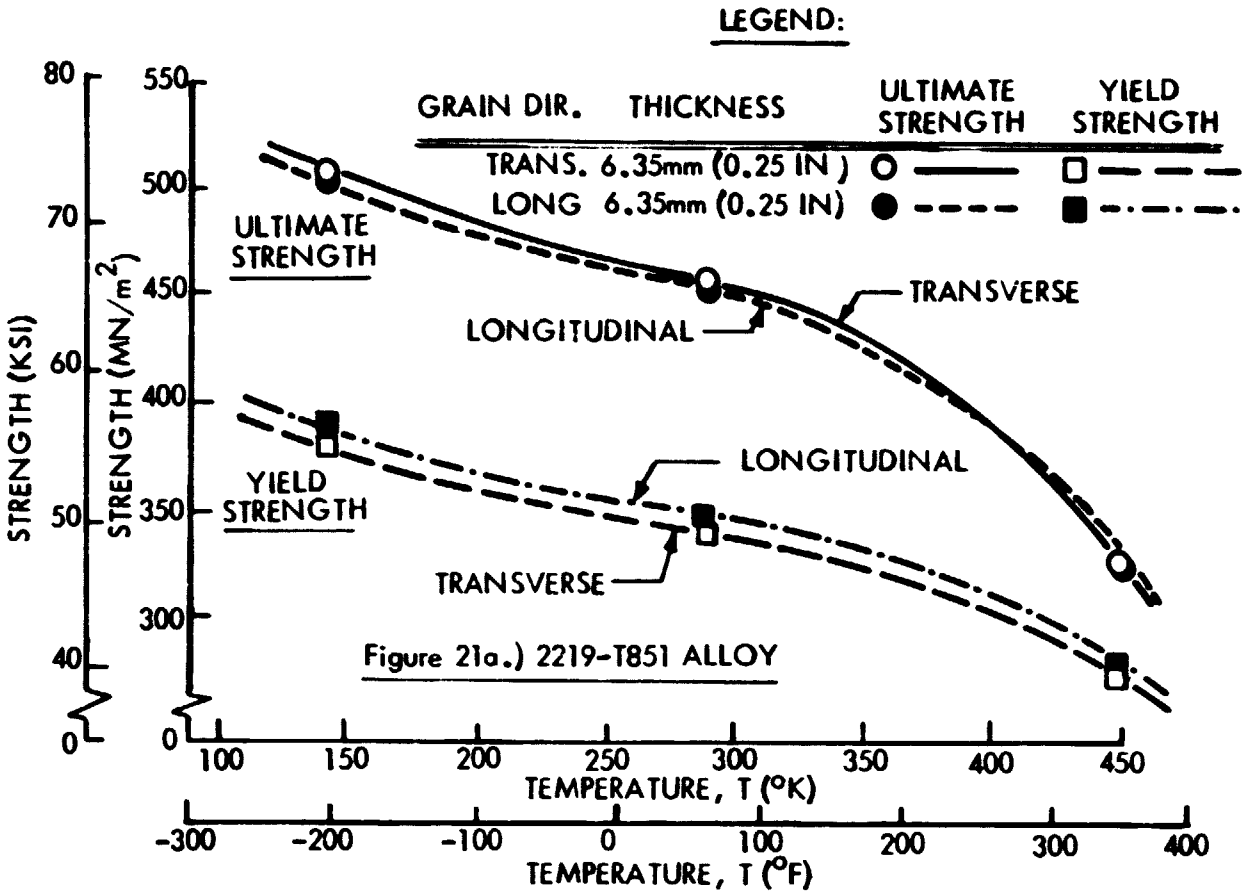


Figure 21a.) 2219-T851 ALLOY

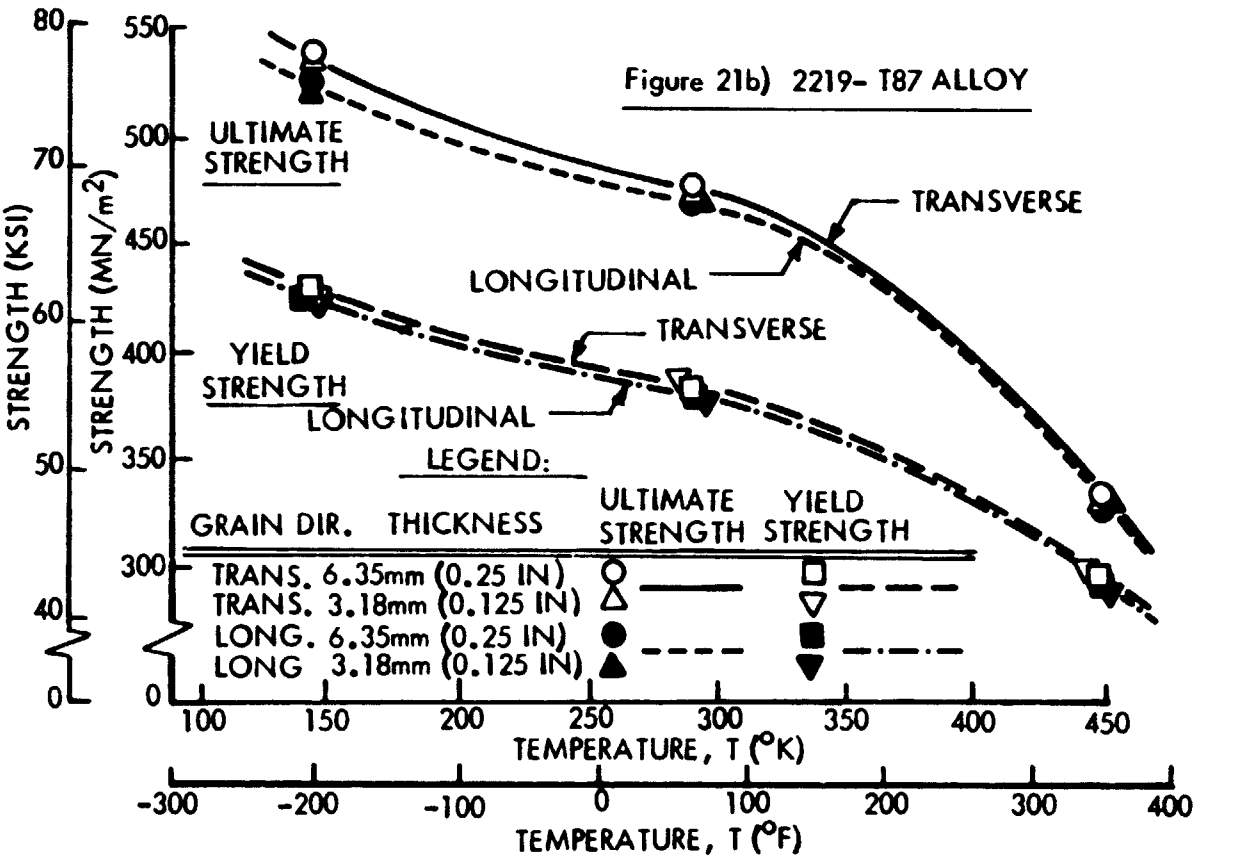


Figure 21b) 2219- T87 ALLOY

Figure 21: PLOT OF VARIATION OF STRENGTH WITH TEMPERATURE, 2219-T851 AND 2219-T87 ALUMINUM ALLOYS (AVERAGE VALUES PLOTTED)

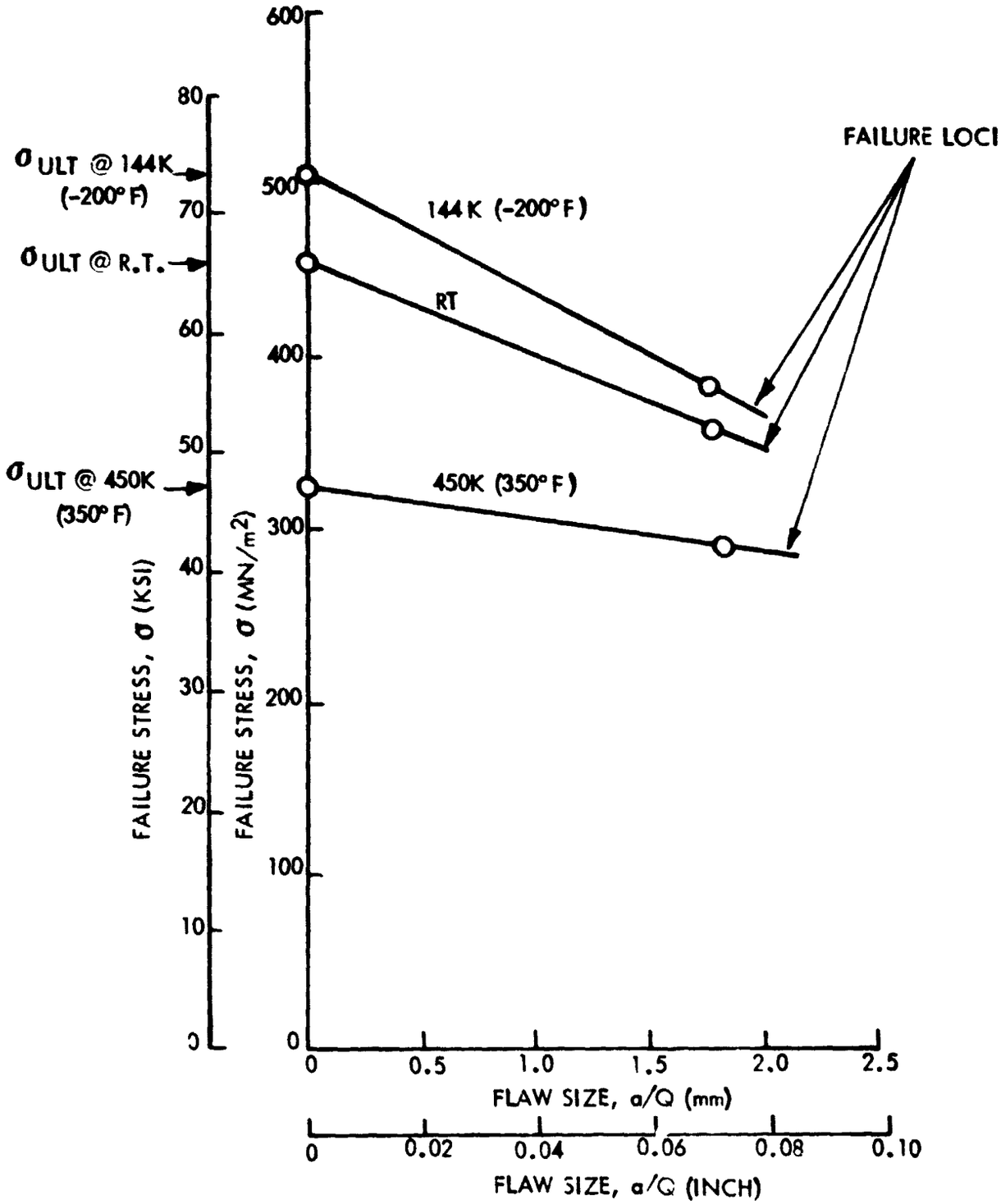


FIGURE 22: PLOT OF FAILURE STRESS VS. FLAW SIZE FOR 6.35 mm (0.250 INCH) 2219-T851 SURFACE FLAW STATIC FRACTURE TESTS, TS PROPAGATION DIRECTION

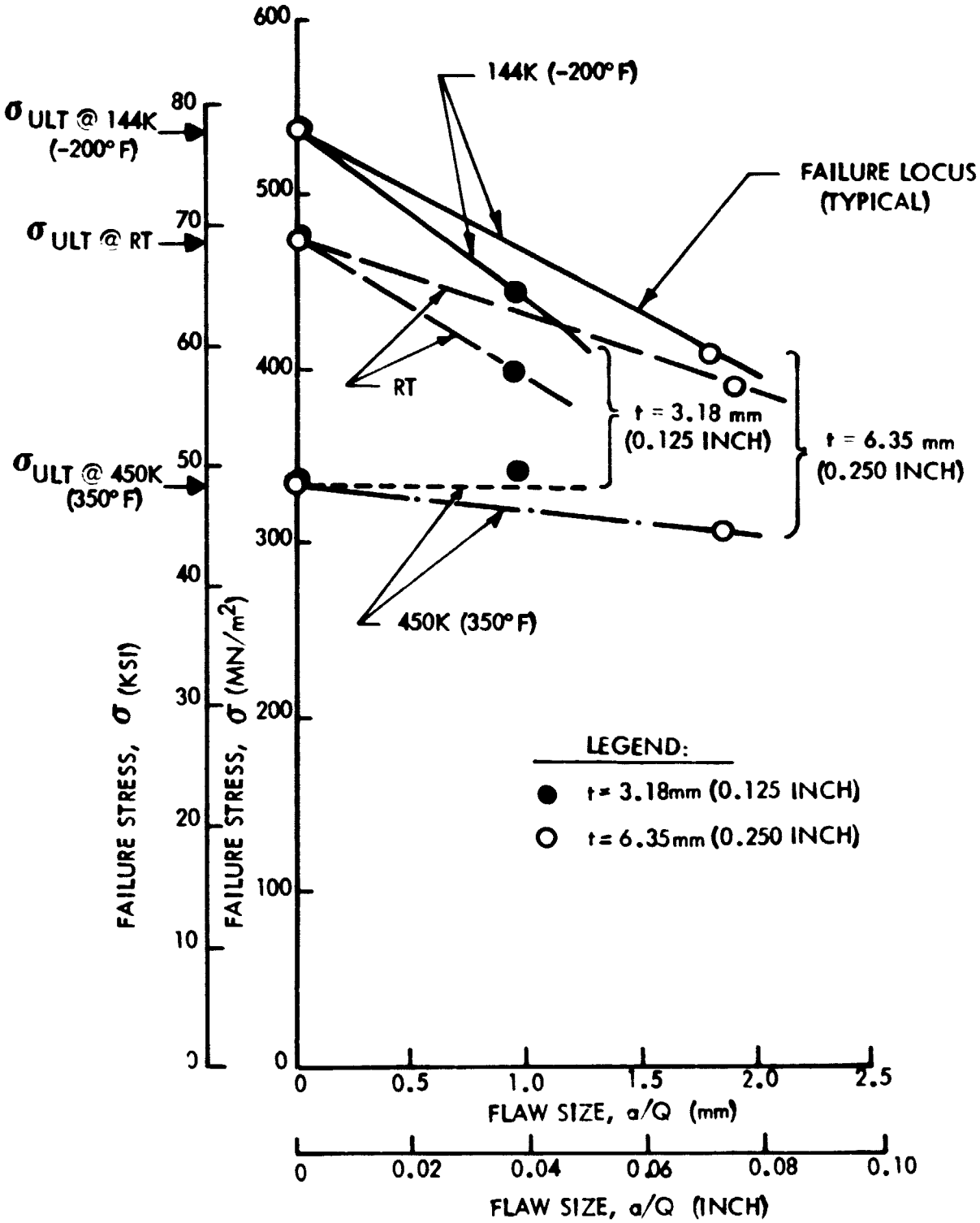


FIGURE 23: PLOT OF FAILURE STRESS VS. FLAW SIZE FOR 6.35mm (0.250 INCH) AND 3.18 mm (0.125 INCH) 2219-T87 SURFACE FLAW STATIC FRACTURE TESTS, TS PROPAGATION DIRECTION

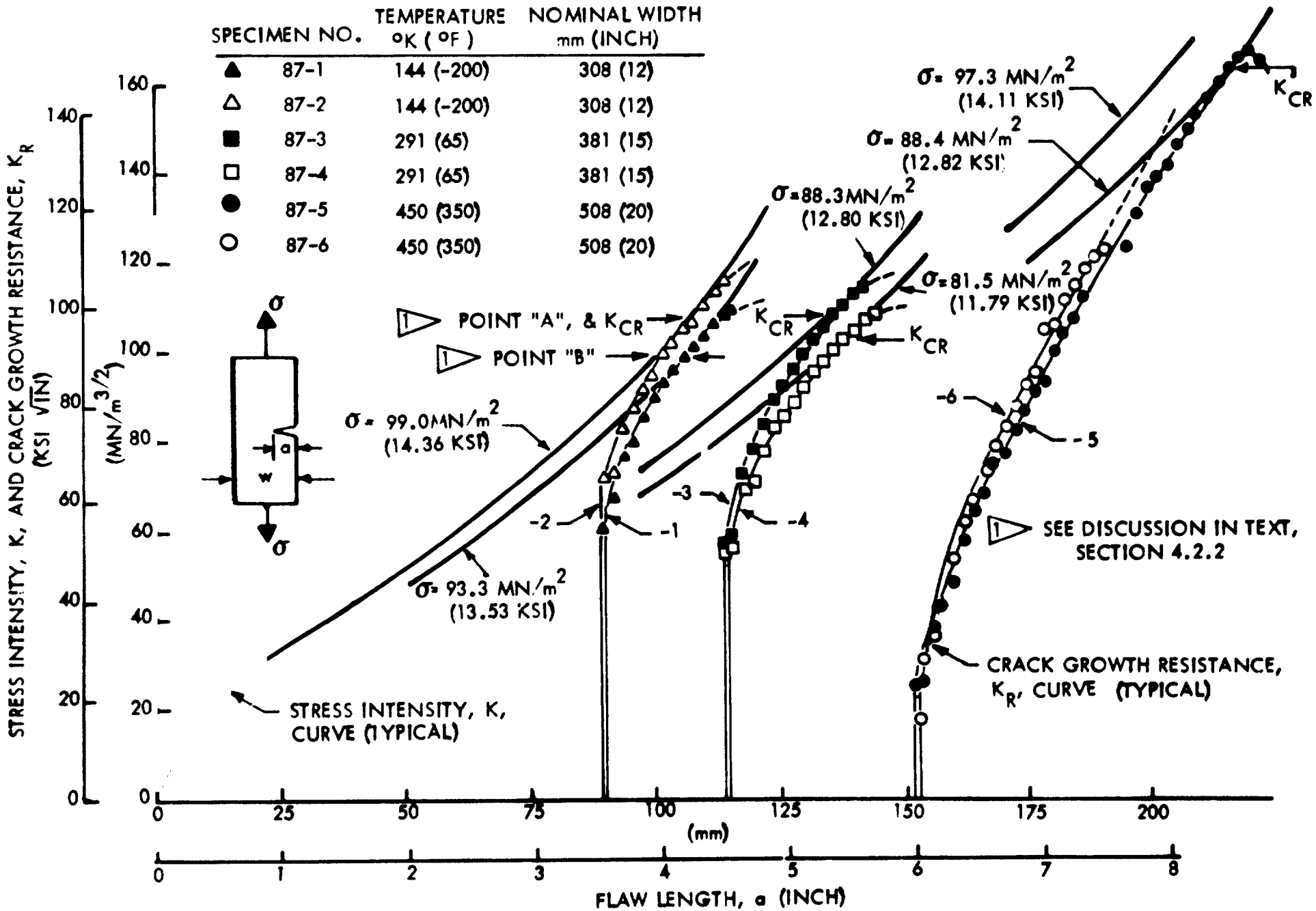


FIGURE 24: PLOT OF STRESS INTENSITY AND CRACK GROWTH RESISTANCE VS. FLAW LENGTH, 2219-T87 ALLOY, 6.35 mm (0.25 INCH)

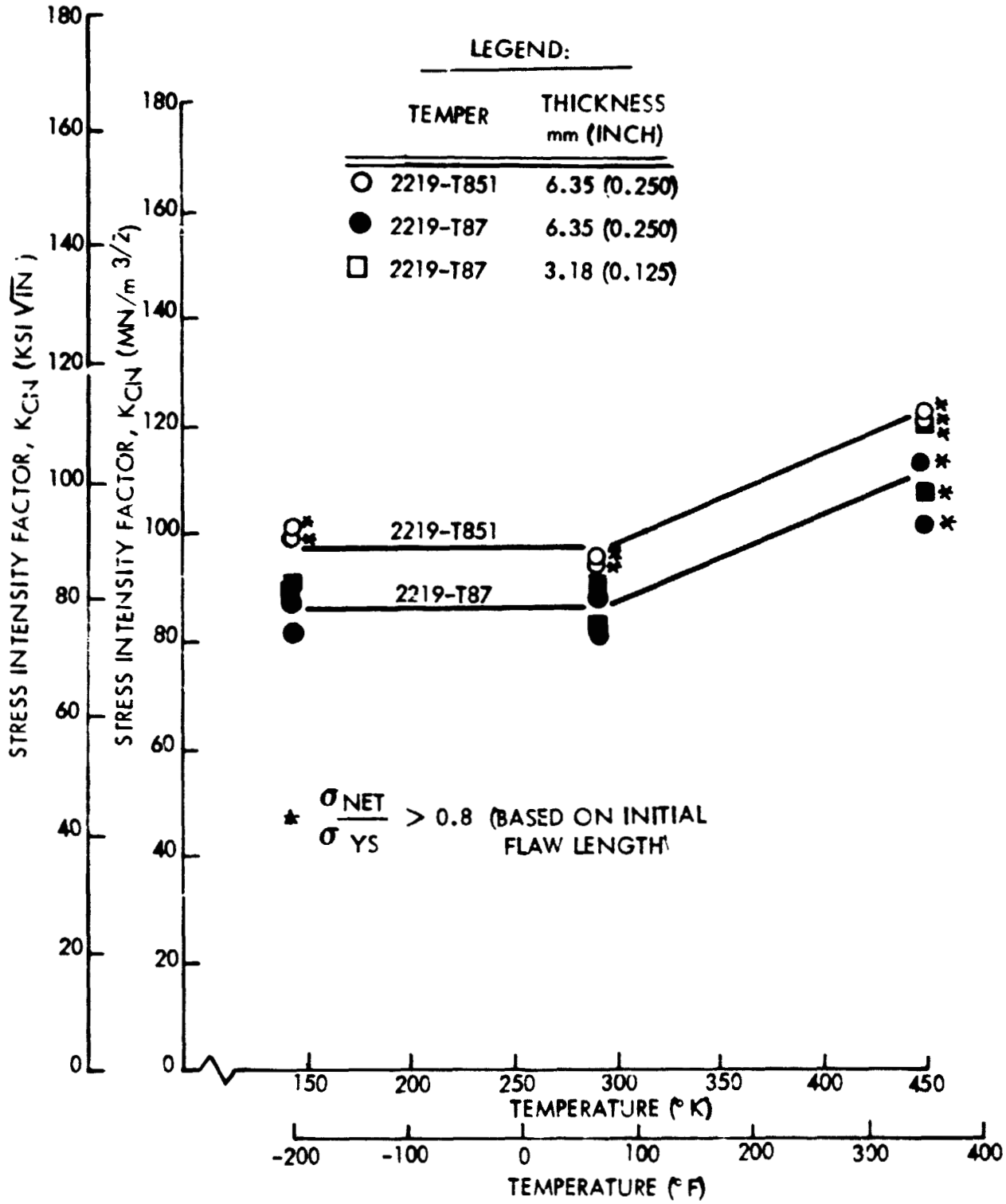


FIGURE 25: PLOT OF STRESS INTENSITY FACTOR, $K_{CN}$, VS. TEMPERATURE FOR 2219 ALUMINUM ALLOY SINGLE EDGE NOTCH TENSION STATIC FRACTURE TESTS, TL PROPAGATION DIRECTION

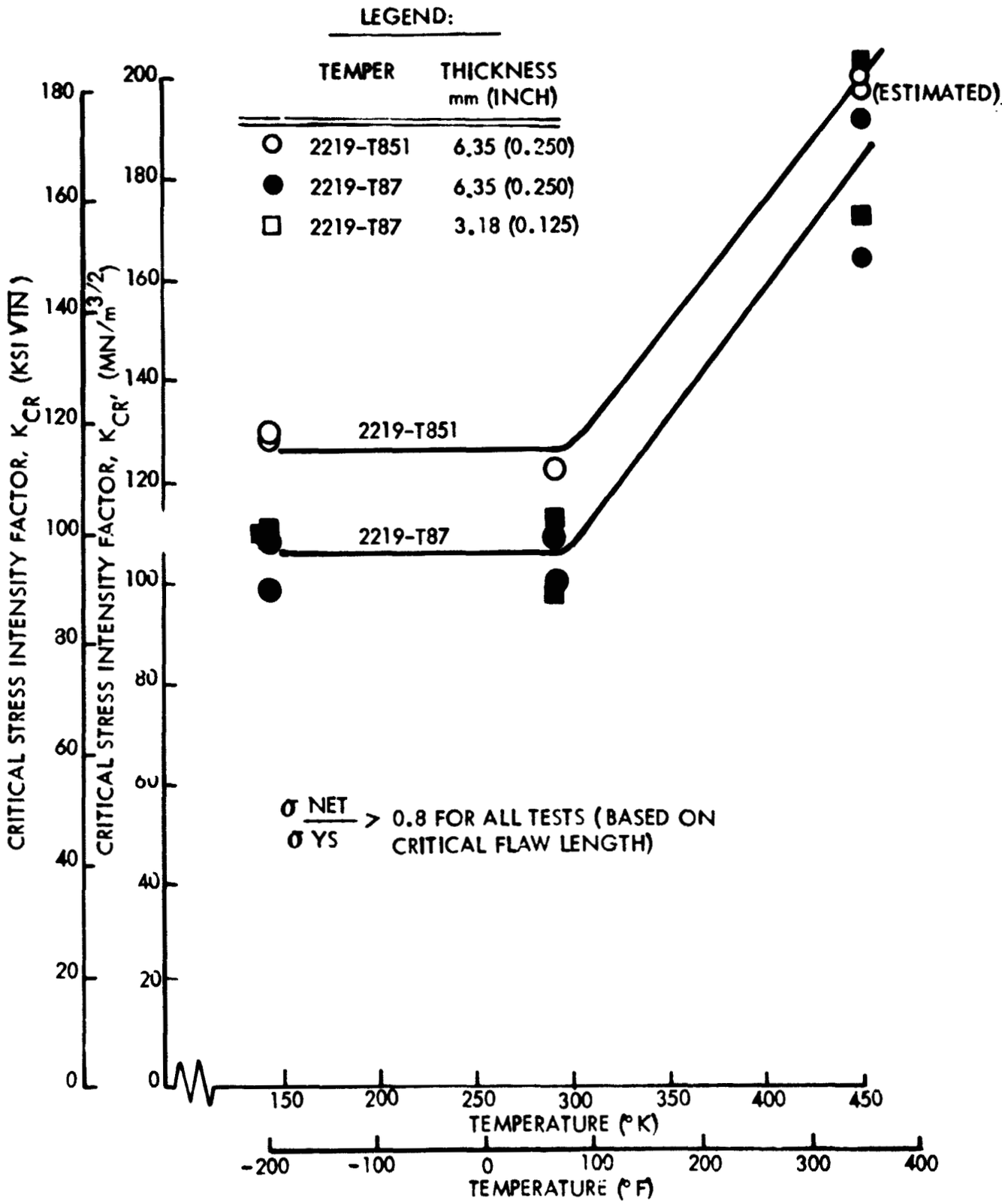


FIGURE 26 : PLOT OF CRITICAL STRESS INTENSITY FACTOR, $K_{CR}$, VS. TEMPERATURE FOR 2219 ALUMINUM ALLOY SINGLE EDGE NOTCH TENSION STATIC FRACTURE TESTS, TL PROPAGATION DIRECTION

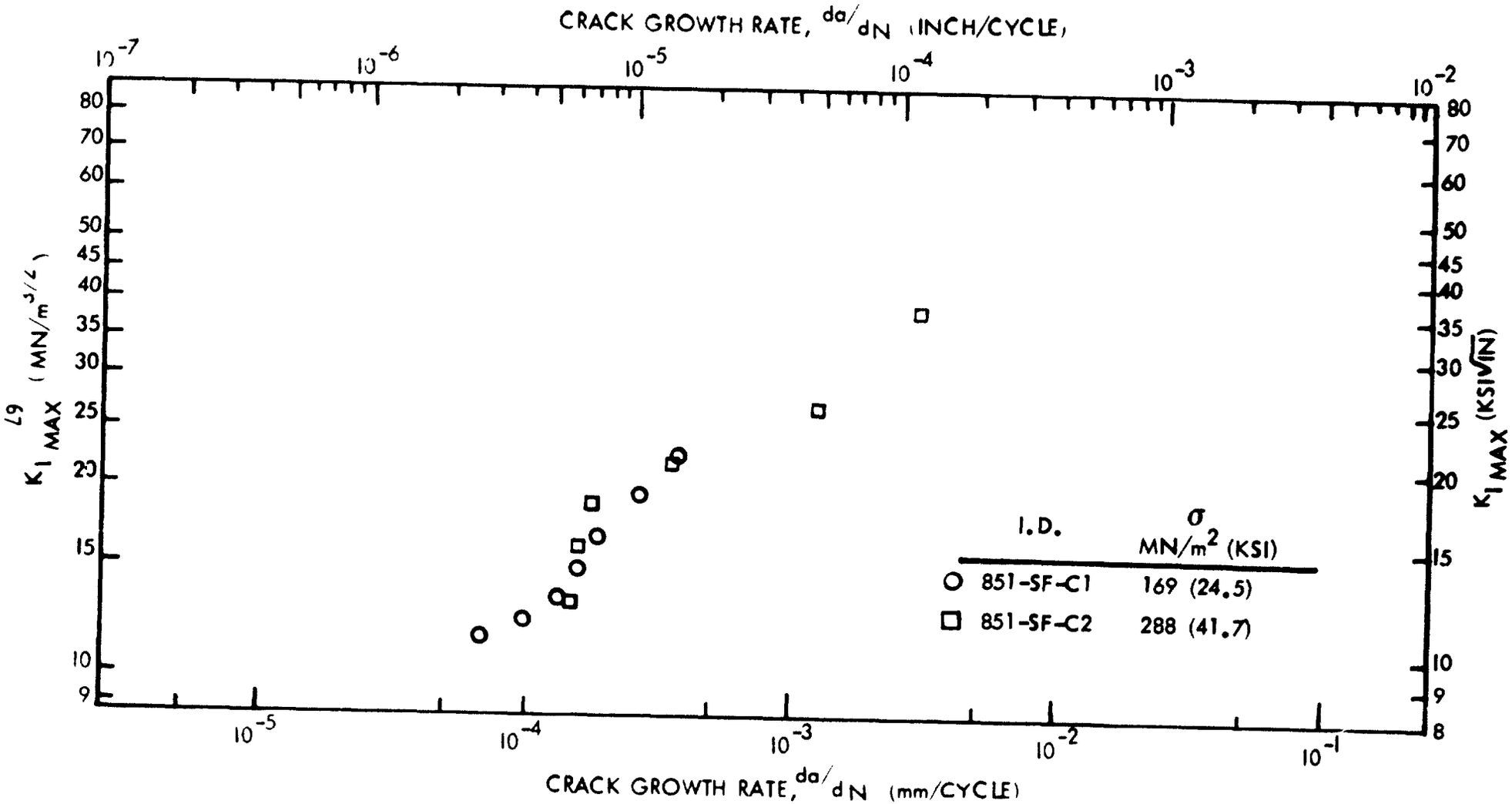


FIGURE 27: PLOT OF CRACK GROWTH RATE VS $K_{I_{MAX}}$, 6.35 mm (0.25 INCH) 2219-T851 SF SPECIMENS TESTED AT ROOM TEMPERATURE, R = 0, FREQ = 1 Hz (60 CPM), TS PROPAGATION DIRECTION

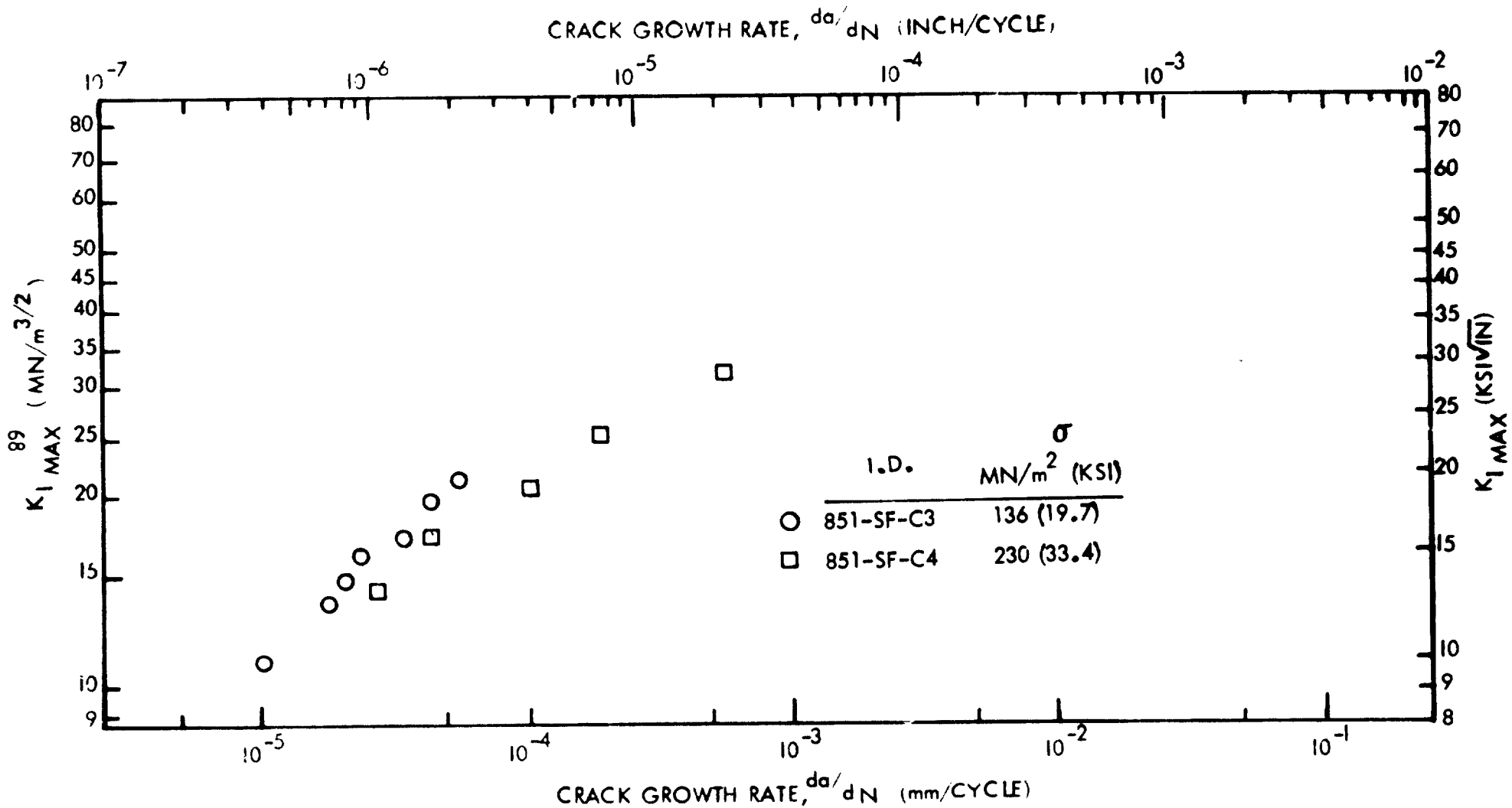


FIGURE 28: PLOT OF CRACK GROWTH RATE VS. $K_{I_{MAX}}$, 6.35 mm (0.25 INCH) 2219-T851 SF SPECIMENS TESTED AT 450° K (350° F), R = 0.5, FREQ = 1 Hz (60 CPM), TS PROPAGATION DIRECTION

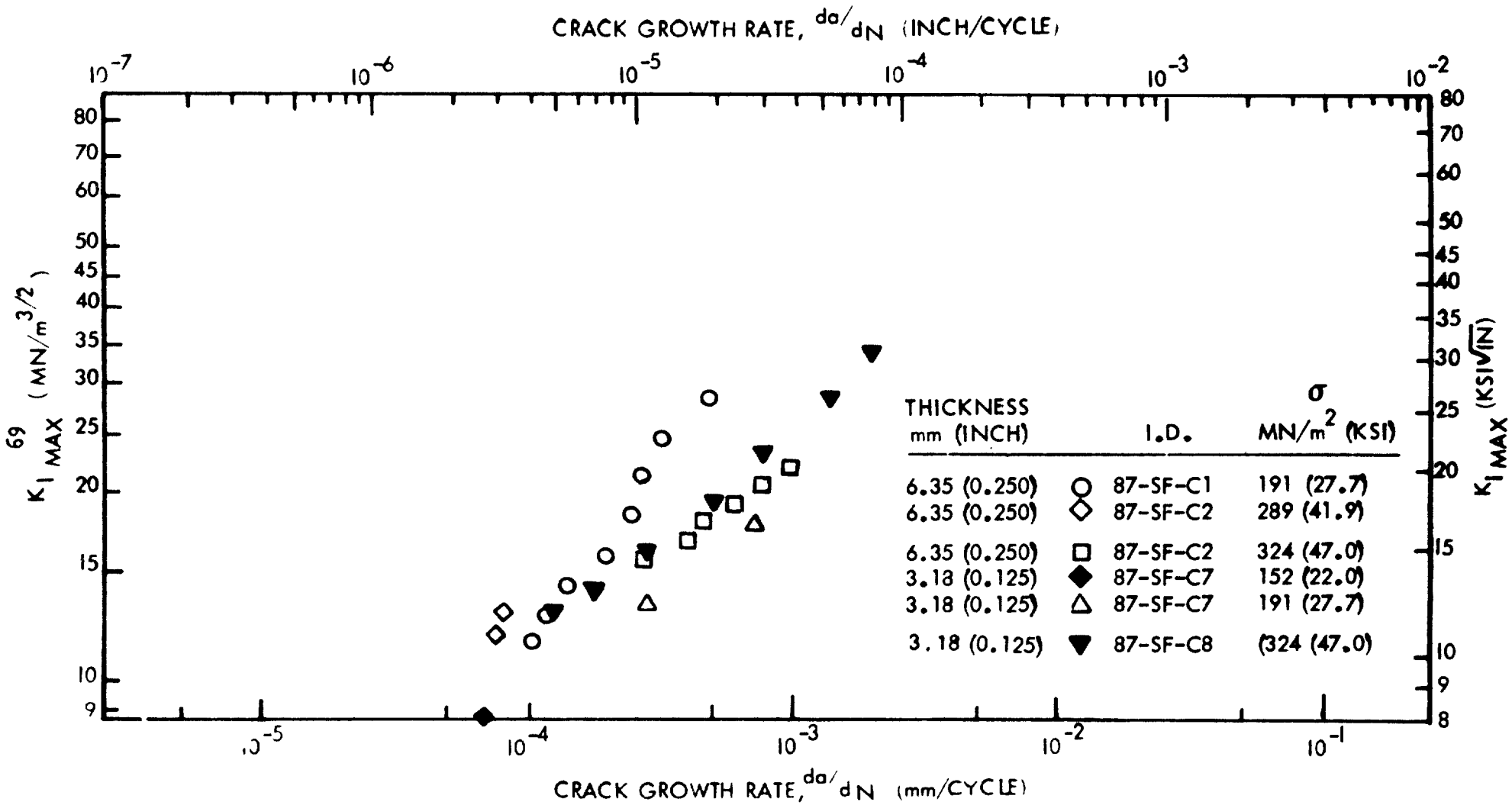


FIGURE 29: PLOT OF CRACK GROWTH RATE VS. $K_{I_{MAX}}$, 6.35 mm (0.250 INCH) AND 3.18 mm (0.125 INCH) 2219-T87 SF SPECIMENS TESTED AT ROOM TEMPERATURE, R = 0, FREQ. = 1 Hz (60 CPM), TS PROPAGATION DIRECTION

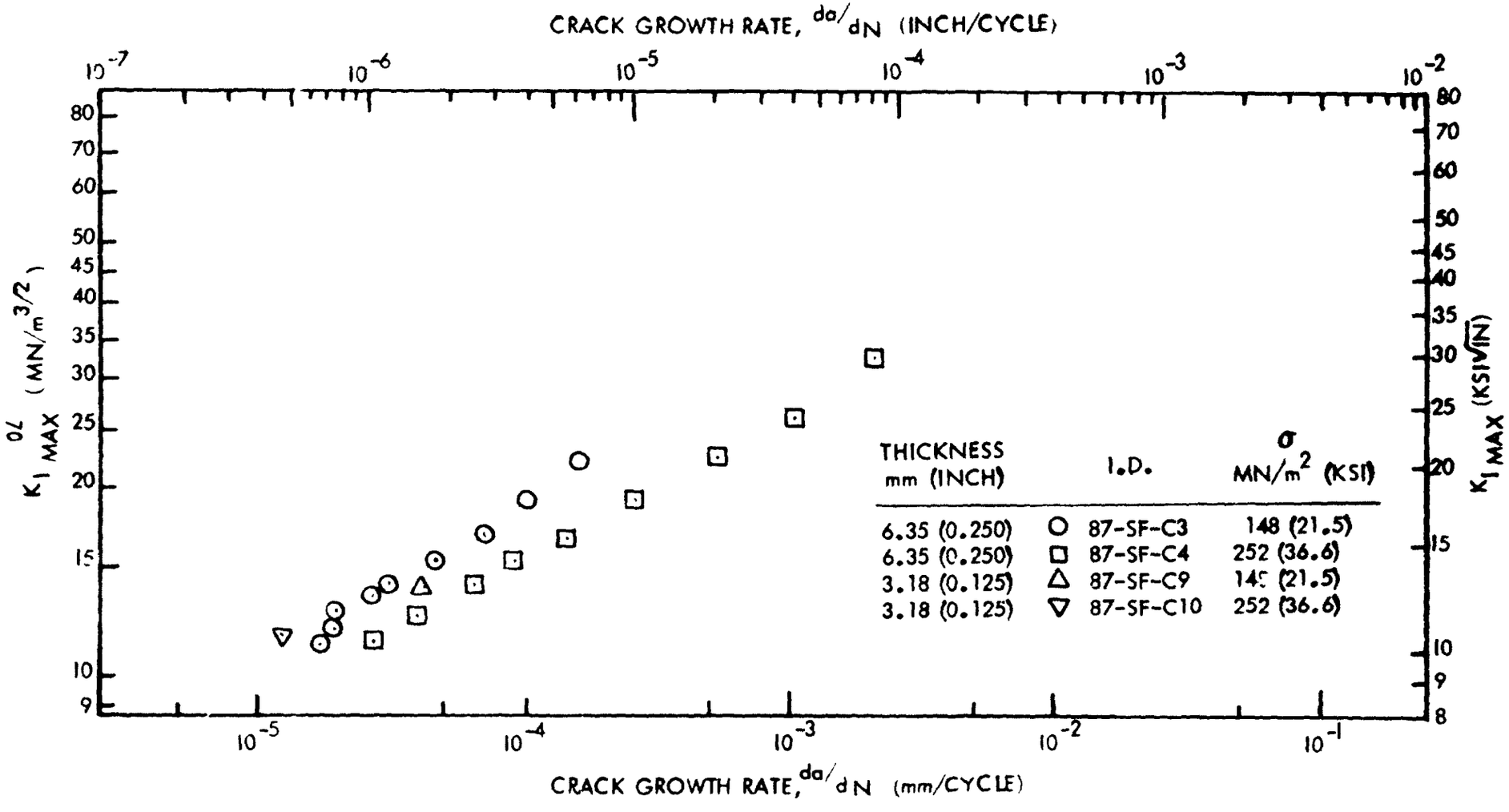


FIGURE 30: PLOT OF CRACK GROWTH RATE VS. $K_{I_{MAX}}$, 6.35 mm (0.250 INCH) AND 3.18 mm (0.125 INCH) 2219-T87 SF SPECIMENS TESTED AT 450°K (350°F), R = 0.5, FREQ. = 1 Hz (60 CPM), TS PROPAGATION DIRECTION

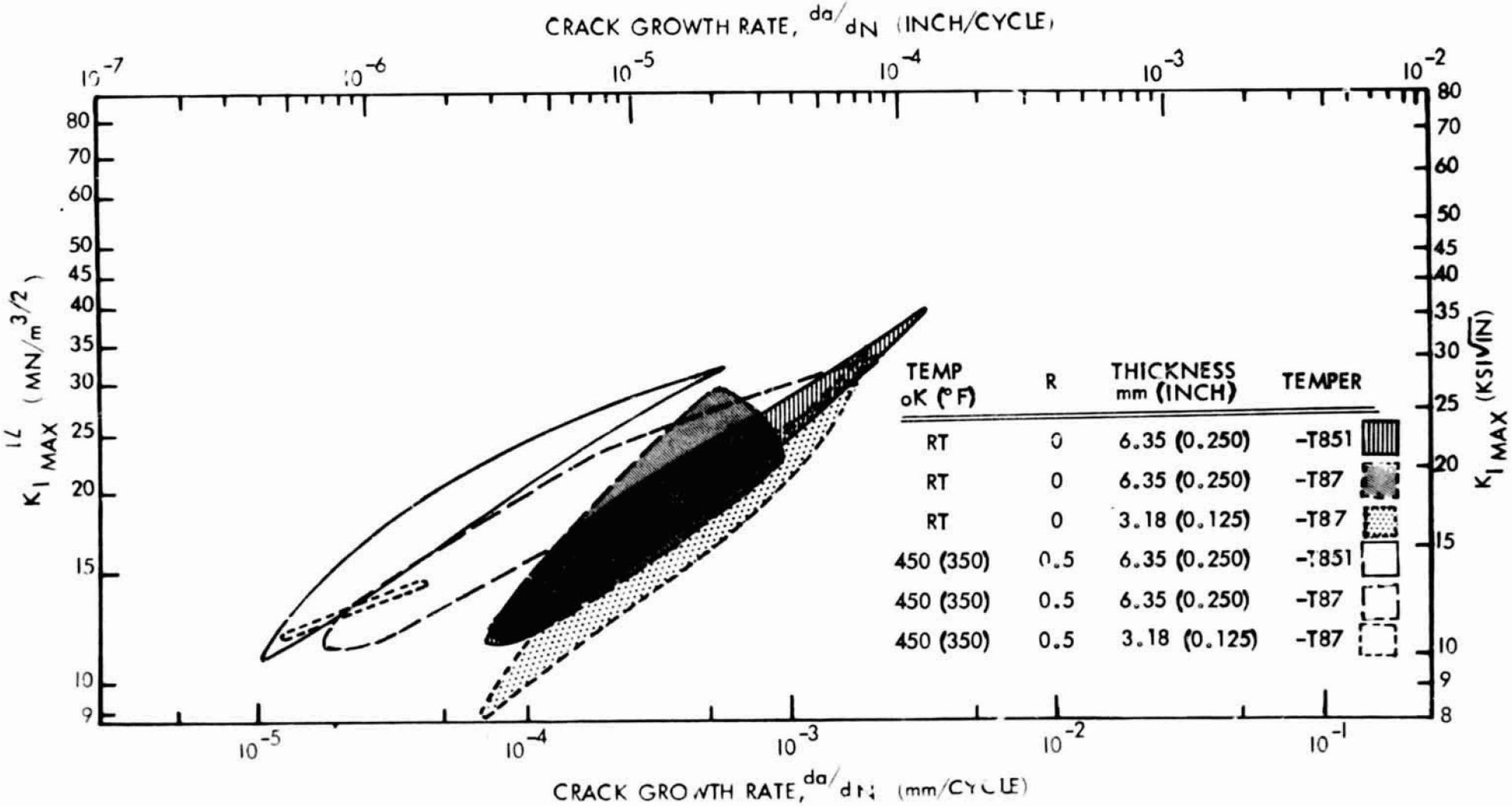


FIGURE 31: PLOT SHOWING SUMMARY OF CRACK GROWTH RATE VS. $K_{I_{MAX}}$ FOR 2219 SF SPECIMENS, FREQ = 1 Hz (60 CPM), TS PROPAGATION DIRECTION

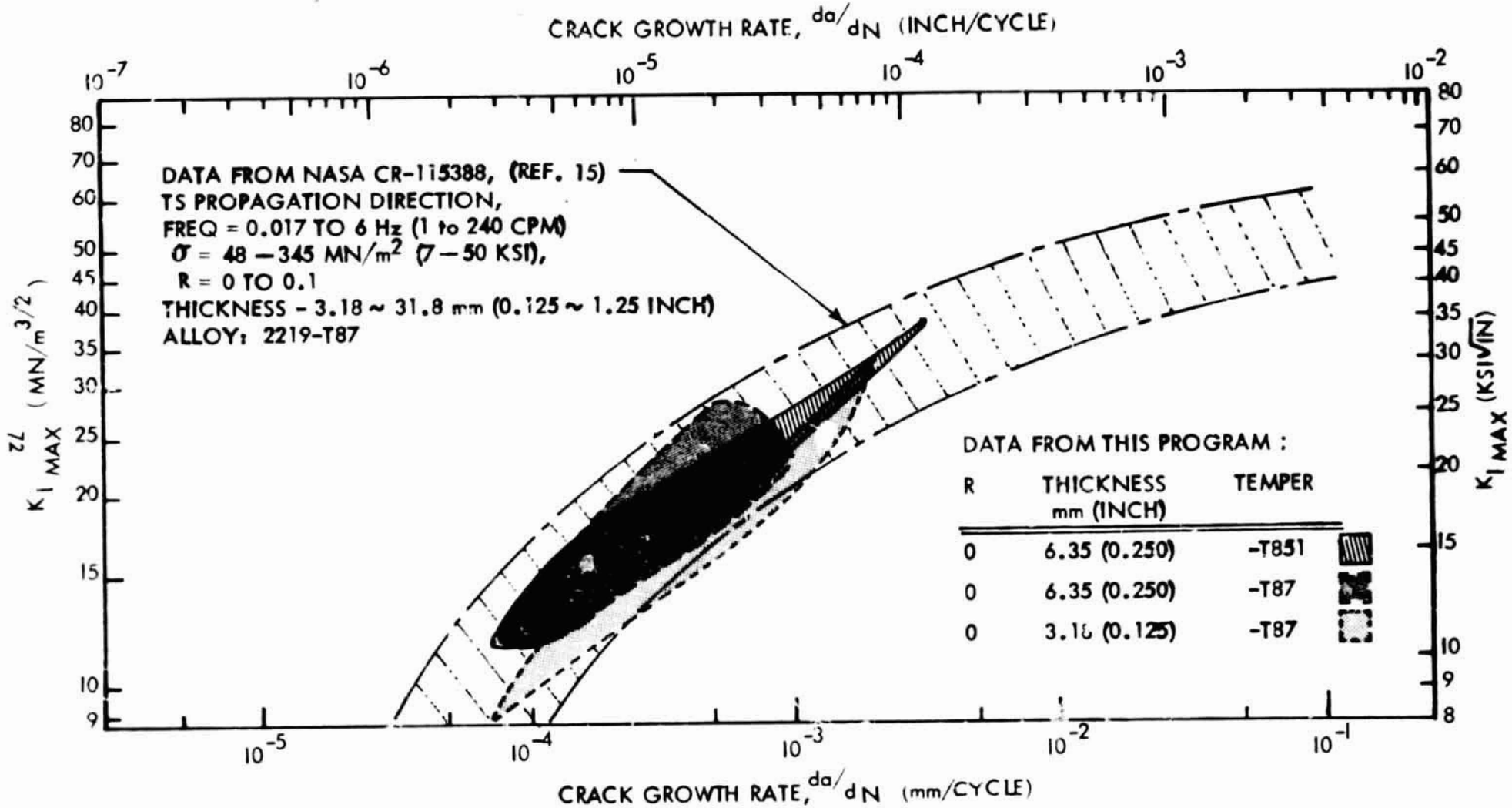


FIGURE 32. PLOT SHOWING COMPARISON OF ROOM TEMPERATURE SF DATA GENERATED ON THIS PROGRAM WITH ROOM TEMPERATURE SF DATA COMPILED IN CR-115388 (REF. 15)

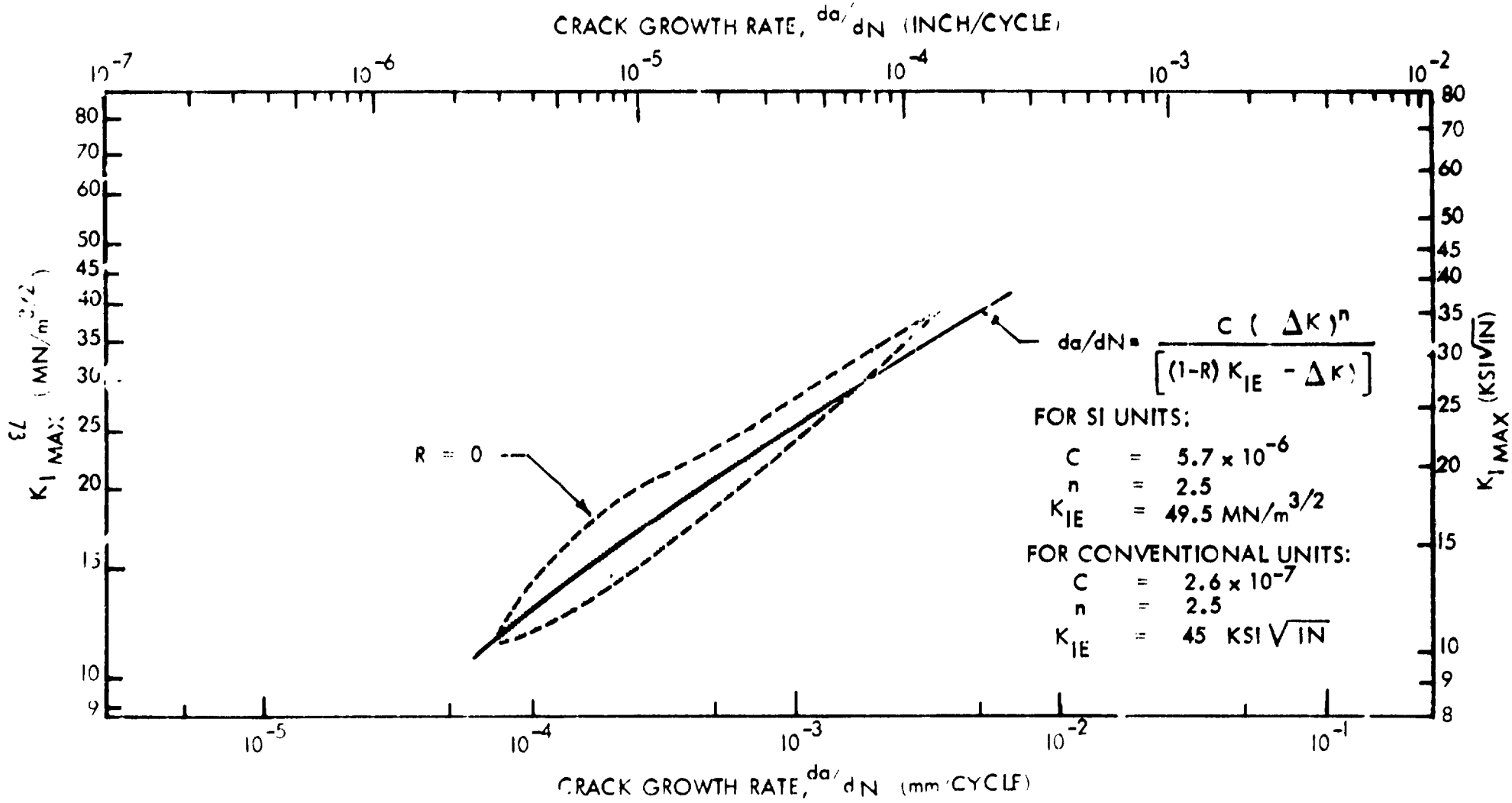


FIGURE 33: PLOT SHOWING FORMAN'S EQUATION FITTED TO ROOM TEMPERATURE 2219-T851 SF CRACK GROWTH DAT

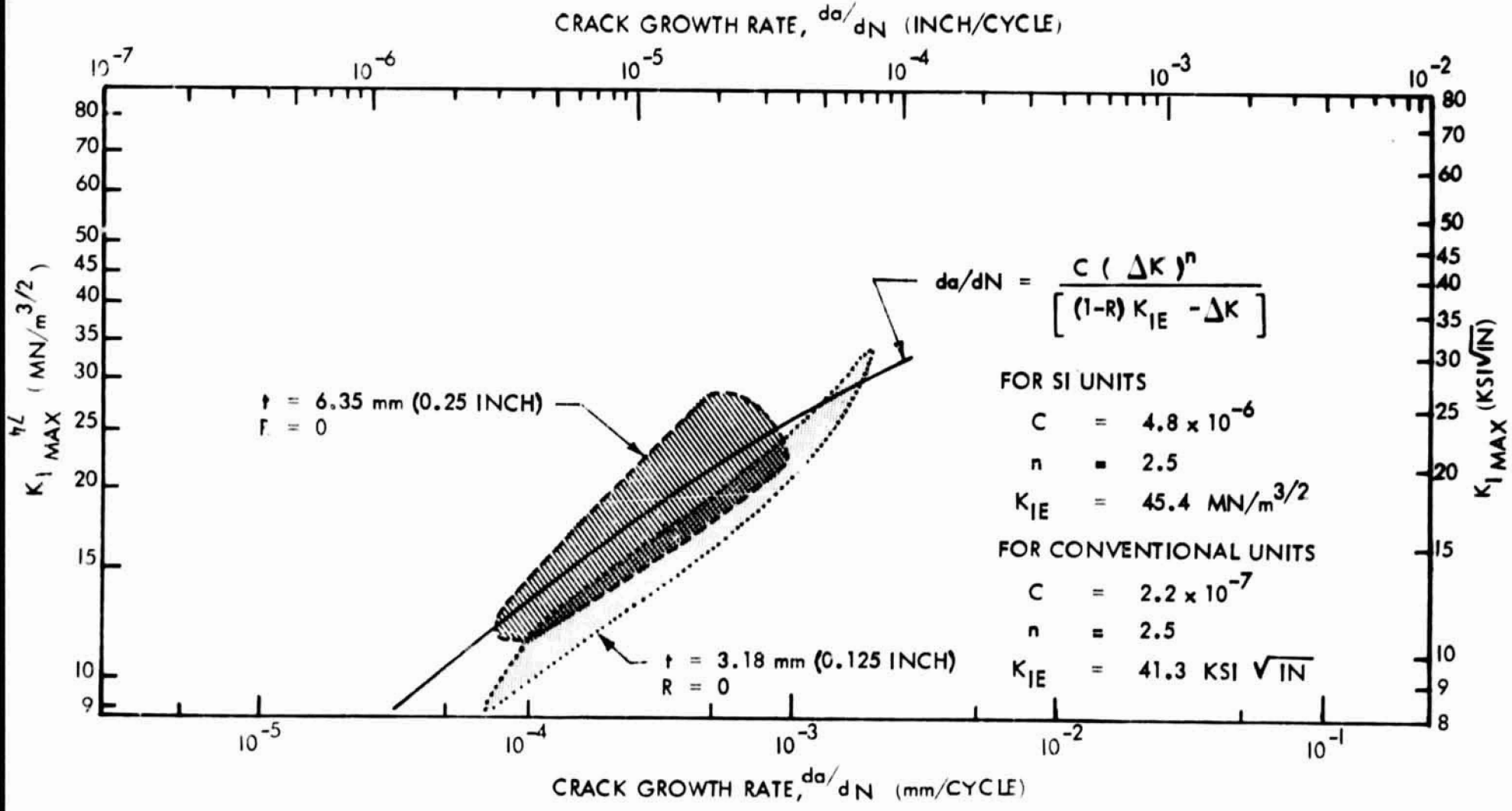


FIGURE 34: PLOT SHOWING FORMAN'S EQUATION FITTED TO ROOM TEMPERATURE 2219-T87 SF CRACK GROWTH DATA

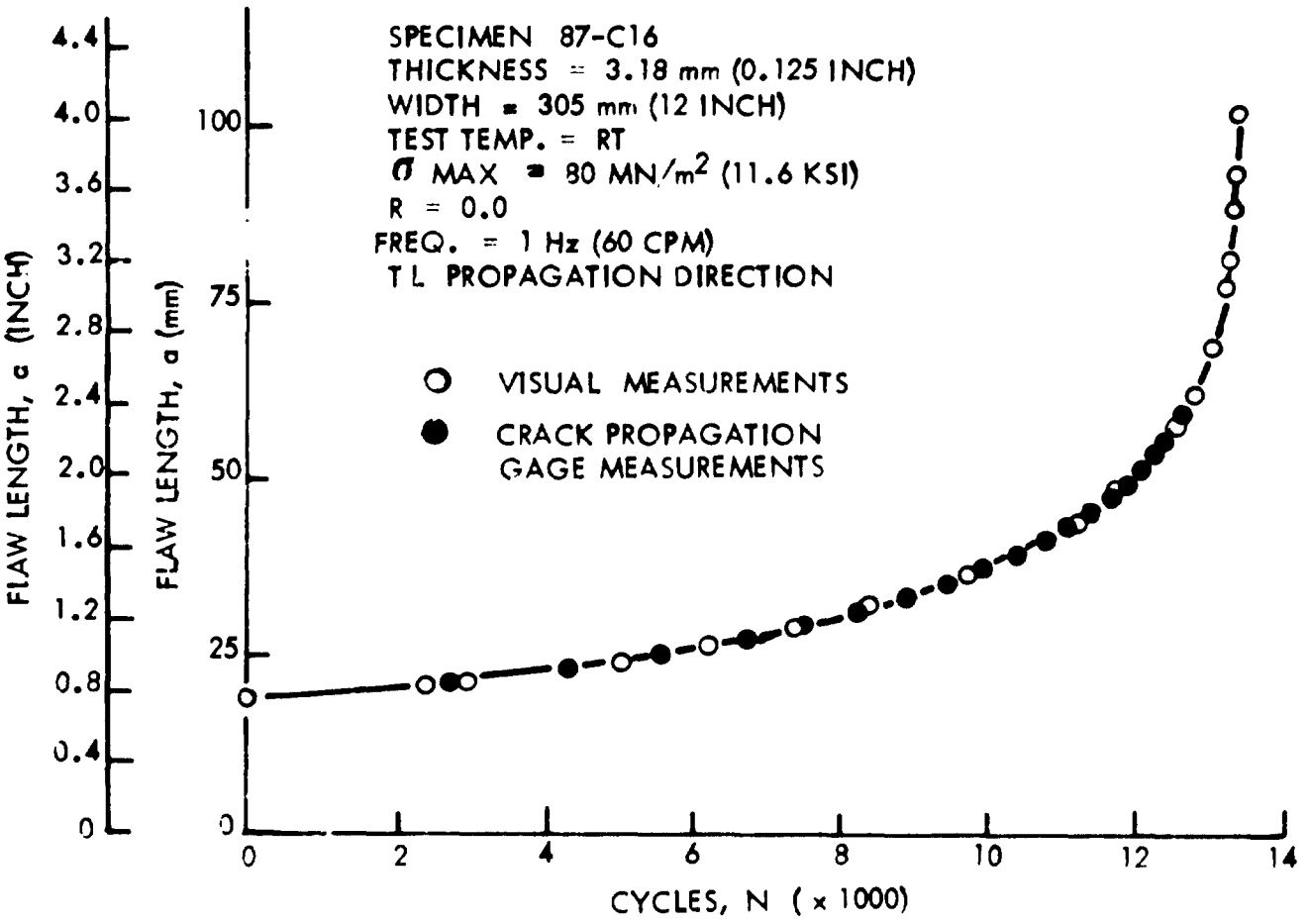


FIGURE 35: PLOT OF FLAW LENGTH VS. CYCLES, 2219-T87 SENT SPECIMEN 87-C16 TESTED AT ROOM TEMPERATURE

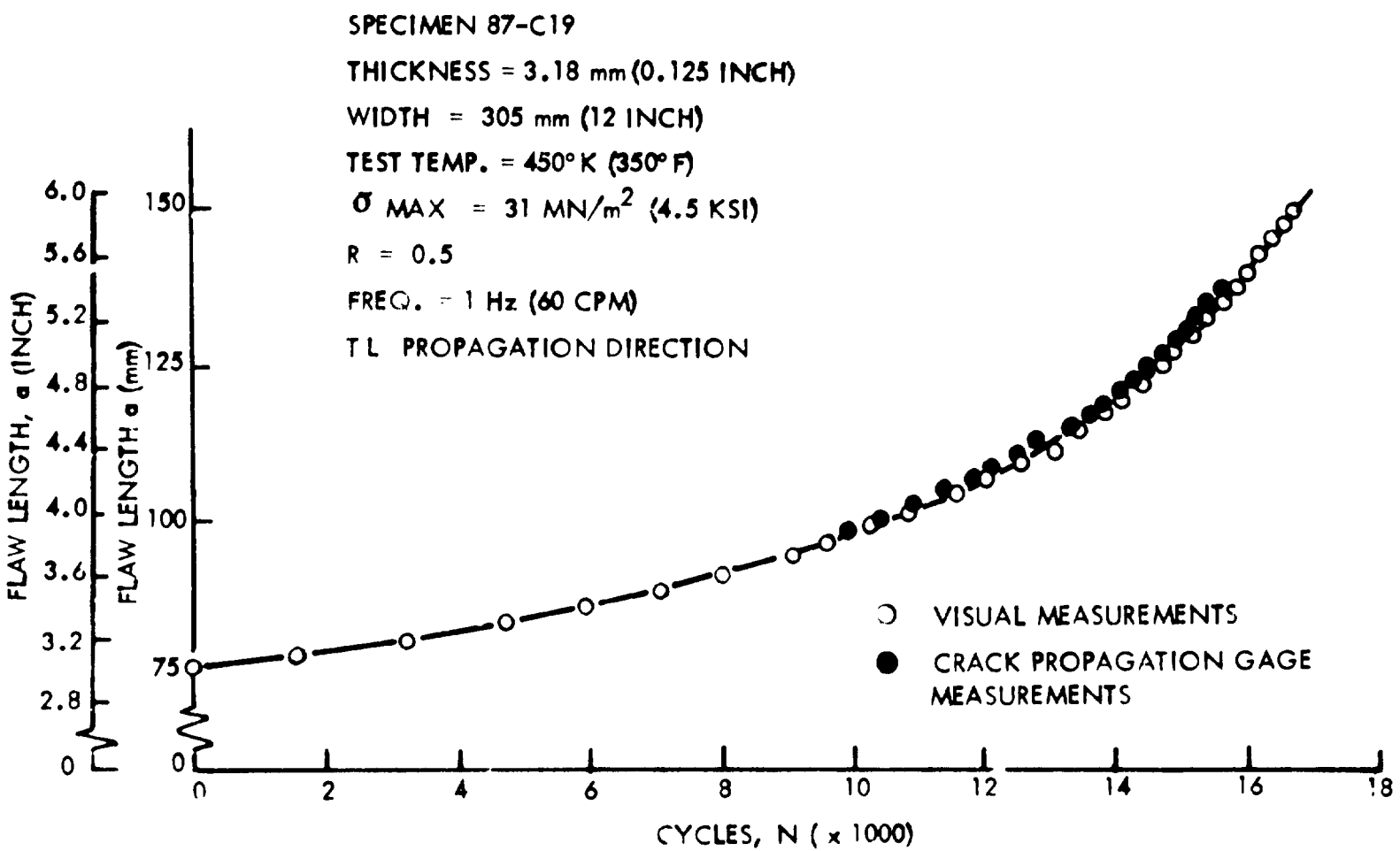


FIGURE 36: PLOT OF FLAW LENGTH VS. CYCLES, 2219-T87 SENT SPECIMEN 87-C19 TESTED AT 450° K (350° F)

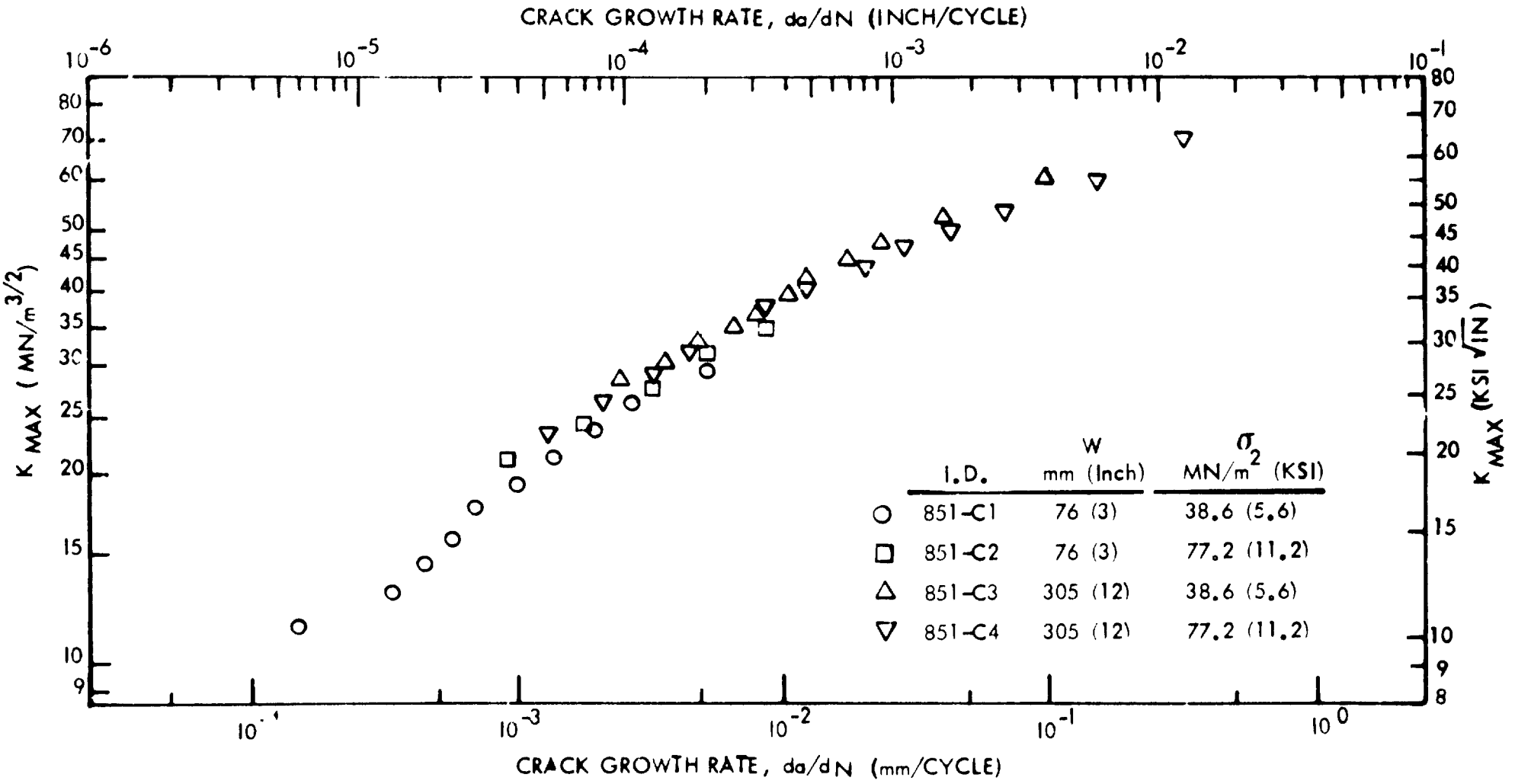


FIGURE 37. PLOT OF CRACK GROWTH RATE VS. $K_{MAX}$, 6.35 mm (0.25 INCH) 2219-T851 SENT SPECIMENS TESTED AT ROOM TEMPERATURE, R = 0, FREQ = 1 Hz, TL PROPAGATION DIRECTION

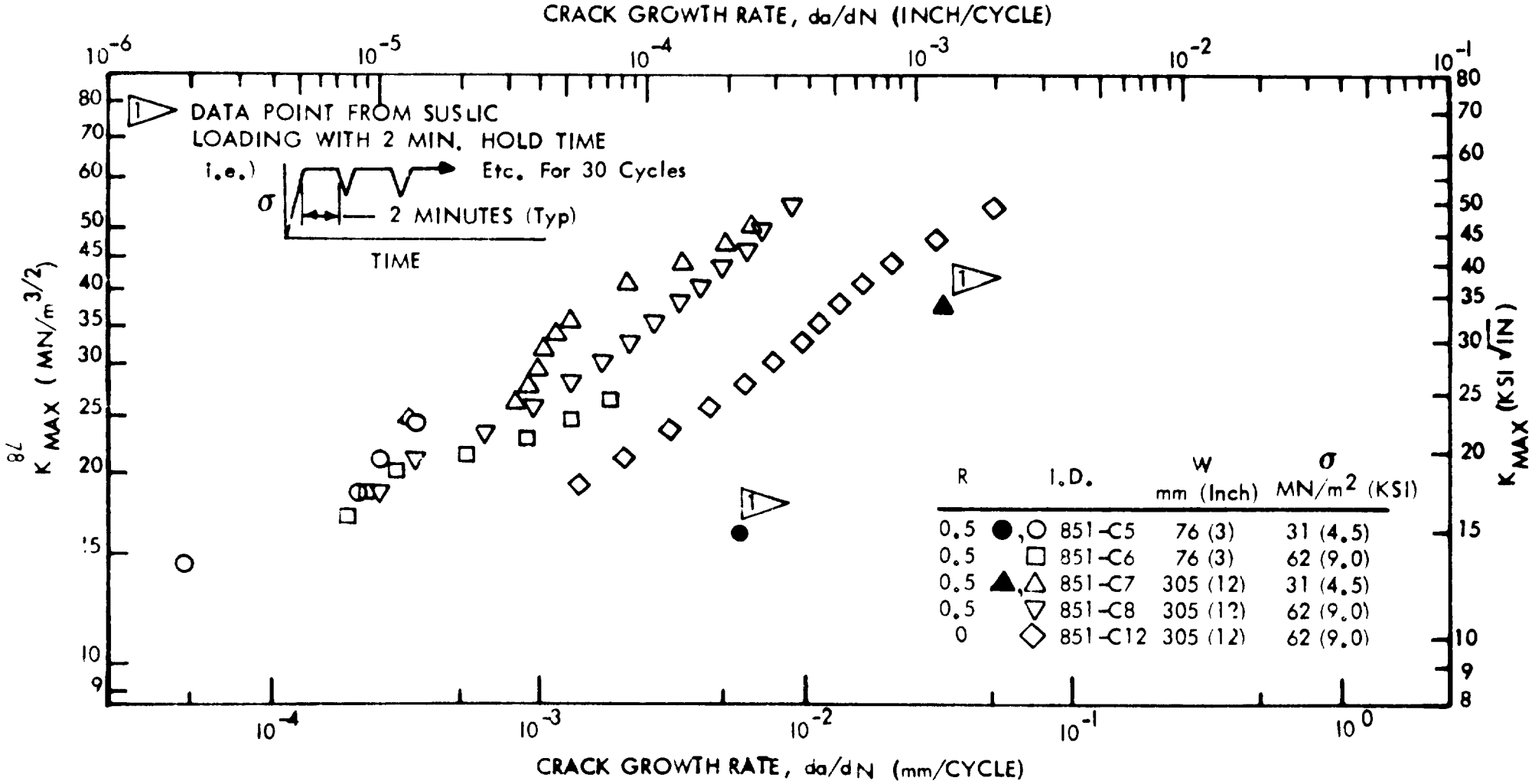


FIGURE 38: PLOT OF CRACK GROWTH RATE VS. $K_{MAX}$, 6.35 mm (0.25 Inch) 2219-T851 SENT SPECIMENS TESTED AT 450°K (350°F), R = 0.5 & 0, FREQ. = 1 Hz (60 CPM), TL PROPAGATION DIRECTION

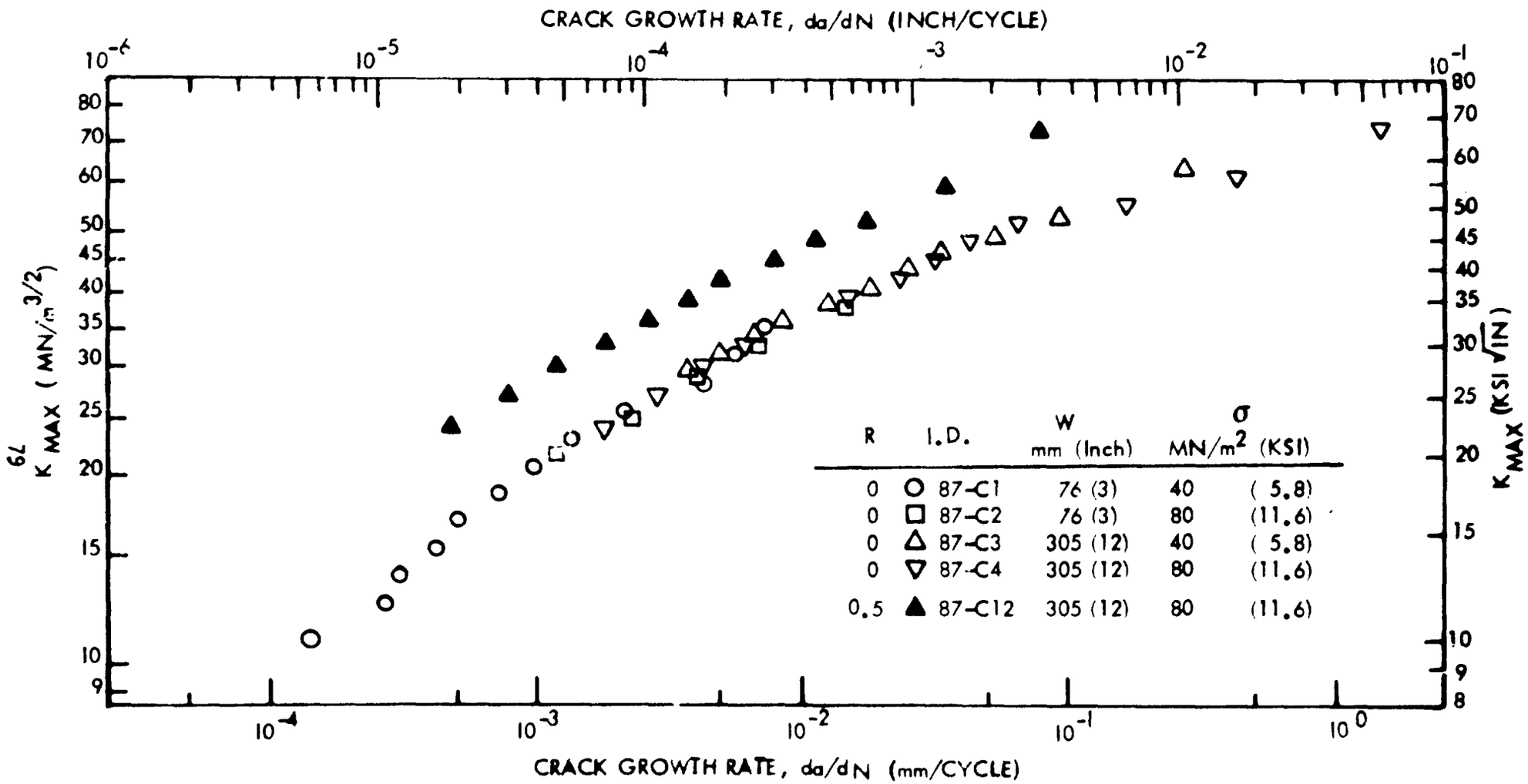


FIGURE 39: PLOT OF CRACK GROWTH RATE VS. $K_{MAX}$, 6.35 mm (0.25 Inch) 2219-T87 SENT SPECIMENS TESTED AT ROOM TEMPERATURE, R = 0 & 0.5, FREQ = 1 Hz (60 CPM), TL PROPAGATION DIRECTION

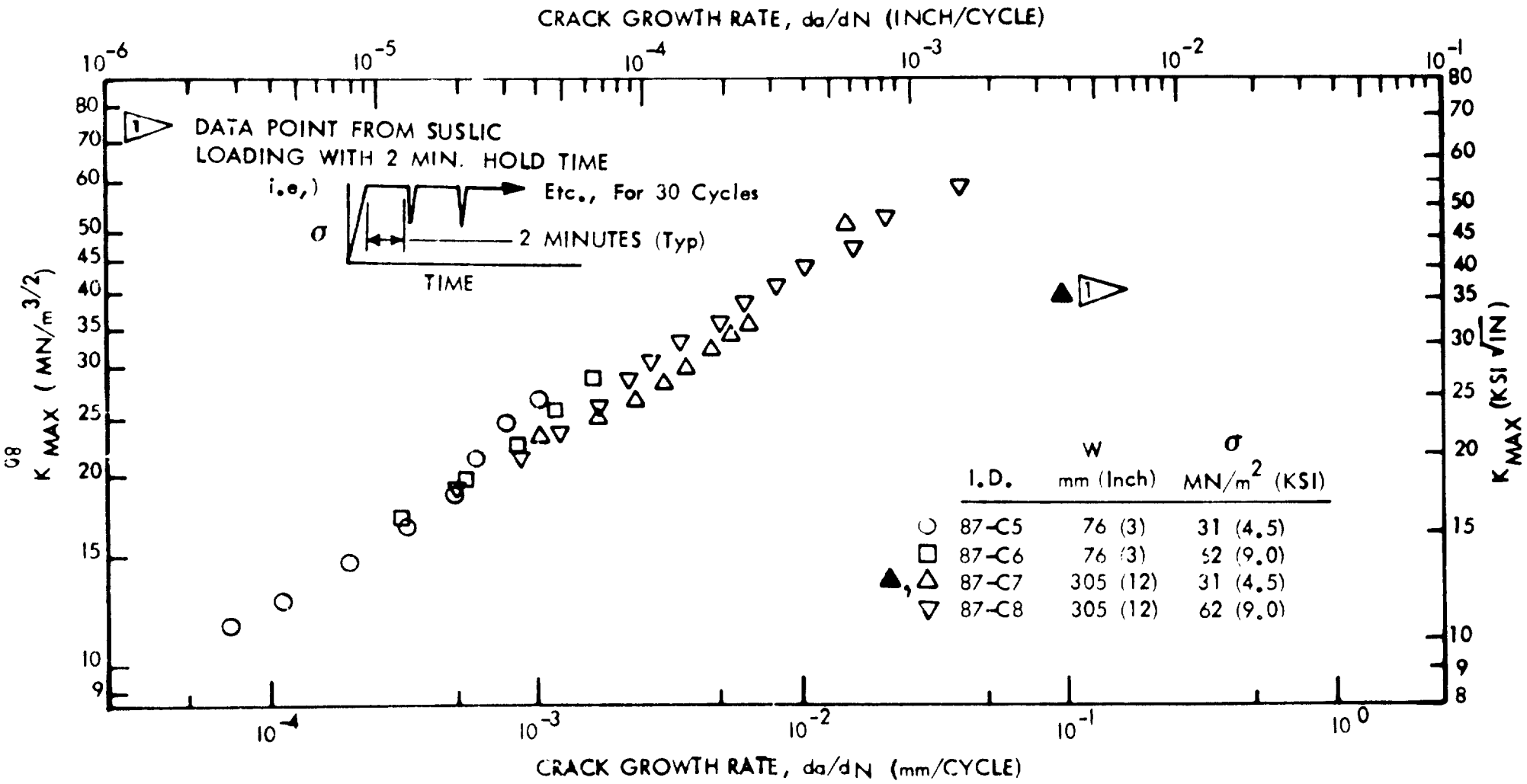


FIGURE 40: PLOT OF CRACK GROWTH RATE VS. $K_{MAX}$, 6.35 mm (0.25 Inch) 2219-T87 SENT SPECIMENS TESTED AT 450°K (350°F), R = 0.5, FREQ. = 1 Hz (60 CPM), TL PROPAGATION DIRECTION

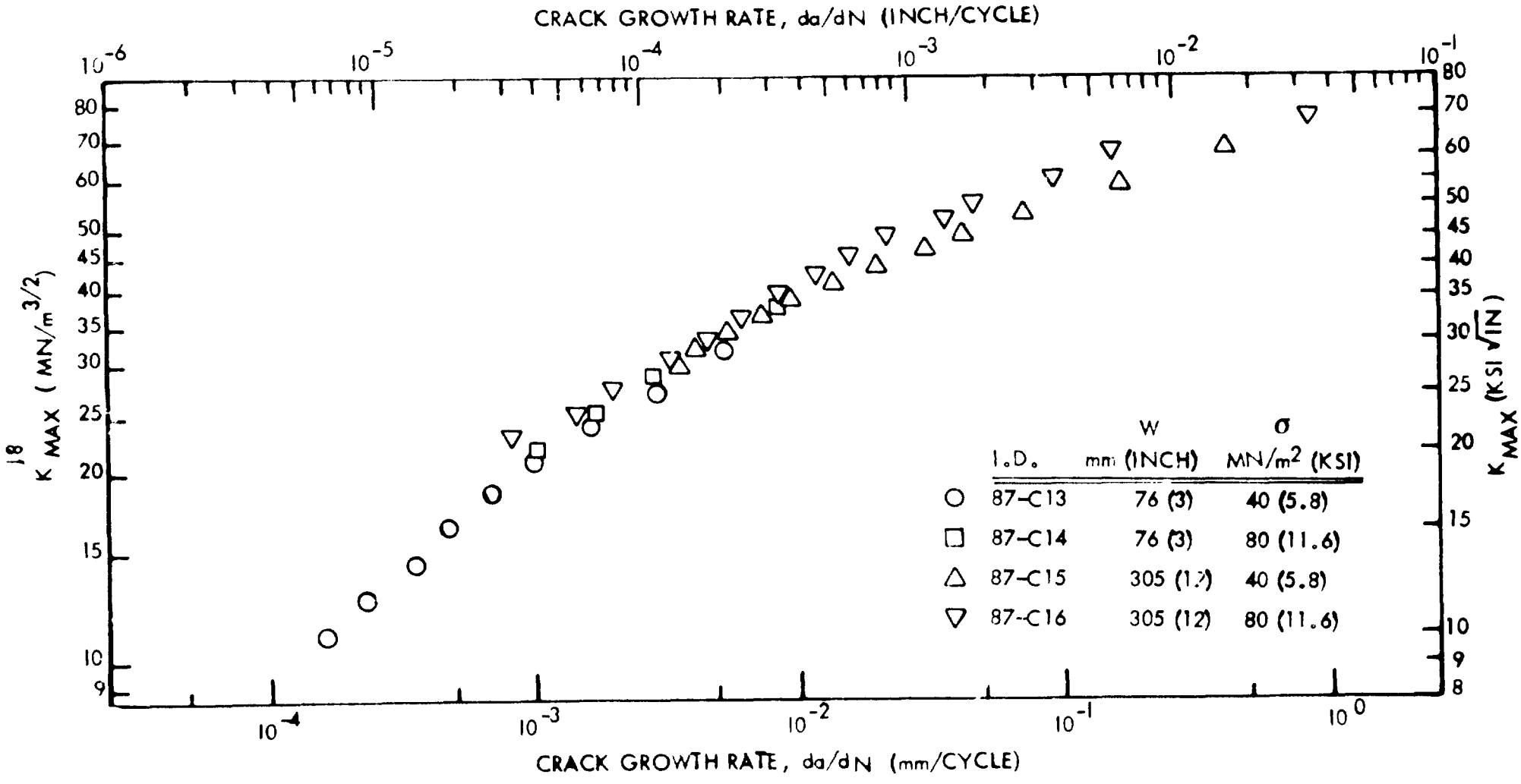


FIGURE 41: PLOT OF CRACK GROWTH RATE VS. $K_{MAX}$, 3.18 mm (0.125) 2219-T87 SENT SPECIMENS TESTED AT ROOM TEMPERATURE, R = 0, FREQ. = 1 Hz (60 CPM), TL PROPAGATION DIRECTION

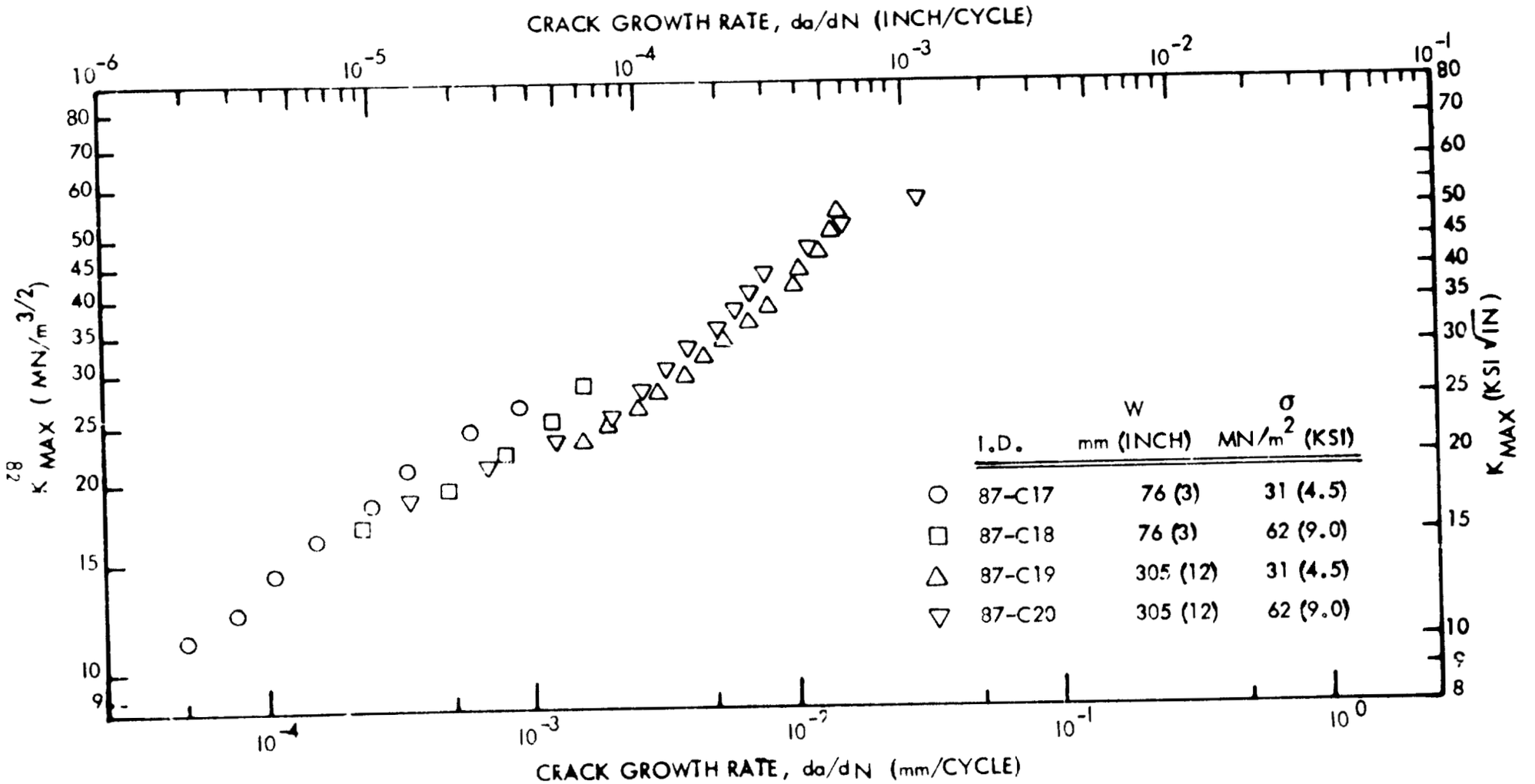


FIGURE 42: PLOT OF CRACK GROWTH RATE VS. $K_{MAX}$, 3.18 mm (0.125 INCH) [illegible] ENT SPECIMENS TESTED AT 450°K (350°F), R = 0.5, FREQ = 1 Hz (60 CPM), TL PROPAGATION DIRECTION

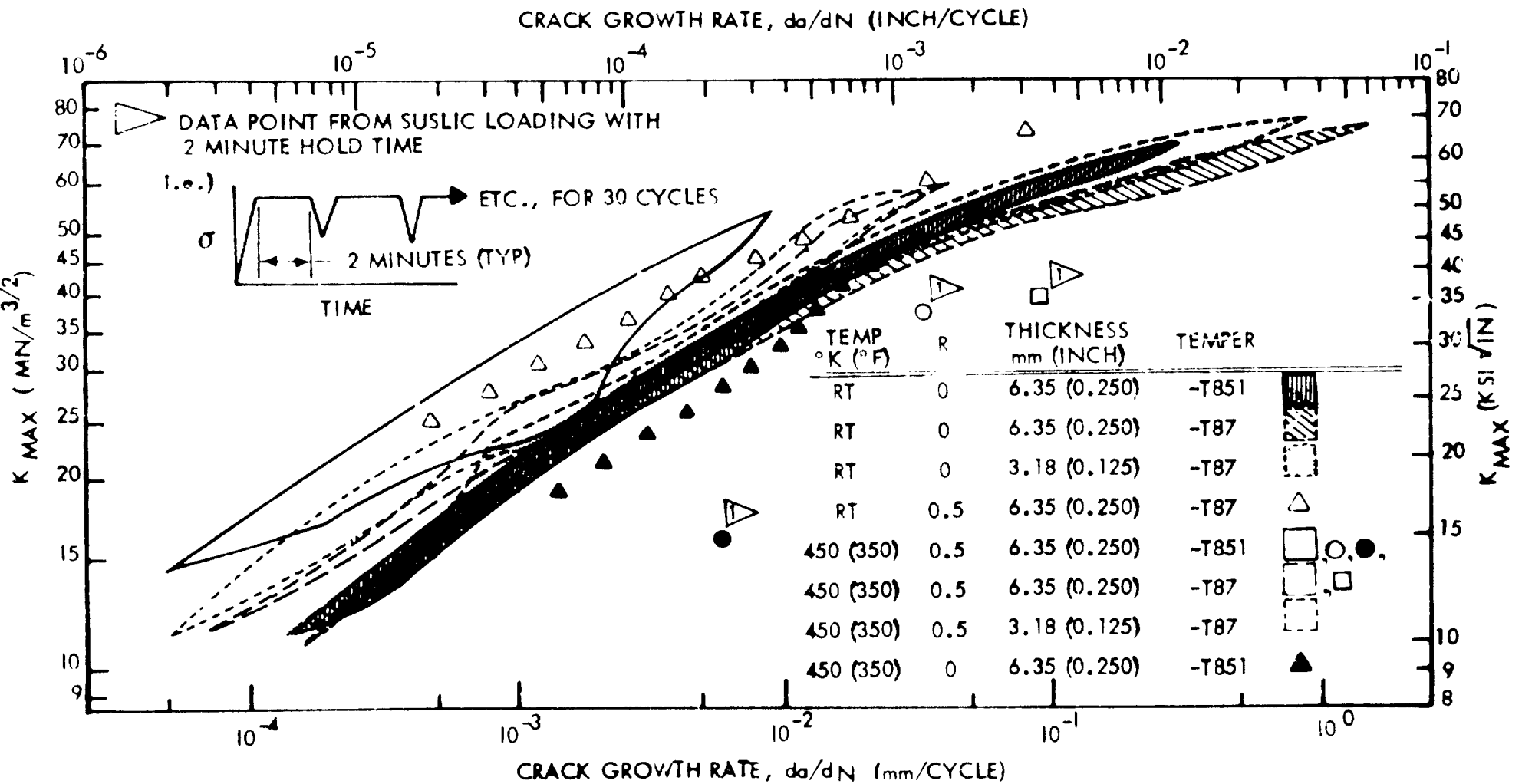


FIGURE 43: PLOT SHOWING SUMMARY OF CRACK GROWTH RATE VS. $K_{MAX}$ FOR 2219 SENT SPECIMENS, FREQ 1 Hz (60 CPM), T L PROPAGATION DIRECTION

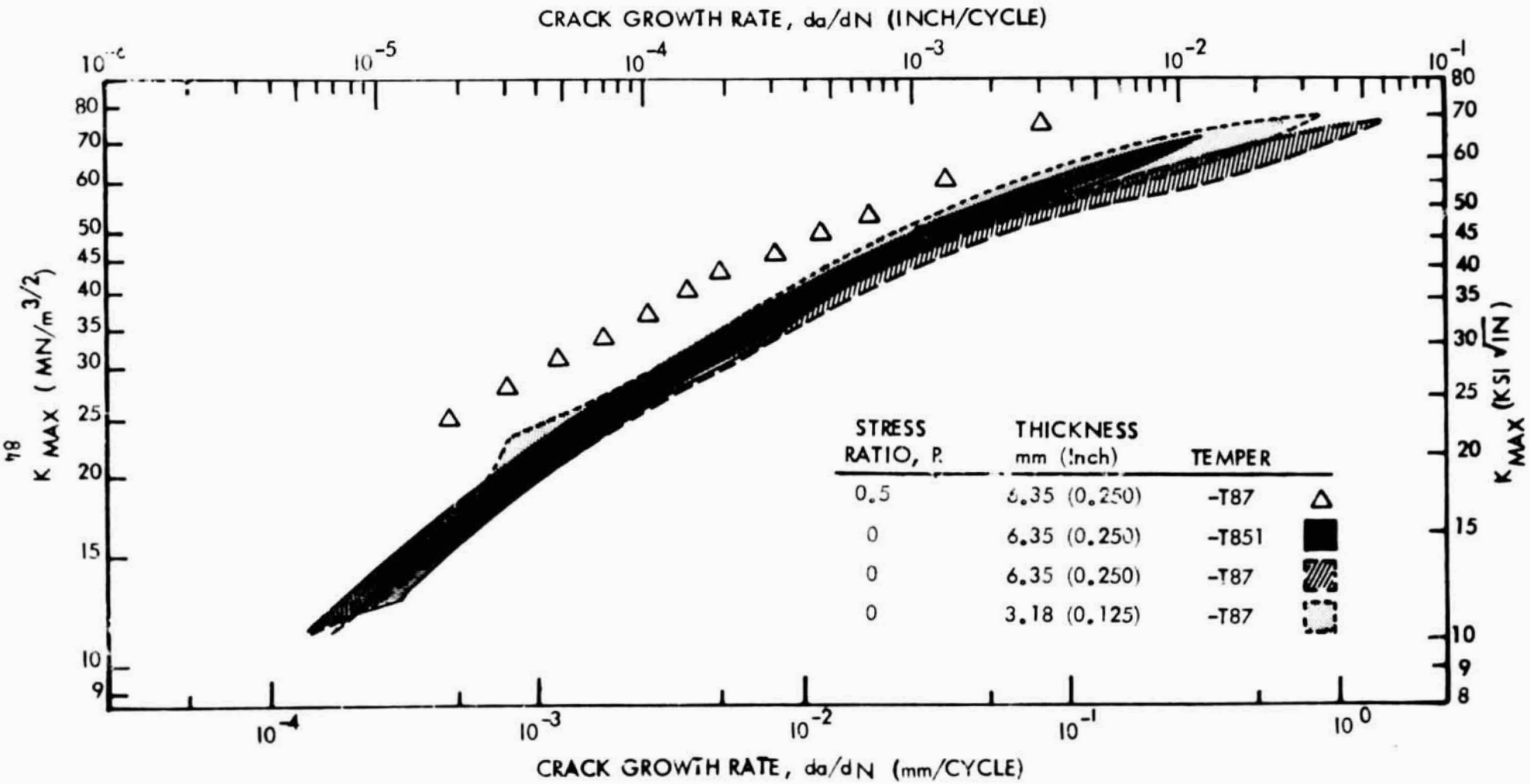


FIGURE 44: PLOT SHOWING EFFECT OF VARYING STRESS RATIO ON 2219 SENT CYCLIC SPECIMENS TESTED AT ROOM TEMPERATURE, FREQ. = 1 Hz (60 CPM), TL PROPAGATION DIRECTION

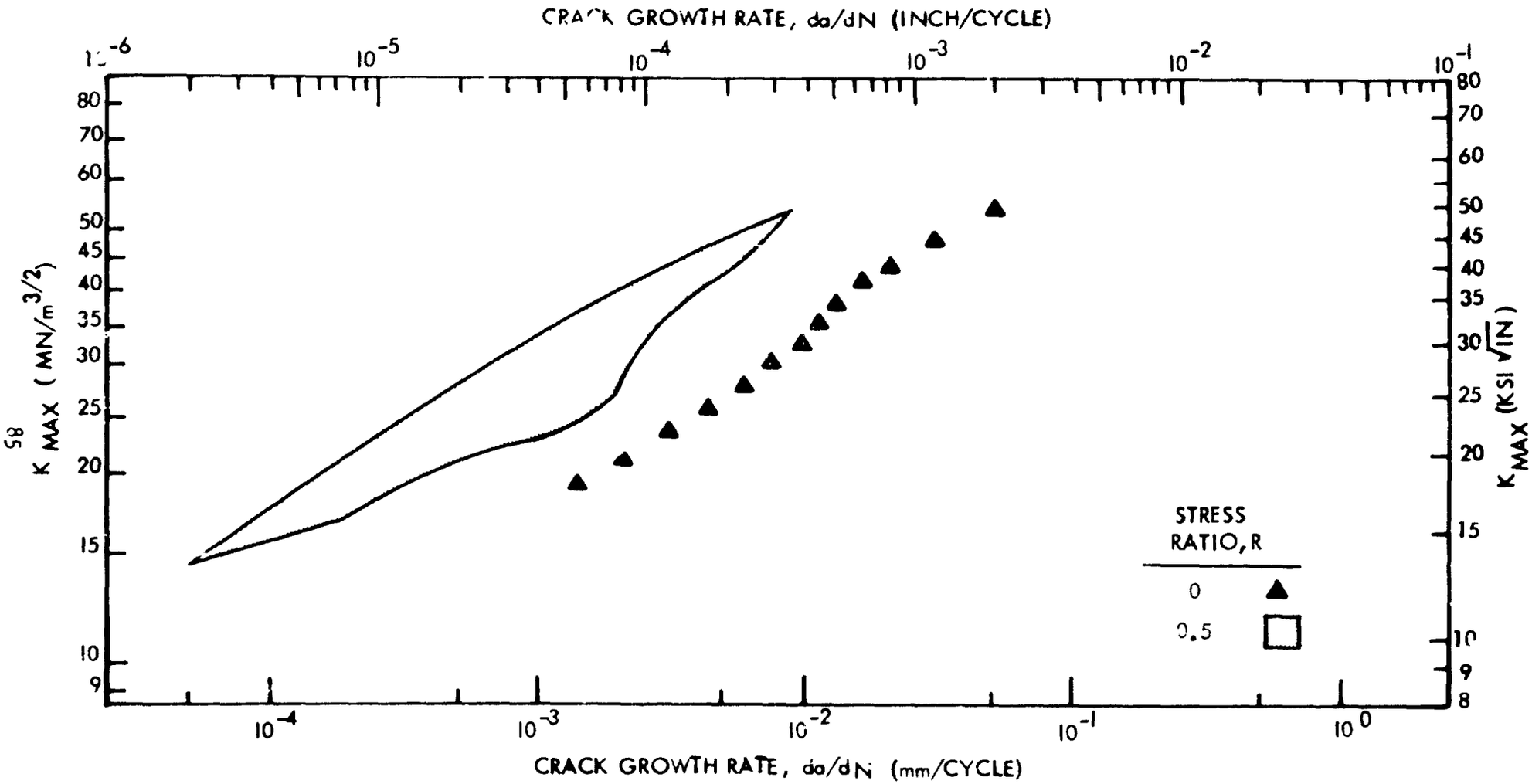


FIGURE 45: PLOT SHOWING EFFECT OF VARYING STRESS RATIO ON 6.35 mm (0.250 INCH) 2219-T851 SENT CYCLIC SPECIMENS TESTED AT 450K (350F), FREQ = 1 Hz (60 CPM), TL PROPAGATION DIRECTION

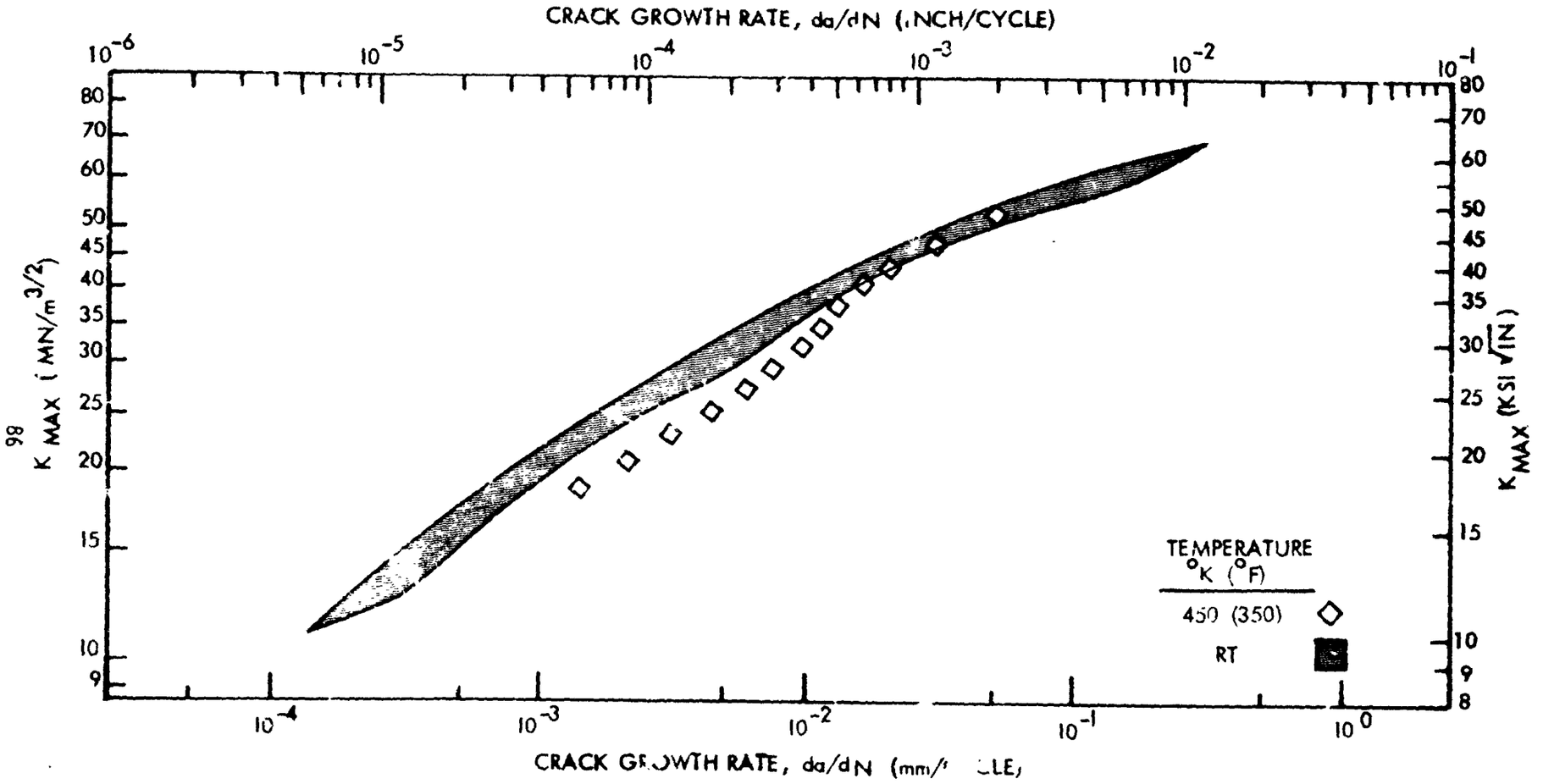


FIGURE 46: PLOT SHOWING EFFECT OF VARYING TEST TEMPERATURE ON 6.35 mm (0.250 INCH) 2219-T851 SENT CYCLIC SPECIMENS TESTED AT R = 0, FREQ = 1 Hz (60 CPM), TL PROPAGATION DIRECTION

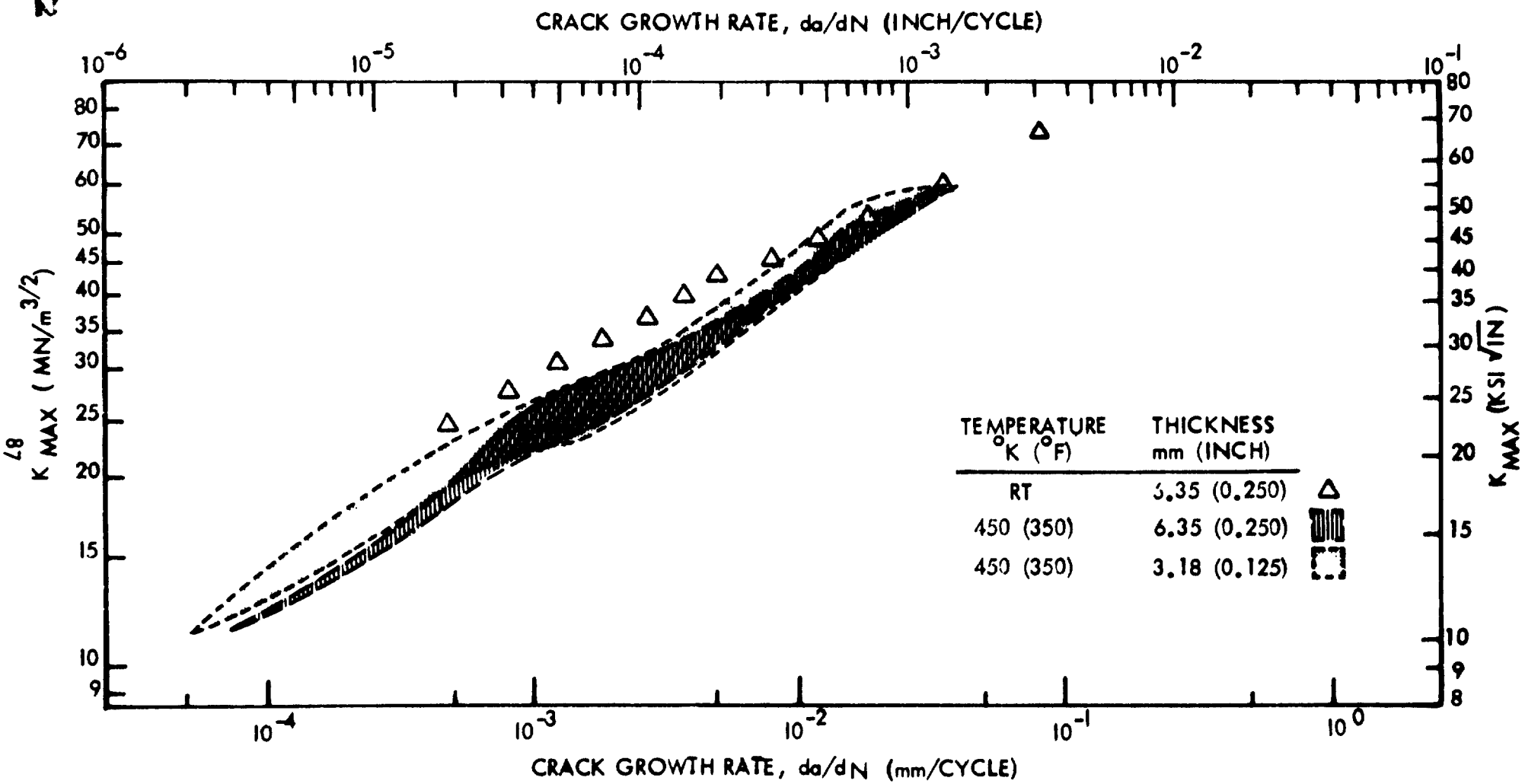


FIGURE 47: PLOT SHOWING EFFECT OF VARYING TEST TEMPERATURE ON 2219-T87 SENT CYCLIC SPECIMENS TESTED AT R = 0.5, FREQ = 1 Hz (60 CPM), TL PROPAGATION DIRECTION

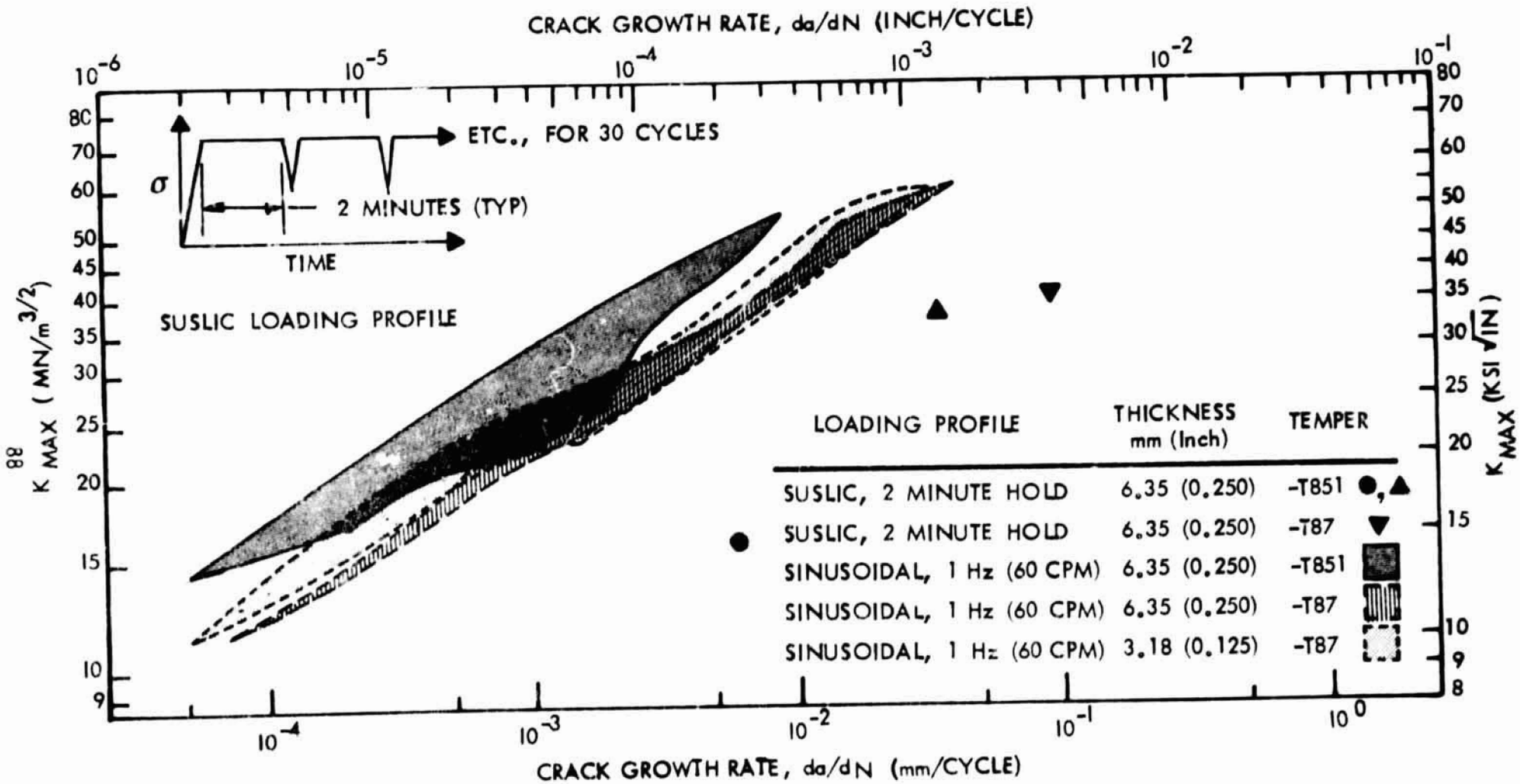


FIGURE 48: PLOT SHOWING EFFECT OF SUSLIC LOADING ON 2219 SENT SPECIMENS TESTED AT 450K (350F), R = 0.5, TL PROPAGATION DIRECTION

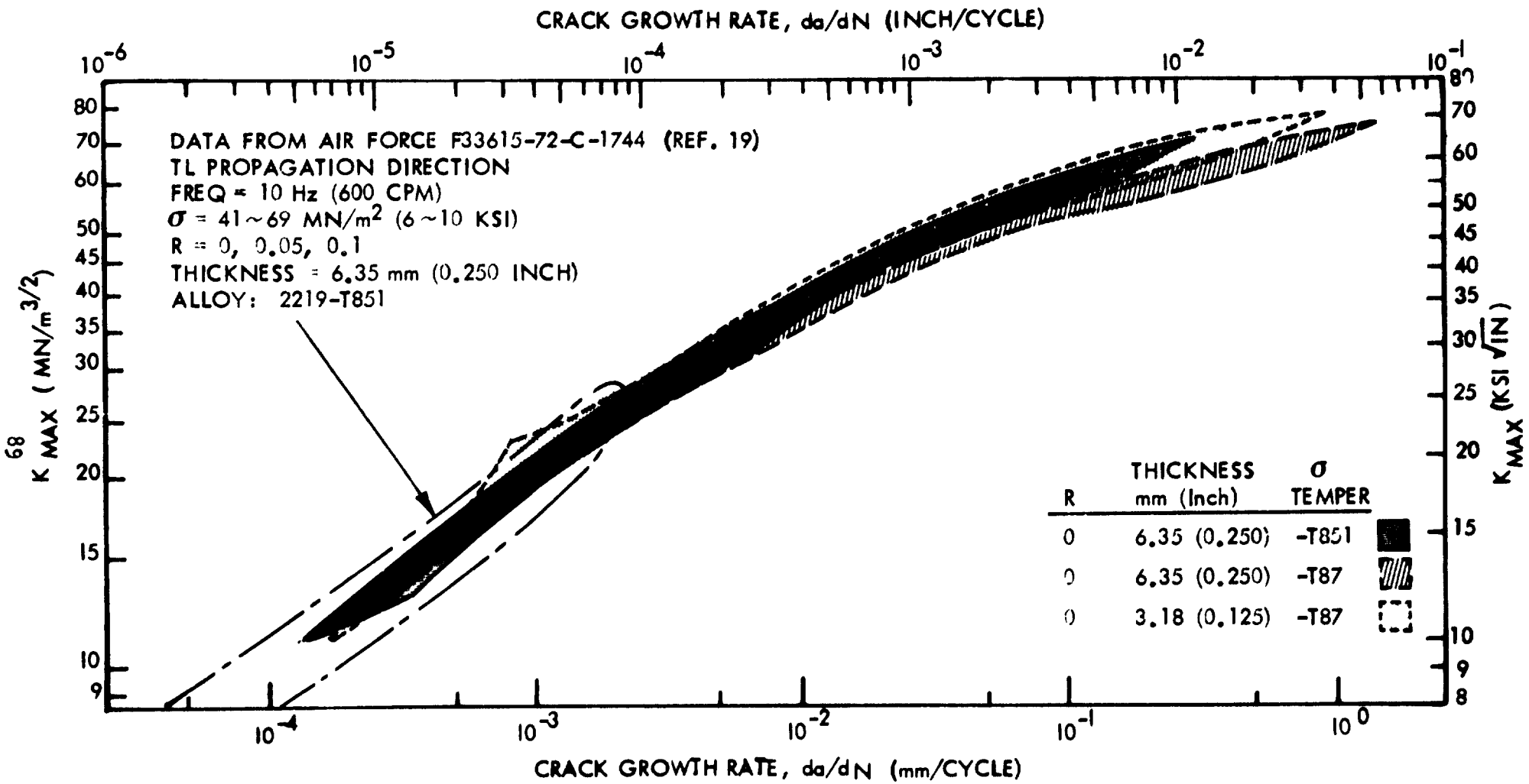


FIGURE 49: PLOT SHOWING COMPARISON OF ROOM TEMPERATURE SENT DATA GENERATED ON THIS PROGRAM WITH ROOM TEMPERATURE DATA GENERATED BY GRUMMAN ON AIR FORCE CONTRACT F33615-72-C-1744 (REF. 19)

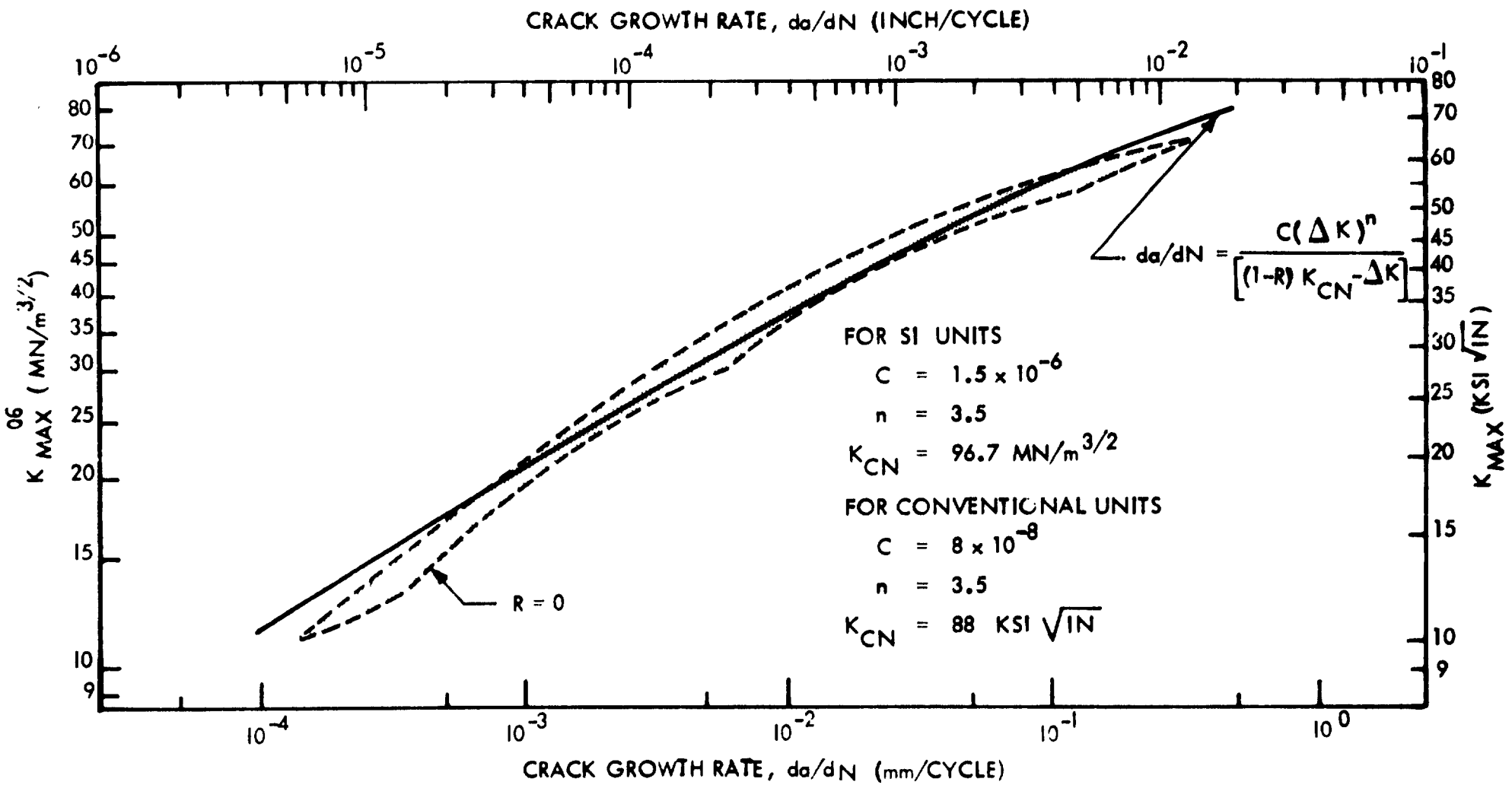


FIGURE 50: PLOT SHOWING FORMAN'S EQUATION FITTED TO ROOM TEMPERATURE 2219-T851 SENT CRACK GROWTH DATA

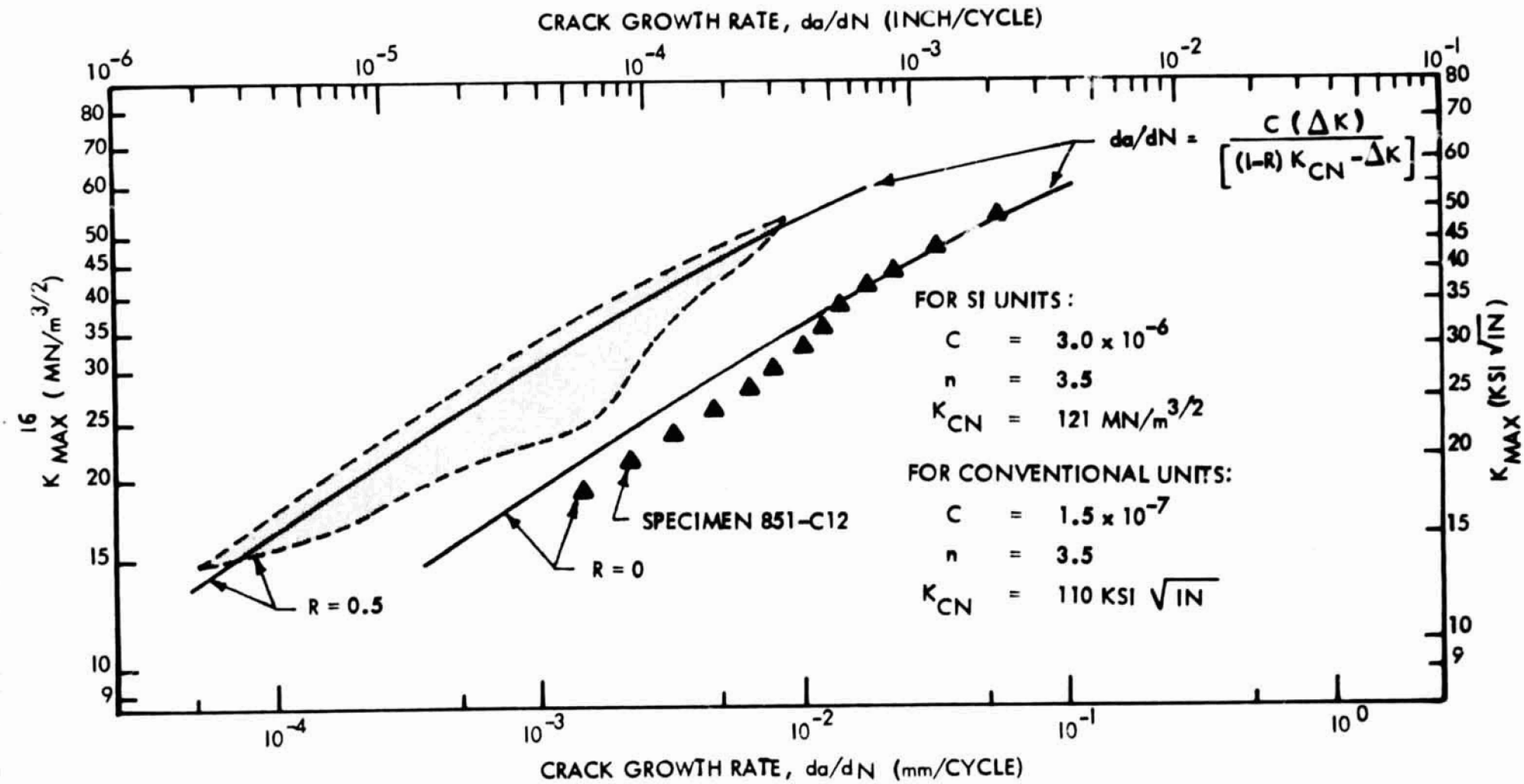


FIGURE 51: PLOT SHOWING FORMAN'S EQUATION FITTED TO 450K (350F) 2219-T851 SENT CRACK GROWTH DATA

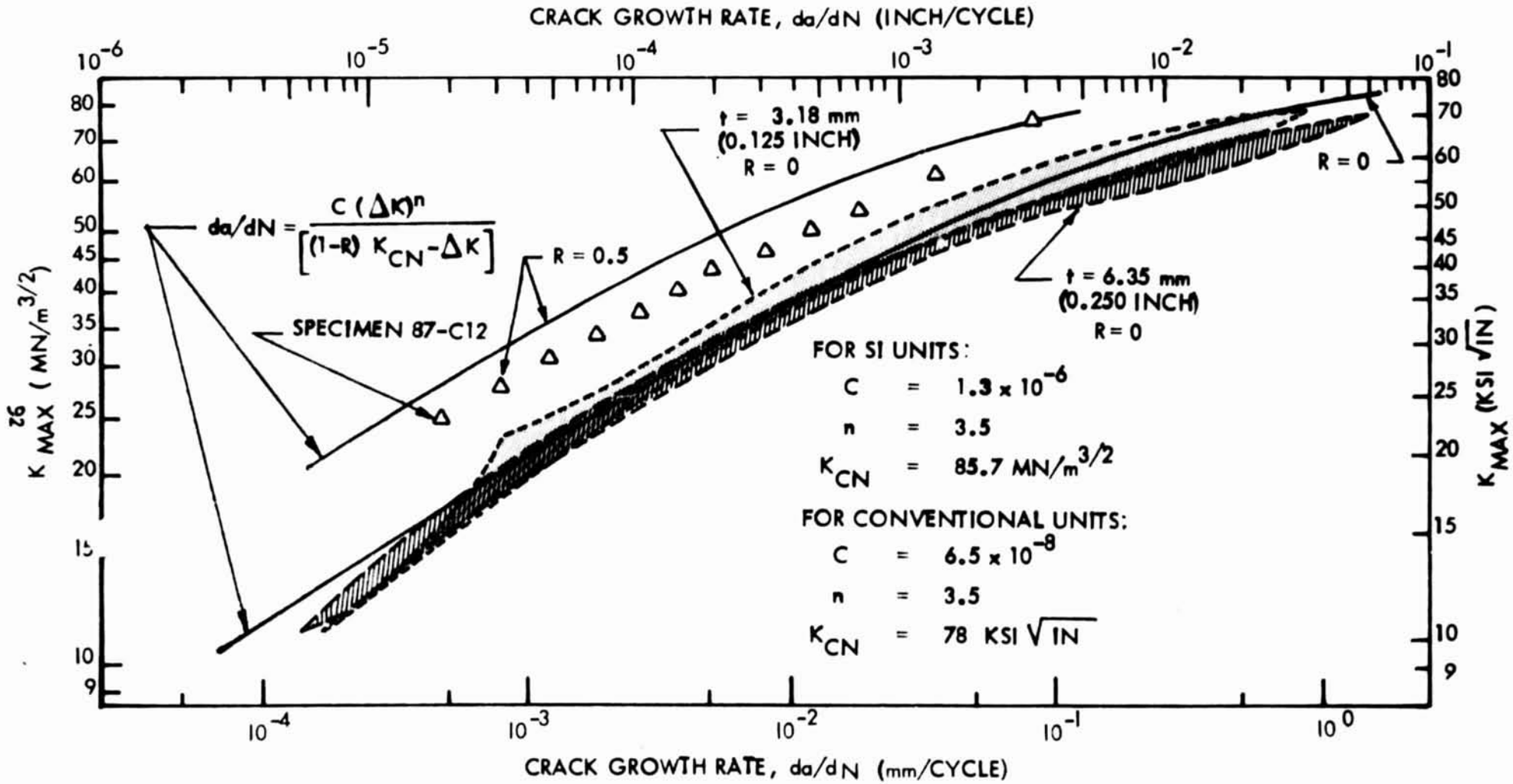


FIGURE 52: PLOT SHOWING FORMAN'S EQUATION FITTED TO ROOM TEMPERATURE 2219-T87 SENT CRACK GROWTH DATA

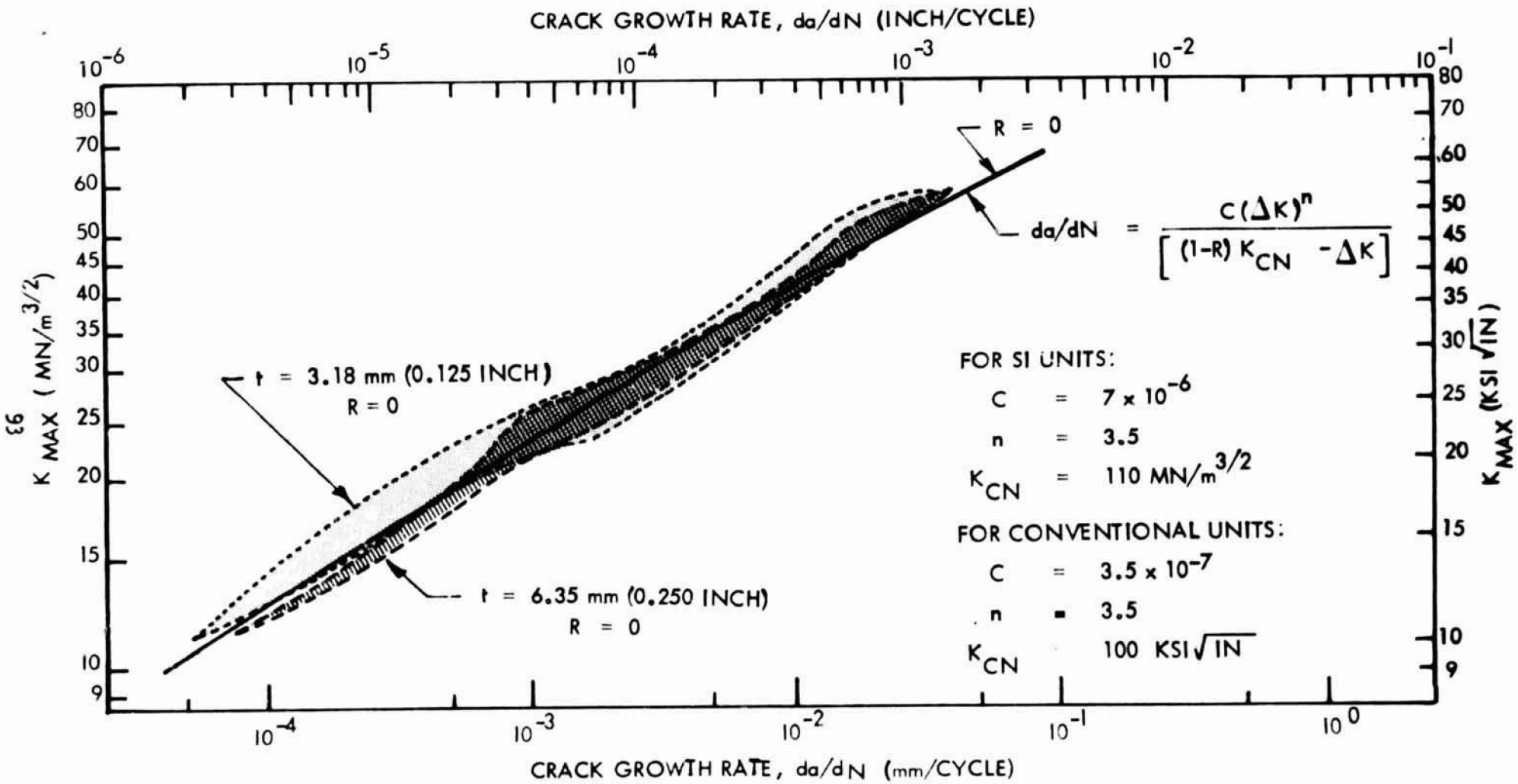


FIGURE 53: PLOT SHOWING FORMAN'S EQUATION FITTED TO 450K (350F) 2219-T87 SENT CRACK GROWTH DATA

| | I.D. | RT $MN/m^2$ (KSI) | ET $MN/m^2$ (KSI) | LOADING PROFILE |
|---|---|---|---|---|
| ○ | 851-SF-C5 | 169 (24.5) | 136 (19.7) | FULL SPECTRUM |
| □ | 851-SF-C6 | 288 (41.7) | 230 (33.4) | FULL SPECTRUM |

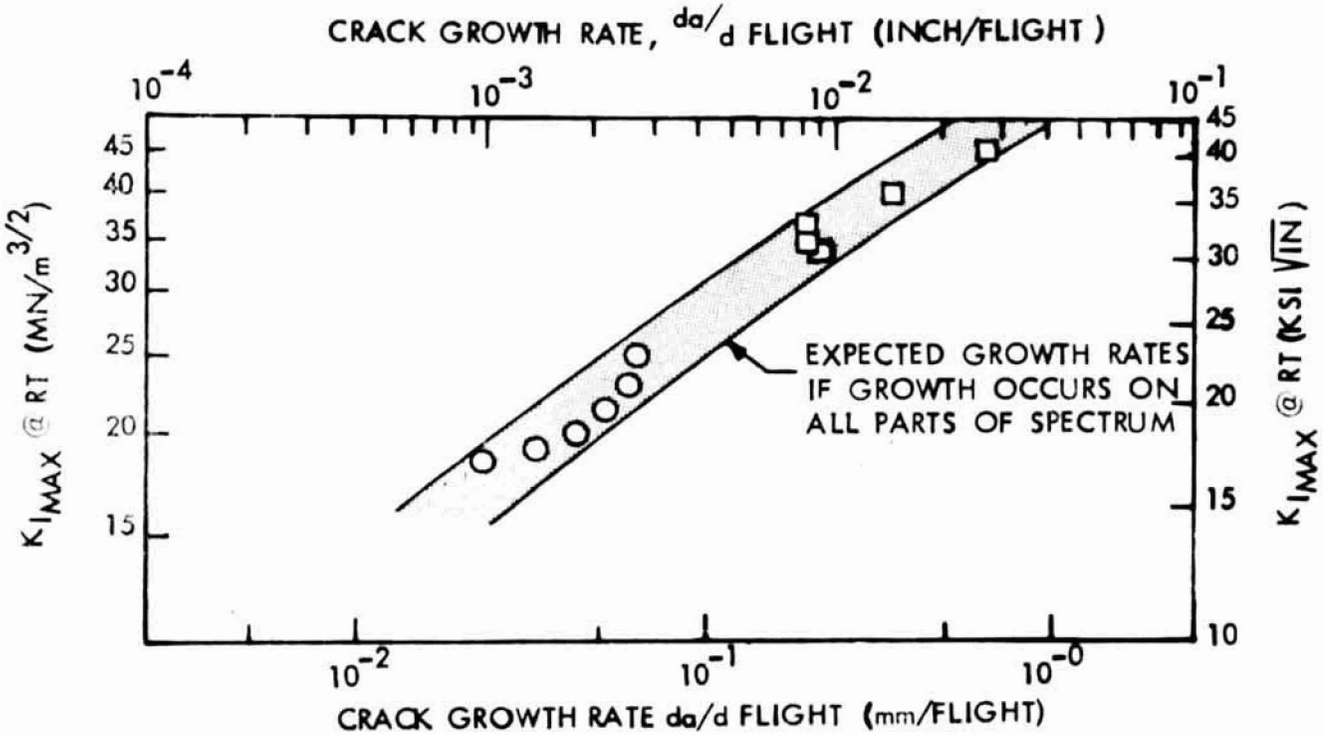


FIGURE 54: PLOT OF CRACK GROWTH RATE VS. $K_{I\,MAX}$ @ R.T. FOR 6.35 mm (0.250 INCH) 2219-T851 SF SPECIMENS TESTED UNDER THERMAL PROFILE LOADING. TS PROPAGATION DIRECTION

| THICKNESS mm (Inch) | | I.D. | RT $MN/m^2$ (KSI) | ET $MN/m^2$ (KSI) | LOADING PROFILE |
|---|---|---|---|---|---|
| 6.35 (0.250) | □ | 87-SF-C5 | 324 (47.0) | 252 (36.6) | FULL SPECTRUM |
| " " | O | 87-SF-C6 | 191 (27.7) | 148 (21.5) | FULL SPECTRUM |
| 3.18 (0.125) | △ | 87-SF-C11 | 324 (47.0) | 252 (36.6) | FULL SPECTRUM |

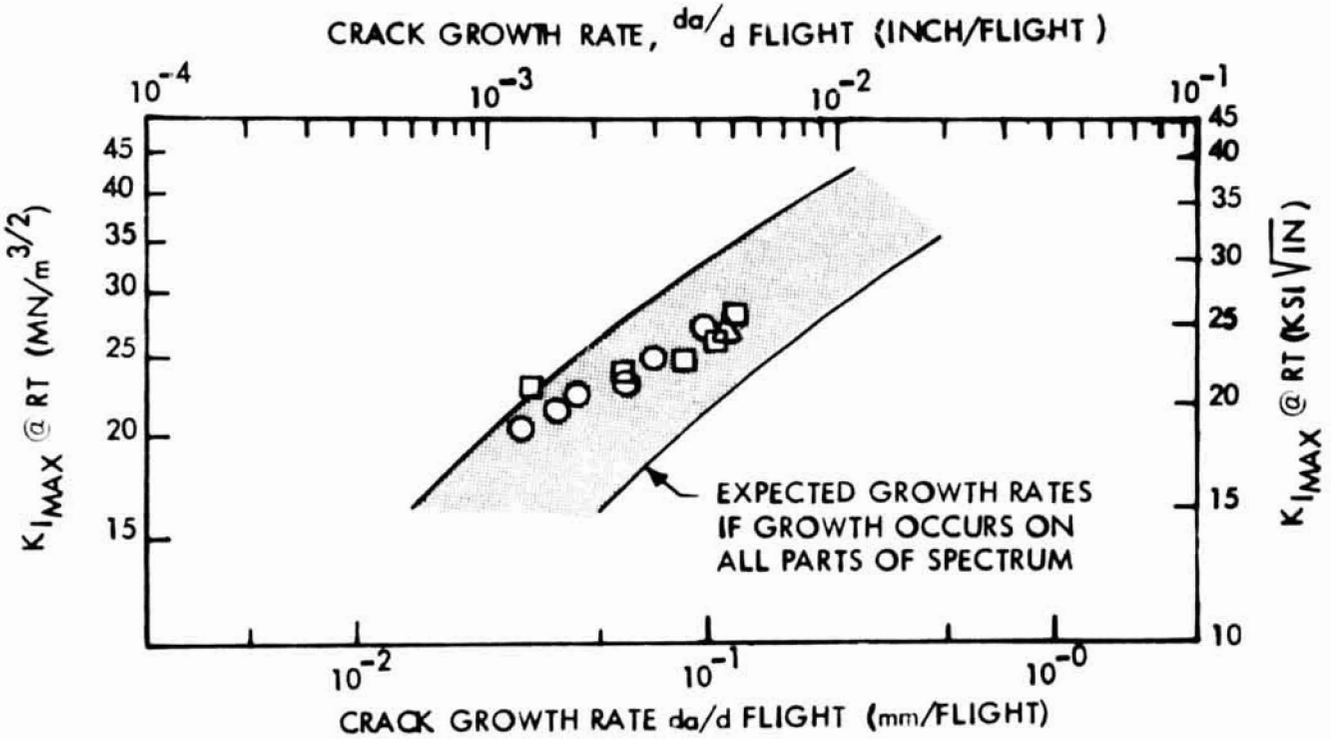


FIGURE 55: PLOT OF CRACK GROWTH RATE VS. $K_{I\ MAX}$ @R.T. FOR 6.35 mm (0.250 INCH) AND 3.18 mm (0.125 INCH) 2219-T87 SF SPECIMENS TESTED UNDER THERMAL PROFILE LOADING. TS PROPAGATION DIRECTION

| | I.D. | RT $MN/m^2$ (KSI) | ET $MN/m^2$ (KSI) | LOADING PROFILE |
|---|---|---|---|---|
| ○ | 851-C9 | 77.2 (11.2) | 62 (9.0) | FULL SPECTRUM |
| ● | 851-C10 | 77.2 (11.2) | 62 (9.0) | MODIFIED FULL SPECTRUM, R = 0, @ ET |
| □ | 851-C11 | 38.6 (5.6) | 31 (4.5) | FULL SPECTRUM |

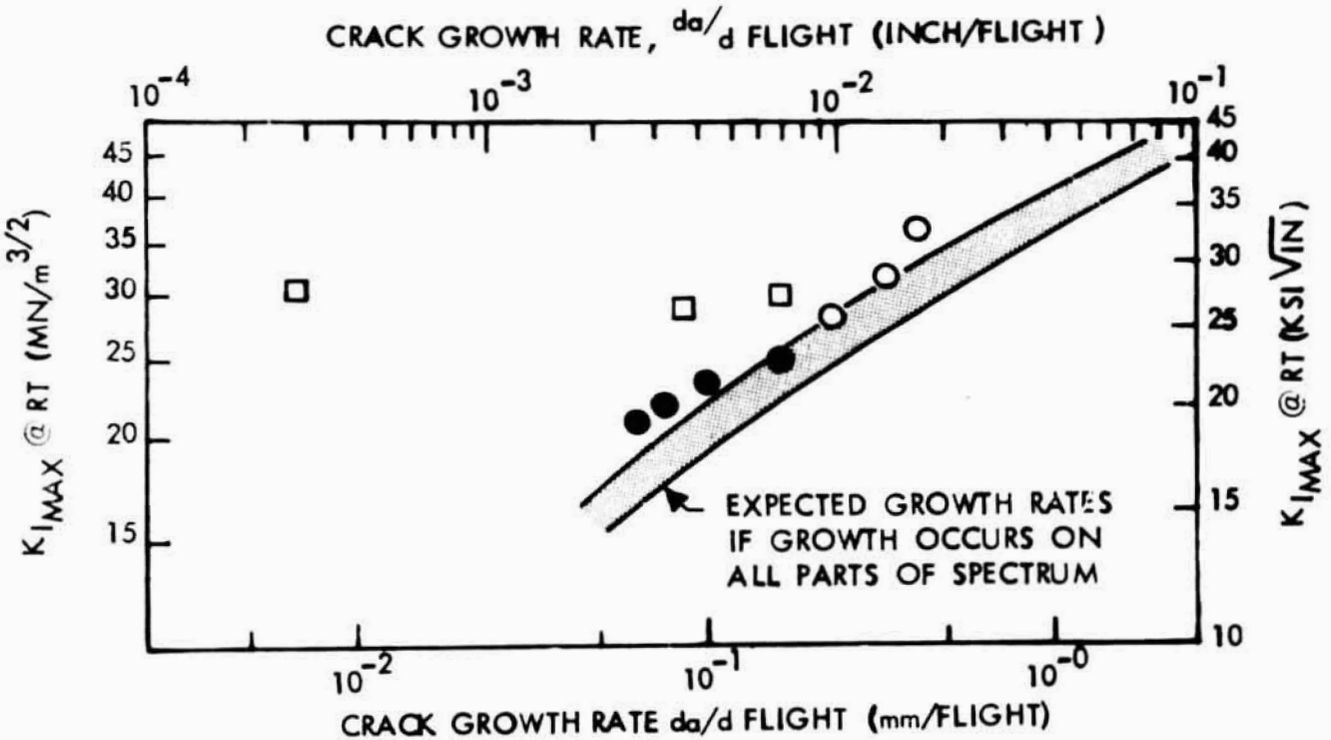


FIGURE 56: PLOT OF CRACK GROWTH RATE VS. $K_{MAX}$ @ RT FOR 6.35 mm (0.250 INCH) 2218-T851 SENT SPECIMENS TESTED UNDER THERMAL PROFILE LOADING. TL PROPAGATION DIRECTION

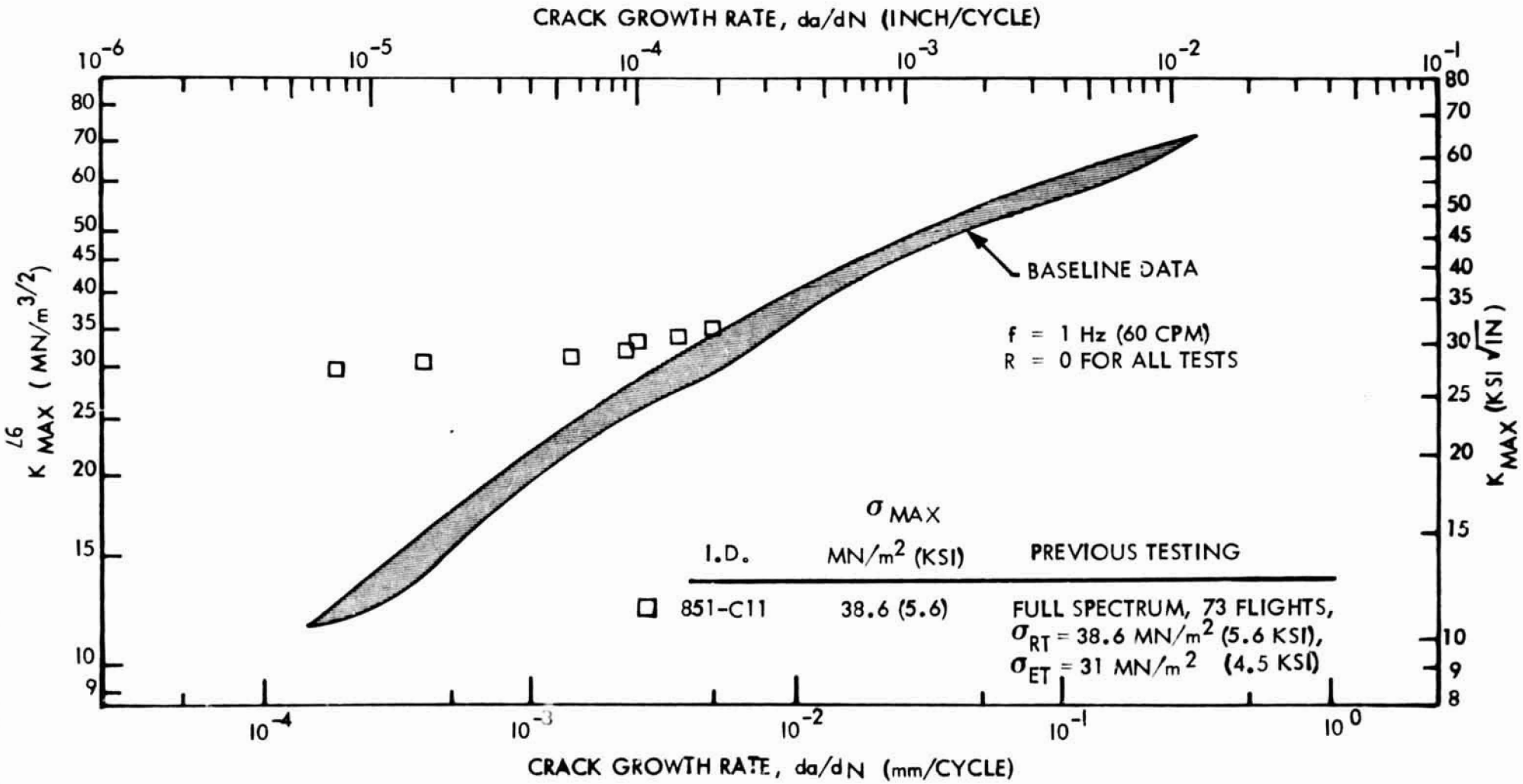


FIGURE 57: PLOT OF CRACK GROWTH RATE VS. $K_{MAX}$ FOR 6.35 mm (0.250 INCH) 2219-T851 SENT SPECIMENS CYCLED AT RT SHOWING RT GROWTH RATE RETARDATION IN SPECIMEN 851-C11

| THICKNESS mm (Inch) | | I.D. | RT $MN/m^2$ (KSI) | ET $MN/m^2$ (KSI) | LOADING PROFILE |
|---|---|---|---|---|---|
| 6.35 (0.250) | ● | 87-C9 | 80 (11.6) | 62 (9.0) | MODIFIED FULL SPECTRUM, ET = 395K(250°F) |
| " " | ○ | 87-C10 | 80 (11.6) | 62 (9.0) | FULL SPECTRUM |
| " " | □ | 87-C11 | 40 ( 5.8) | 31 (4.5) | FULL SPECTRUM |
| 3.18 (0.125) | ▲ | 87-C21 | 80 (11.6) | 62 (9.0) | MODIFIED FULL SPECTRUM, ET = 422K(300°F) |
| " " | ▽ | 87-C23 | 40 ( 5.8) | 31 (4.5) | FULL SPECTRUM |
| " " | ▼ | 87-C24 | 80 (11.6) | 31 (4.5) | MODIFIED FULL SPECTRUM, NO SUSTAINED LOAD AT ET, $\frac{\sigma ET}{\sigma RT} = .5 \frac{\sigma_{ys} @ ET}{\sigma_{ys} @ RT}$ |

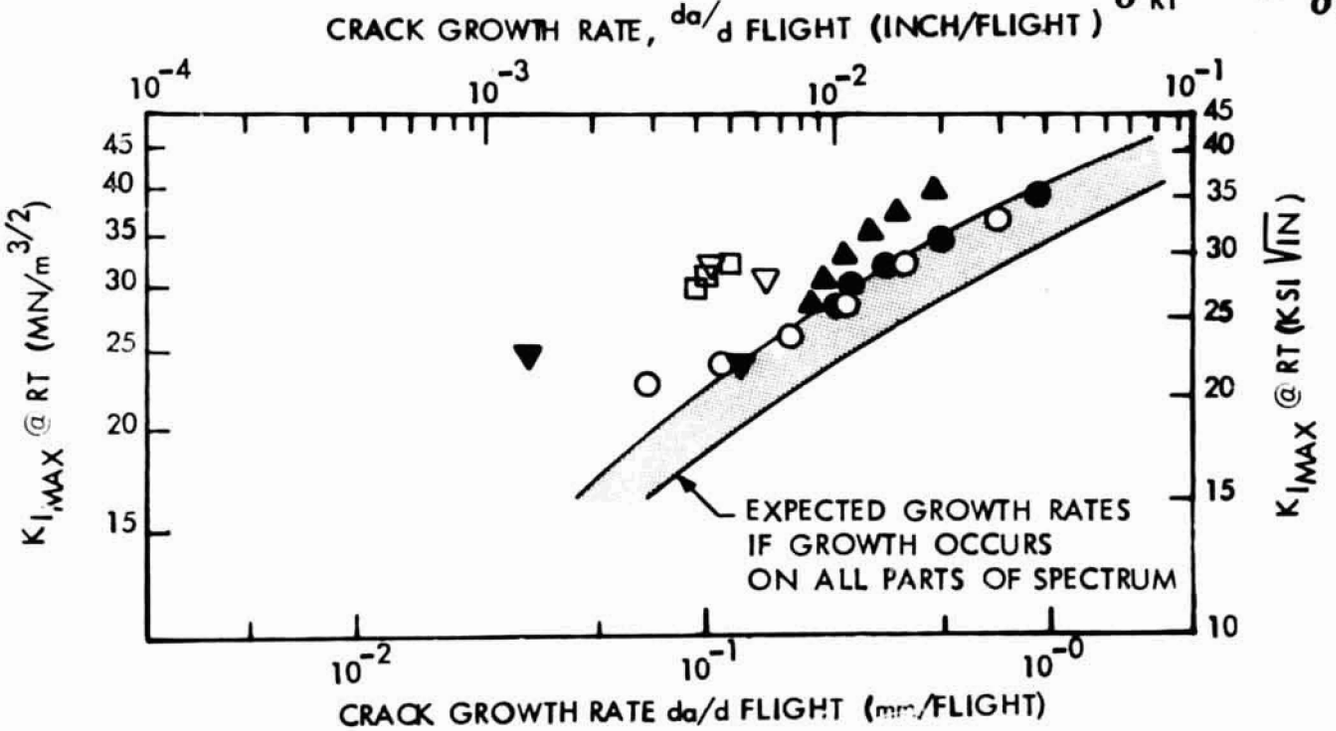


FIGURE 58: PLOT OF CRACK GROWTH RATE VS $K_{MAX}$ @ RT FOR 6.35 mm (0.250 Inch) AND 3.18 mm (0.125 Inch) 2219-T87 SENT SPECIMENS TESTED UNDER THERMAL PROFILE TL PROPAGATION DIRECTION

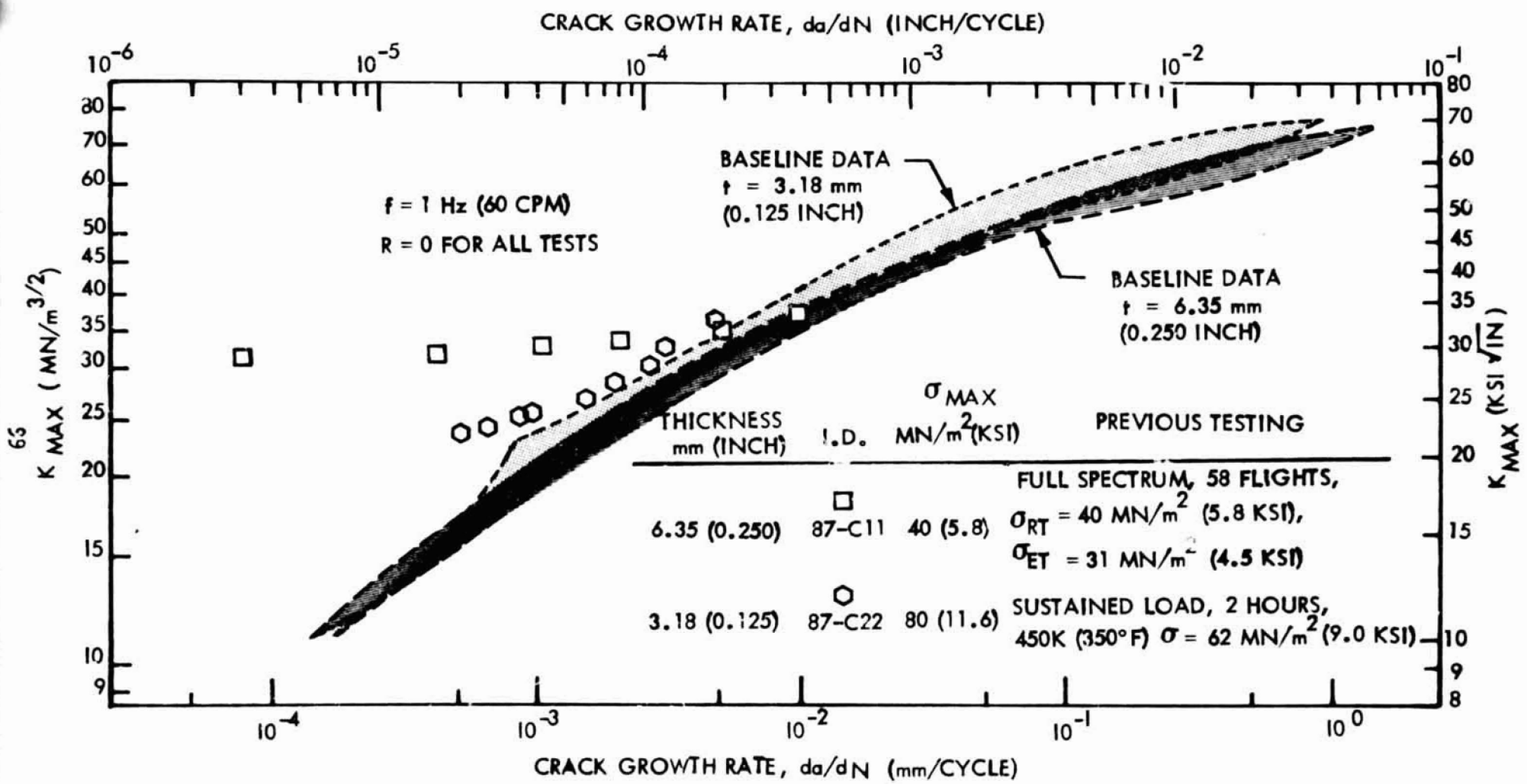


FIGURE 59: PLOT OF CRACK GROWTH RATE VS. $K_{MAX}$ FOR 6.35mm (0.250 INCH) AND 3.18 mm (0.125 INCH) 2219-T87 SENT SPECIMENS CYCLED AT RT SHOWING RT CRACK GROWTH RATE RETARDATION IN SPECIMENS 87-C11 and 87-C22

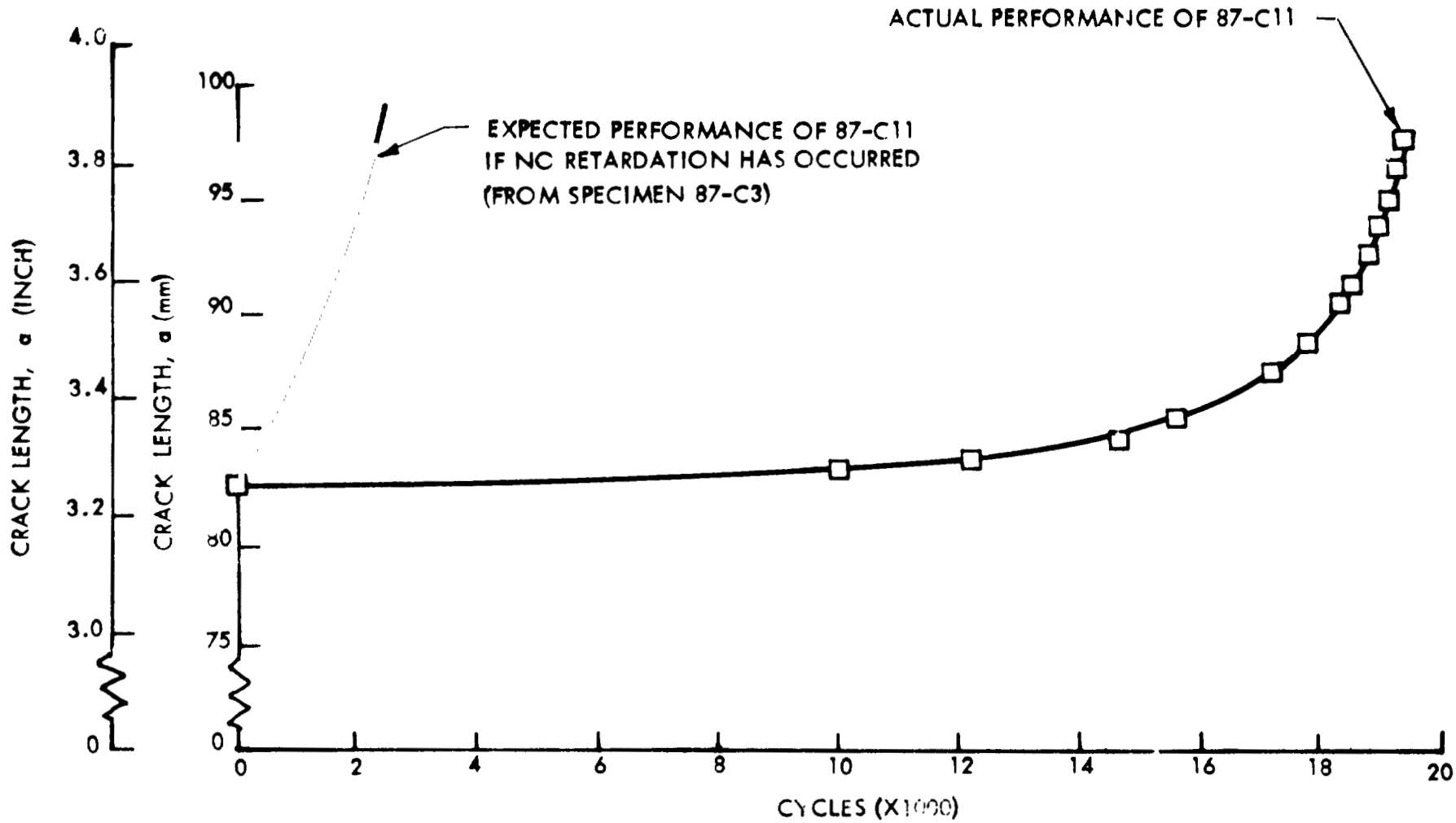


FIGURE 60: PLOT OF CRACK LENGTH VS. CYCLES FOR SENT SPECIMEN 87-C11 CYCLED AT ROOM TEMPERATURE, $\sigma$=40 MN/m$^2$ (5.8 KSI), R = 0 AFTER HAVING BEEN SUBJECTED TO 58 THERMAL PROFILE FLIGHTS

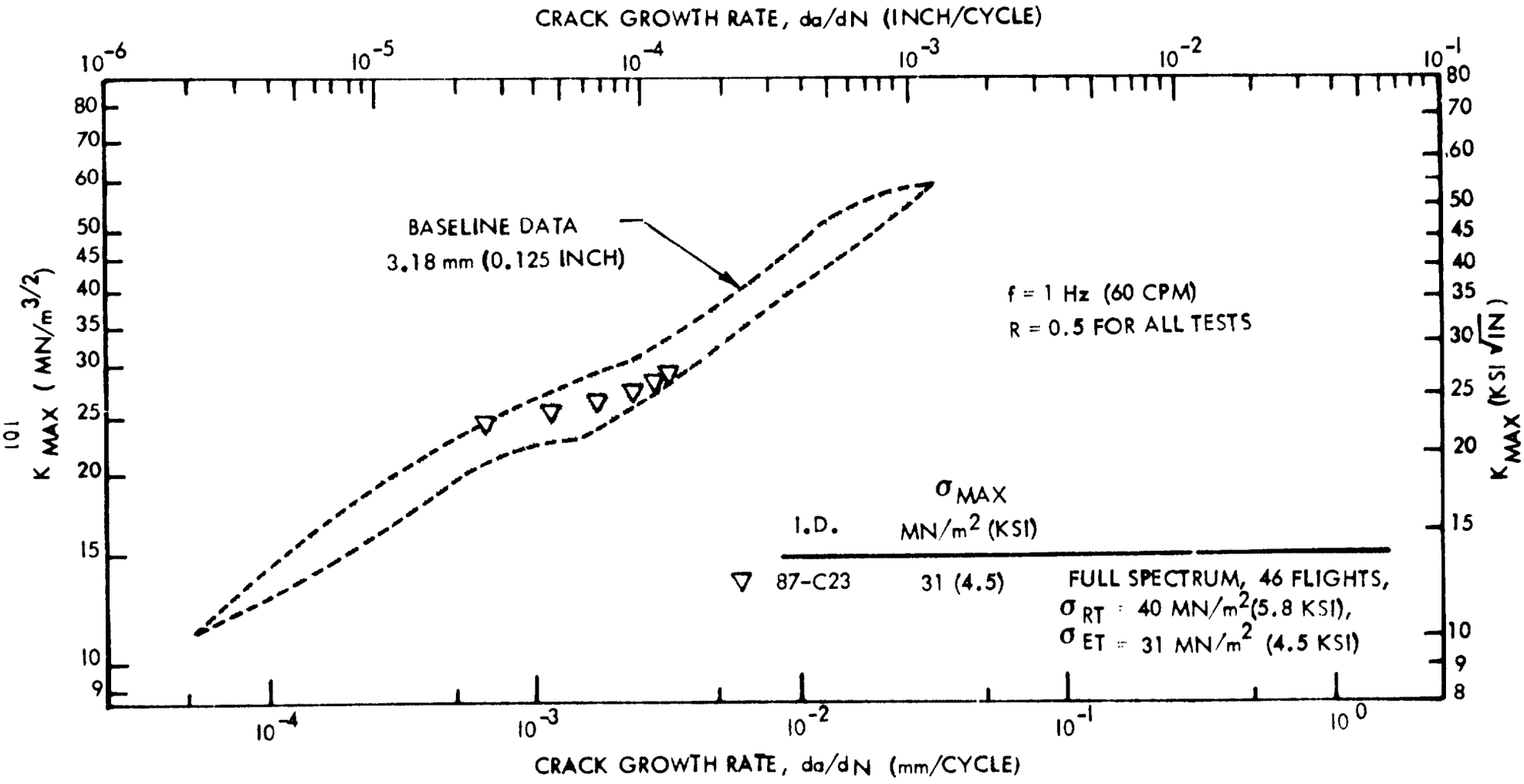


FIGURE 61: PLOT OF CRACK GROWTH RATE VS. $K_{MAX}$ FOR 3.18 mm (0.125 INCH) 2219-T87 SENT SPE MENS CYCLED AT ET SHOWING NO ET CRACK GROWTH RETA..DATION IN S' CIMEN 87-C23.

ORIGINAL PAGE IS
OF POOR QUALITY

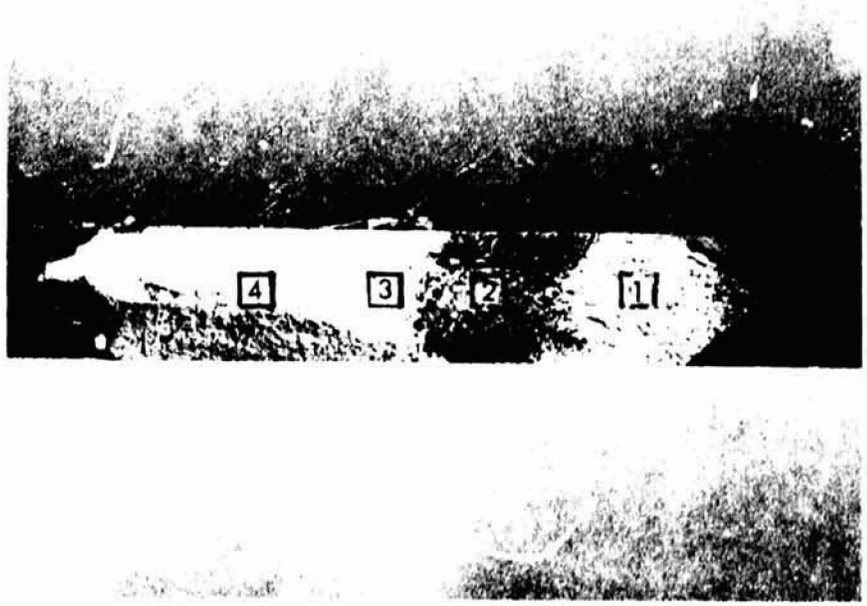


MAG. 3X

1. PRECRACK REGION (Figure 64)
2. THERMAL PROFILE TEST REGION (Figures 65,66 and 67)
3. CONSTANT TEMPERATURE, CONSTANT AMPLITUDE CYCLIC REGION WHERE RETARDED GROWTH RATES WERE APPARENT (Figures 68, 69 and 70)
4. CONSTANT TEMPERATURE CONSTANT AMPLITUDE CYCLIC REGION WHERE CRACK GROWTH RETARDATION WAS DIMINISHED (Figure 71)

FIGURE 62: FRACTURE SURFACE OF 87-C11 AND LOCATIONS FROM WHICH REPLICAS WERE TAKEN

ORIGINAL PAGE IS
OF POOR QUALITY

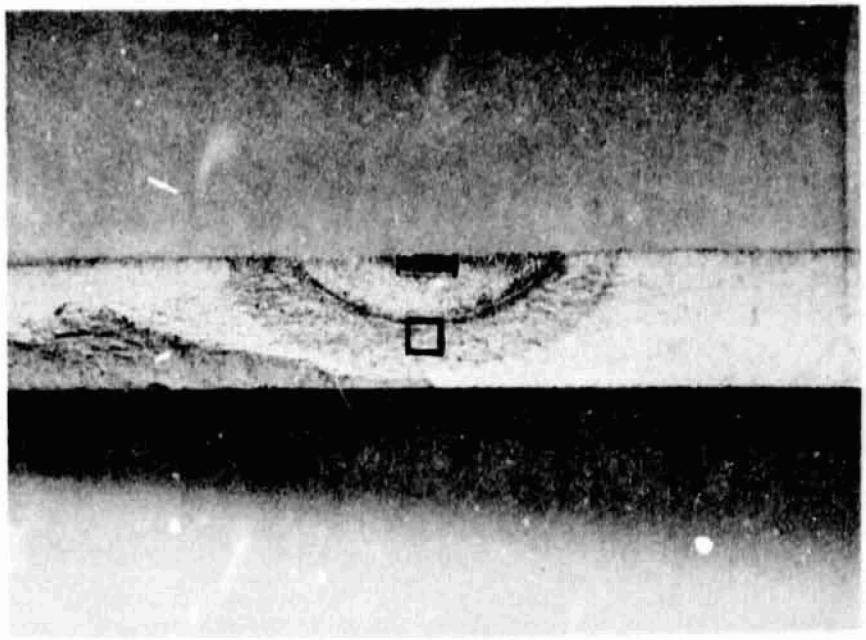

MAG. 3X

FIGURE 63: FRACTURE SURFACE OF 87-SF-C6 AND LOCATION FROM WHICH REPLICA WAS TAKEN

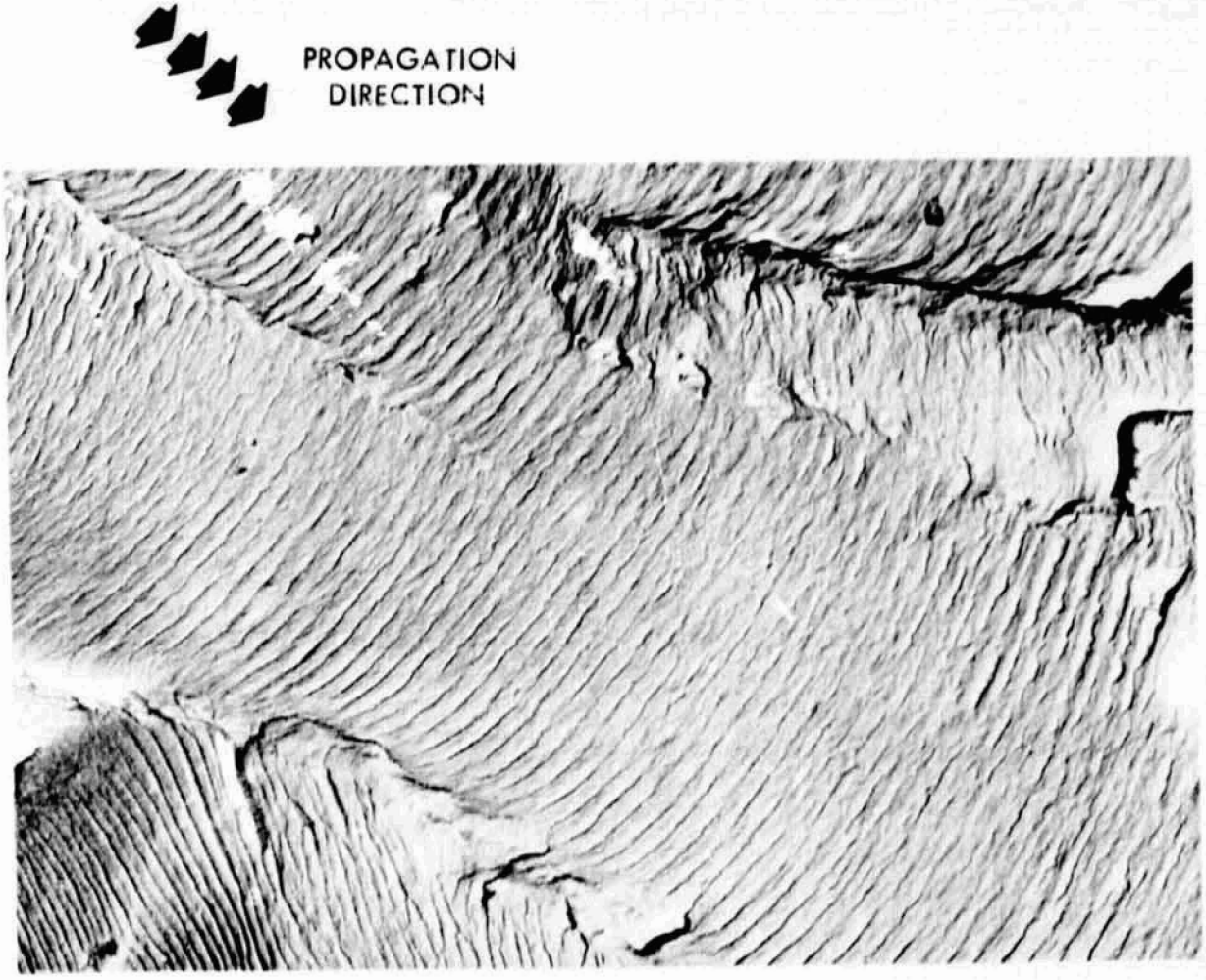


MAG. 4700X

FIGURE 64: TYPICAL FATIGUE STRIATIONS IN THE PRECRACK REGION OF 87-C11

PROPAGATION
DIRECTION

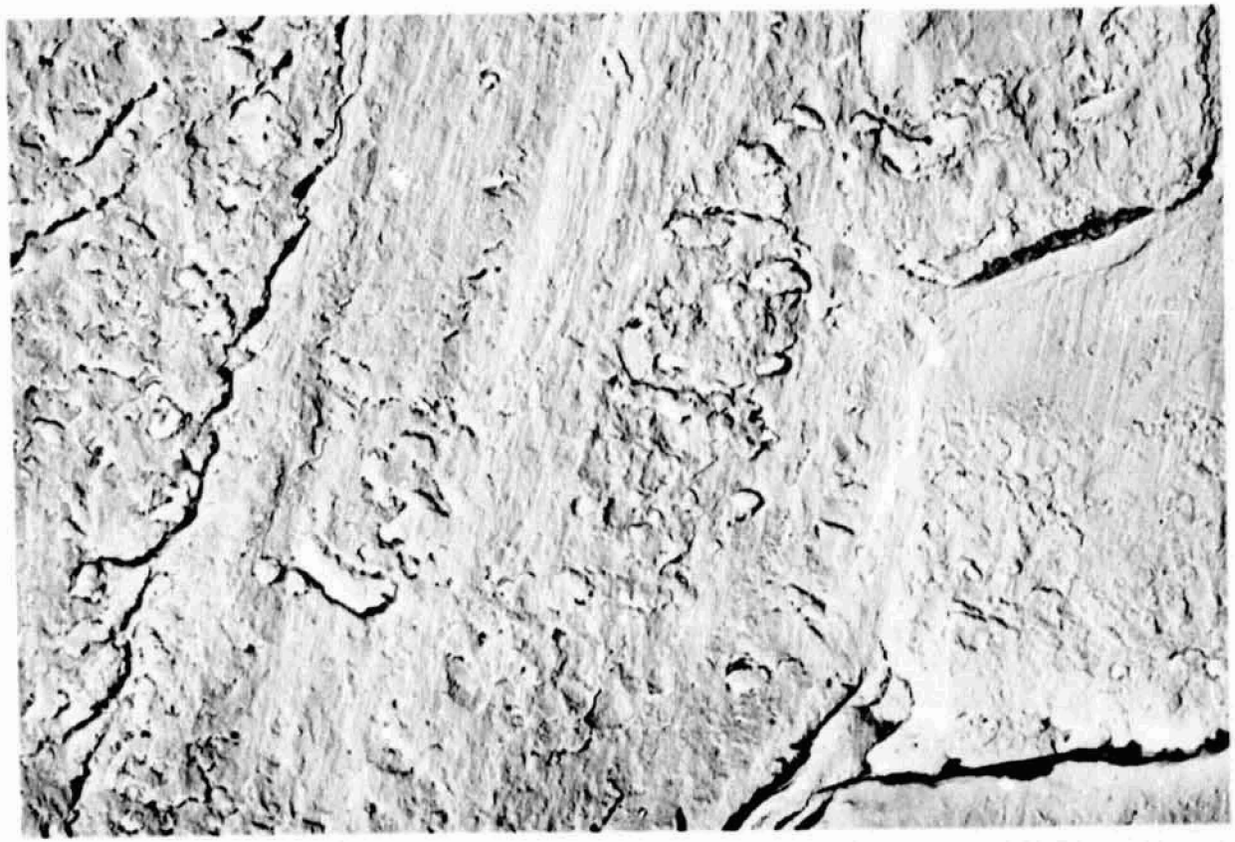

MAG. 5750X

NOTE: "TIRE" TRACKS IN THE MIDDLE, RIGHT SECTION OF PHOTO

FIGURE 65: TYPICAL AREA IN THE THERMAL PROFILE REGION OF SPECIMEN 87-C11

ORIGINAL PAGE IS
OF POOR QUALITY

PROPAGATION
DIRECTION

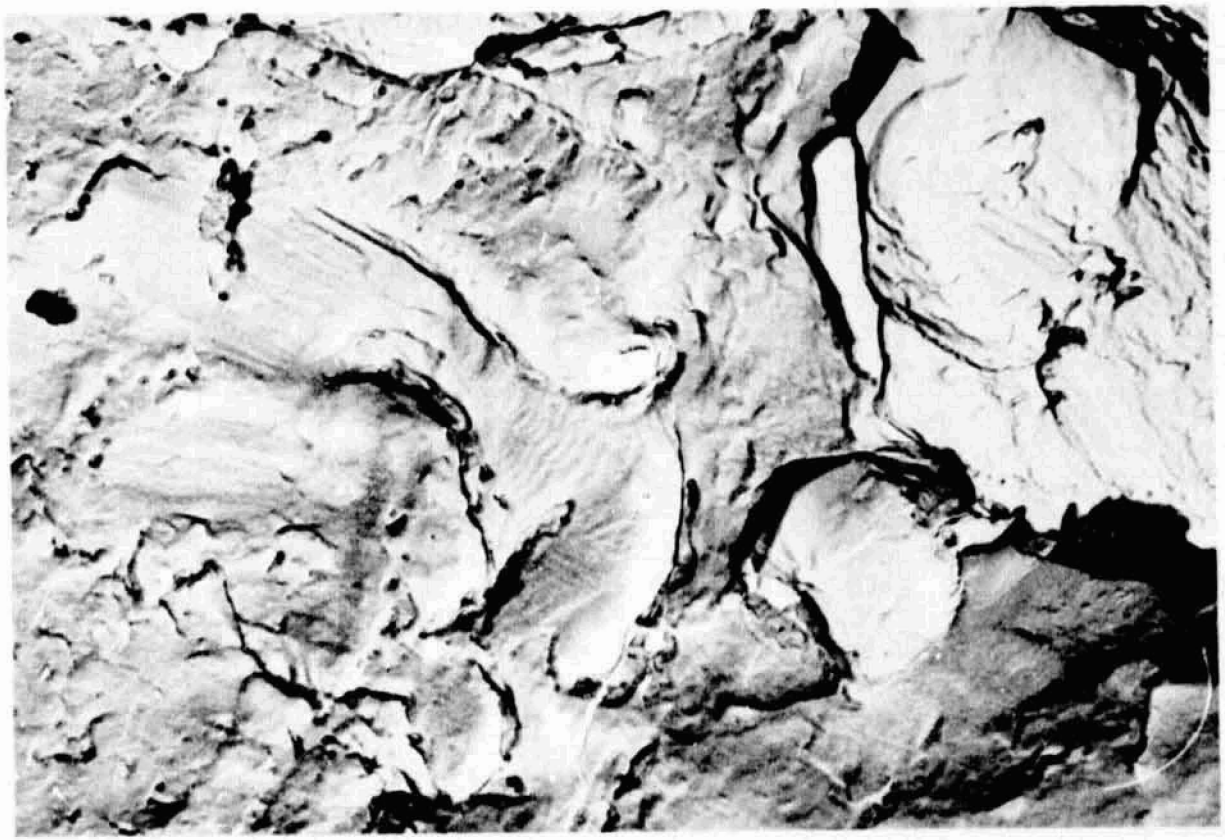

MAG. 17,200 X

NOTE: THE WAVY LINES IN THE CENTER OF THE PHOTO ARE POSSIBLY FATIGUE STRIATIONS.

FIGURE 66: FRACTOGRAPH FROM THE THERMAL PROFILE REGION OF SPECIMEN 87-C11.

PROPAGATION
DIRECTION

MAG. 5750X

FIGURE 67: ELONGATED DIMPLES OCCASIONALLY OBSERVED IN THE THERMAL PROFILE REGION OF SPECIMEN 87-C11.

ORIGINAL PAGE IS
OF POOR QUALITY

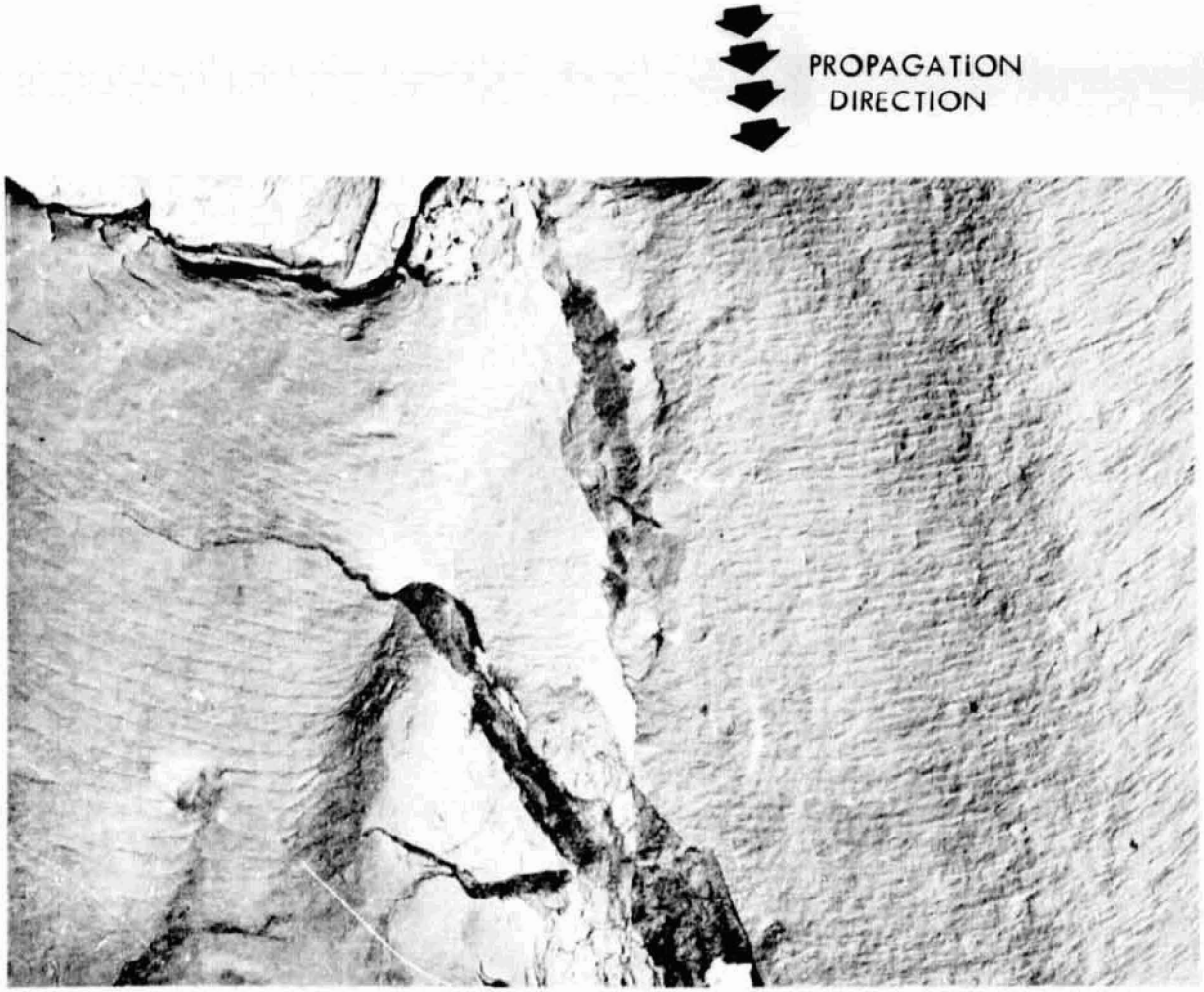


MAG. 5750X

FIGURE 68: FATIGUE STRIATIONS OBSERVED IN THE CONSTANT TEMPERATURE, CONSTANT AMPLITUDE REGION, RIGHT AFTER THE THERMAL PROFILE REGION OF SPECIMEN 87-C11.

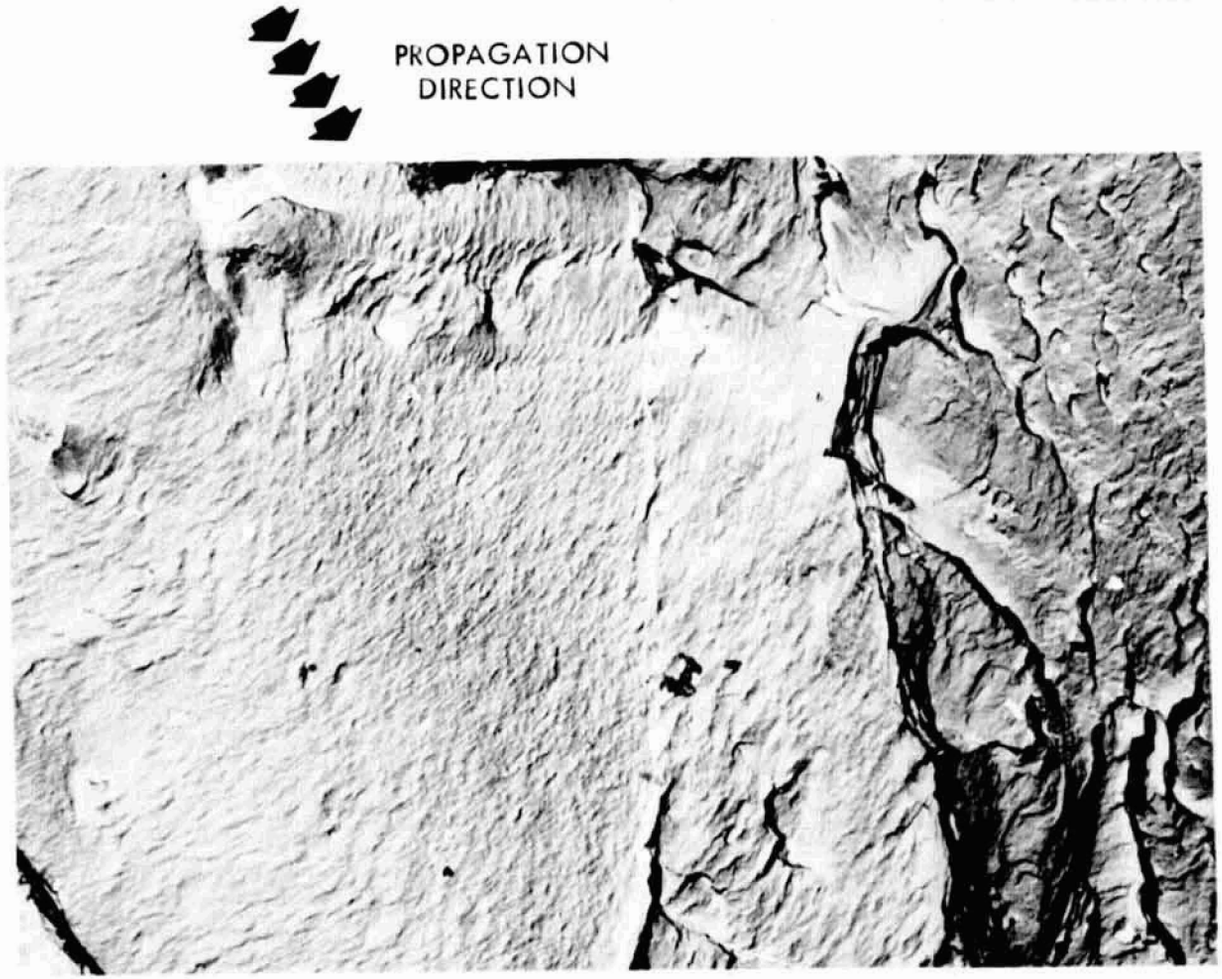


MAG. 5750X

FIGURE 69: FATIGUE STRIATIONS OBSERVED IN THE CONSTANT TEMPERATURE, CONSTANT AMPLITUDE REGION OF SPECIMEN 87-C11, 0.64mm (0.025 INCH) FURTHER FROM ORIGIN THAN Figure 68.

ORIGINAL PAGE IS
OF POOR QUALITY

PROPAGATION
DIRECTION

MAG 5750X

FIGURE 70: TYPICAL APPEARANCE OF THE CONSTANT TEMPERATURE, CONSTANT AMPLITUDE REGION OF 87-C11, AFTER THE THERMAL PROFILE REGION.

PROPAGATION
DIRECTION

MAG. 5750X

FIGURE 71: FATIGUE STRIATIONS FURTHER ALONG IN CONSTANT TEMPERATURE, CONSTANT AMPLITUDE REGION OF SPECIMEN 87-C11, WHERE CRACK GROWTH RETARDATION WAS DIMINISHED.

ORIGINAL PAGE IS
OF POOR QUALITY

PROPAGATION
DIRECTION

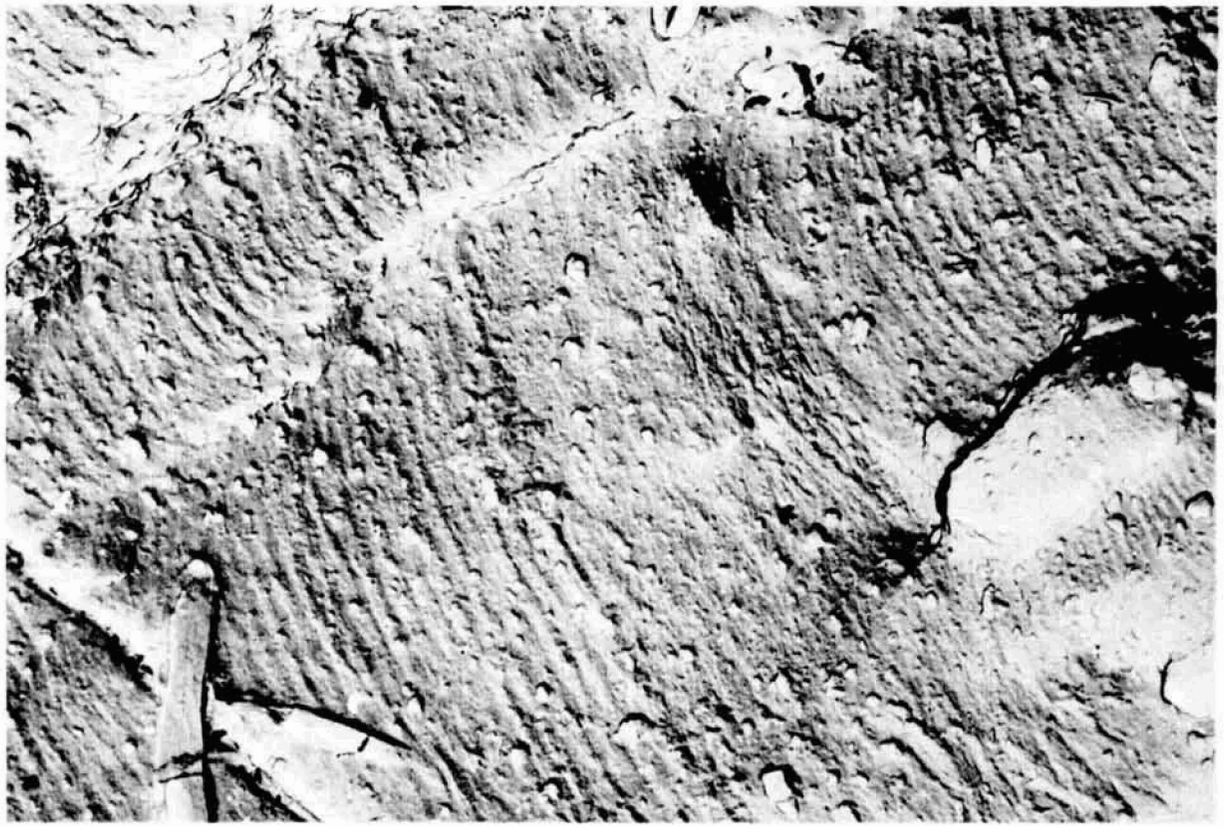

MAG. 5750X

NOTE: THE WIDE STRIATION IN THE CENTRAL PART OF THE PHOTOGRAPH IS PROBABLY A RESULT OF THE SINGLE LOAD APPLICATION AND HOLD WHERE TEMPERATURE INCREASED FROM 155K (-200°K) TO 450K (350°F). (Reentry Portion of Spectrum)

FIGURE 72: THERMAL PROFILE REGION ON THE SURFACE FLAW SPECIMEN.

PROPAGATION
DIRECTION

MAG. 5750 X

FIGURE 73: THERMAL PROFILE REGION ON SURFACE OF FLAW SPECIMEN SHOWING ACICULAR MATERIAL OBSERVED THROUGHOUT MUCH OF THE REPLICA.

ORIGINAL PAGE IS
OF POOR QUALITY

TABLE 1 : SUMMARY OF MECHANICAL PROPERTY, STATIC FRACTURE AND CONSTANT AMPLITUDE, CONSTANT TEMPERATURE CYCLIC TESTS

| ALLOY & TEMPER | THICKNESS mm (Inch) | MECHANICAL PROPERTY TESTS | | | STATIC FRACTURE TESTS | | | | | | CONSTANT AMPLITUDE, CONSTANT TEMPERATURE CYCLIC TESTS | | | | | | |
|---|---|---|---|---|---|---|---|---|---|---|---|---|---|---|---|---|---|
| | | | | | * SF SPECIMEN (a/2c = 0.3) | | | SENT ** SPECIMEN | | | SF SPECIMEN (a/2c = 0.3) | | SENT SPECIMEN | | | | |
| | | | | | | | | | | | | | RT | | 450K (350°F) | | |
| | | 144K (-200°F) | RT | 450K (350°F) | 144K (-200°F) | RT | 450K (350°F) | 144K (-200°F) | RT | 450K (350°F) | RT R = 0 | 450K (350°F) R = 0.5 | R = 0 | R = 0.5 | R = 0 | R = 0.5 | R = 0.5 ▷1▷2 |
| 2219-T851 | 6.35 (0.250) | 4 | 4 | 4 | 1 | 1 | 1 | 2 | 2 | 2 | 2 | 2 | 4 | — | 1 | 4 | 2 |
| 2219-T87 | 6.35 (0.250) | 4 | 4 | 4 | 1 | 2 | 1 | 2 | 2 | 2 | 2 | 2 | 4 | 1 | — | 4 | 1 |
| | 3.18 (0.125) | 4 | 4 | 4 | 1 | 1 | 1 | 2 | 2 | 2 | 2 | 2 | 4 | — | — | 4 | — |

* SF = SURFACE FLAW
** SENT = SINGLE EDGE NOTCH TENSION
▷1▷ 2 MINUTE HOLD AT MAXIMUM STRESS DURING EACH CYCLE
▷2▷ SUSLIC TEST

PRECEDING PAGE BLANK NOT FILMED

TABLE 2: SUMMARY OF LOAD/ THERMAL PROFILE TESTS

| ALLOY & TEMPER | THICKNESS mm (Inch) | THERMAL PROFILE TESTS | | CONSTANT AMPLITUDE CONSTANT TEMPERATURE CYCLIC TEST FOLLOWING THERMAL PROFILE LOADING | SUSTAINED LOAD TEST FOLLOWED BY CONSTANT AMPLITUDE CONSTANT TEMPERATURE CYCLIC TEST |
|---|---|---|---|---|---|
| | | * SF SPECIMEN (a/2c = .3) | ** SENT SPECIMEN | ** SENT SPECIMEN | ** SENT SPECIMEN |
| 2219-T851 | 6.35 (0.250) | 2 | 3 | 1 | — |
| 2219-T87 | 6.35 (0.250) | 2 | 3 | 1 | — |
| | 3.18 (0.125) | 2 | 3 | 1 | 1 |

* SF = SURFACE FLAW

** SENT = SINGLE EDGE NOTCH SPECIMEN

TABLE 3: CHEMICAL COMPOSITION OF ALUMINUM ALLOYS (% BY WEIGHT) AS DETERMINED BY BOEING AEROSPACE COMPANY TESTS

| ELEMENT | 2219-T851 PL 6.35 mm (0.25 INCH) ALCOA HEAT 215061 | 2219-T87 PL 6.35 mm (0.25 INCH) ALCOA HEAT 215091 |
|---|---|---|
| COPPER | 6.40 | 6.33 |
| MANGANESE | 0.30 | 0.30 |
| VANADIUM | 0.08 | 0.06 |
| SILICON | 0.10 | 0.12 |
| IRON | 0.21 | 0.19 |
| MAGNESIUM | 0.016 | 0.018 |
| ZINC | 0.03 | 0.03 |
| TITANIUM | 0.04 | 0.04 |
| ZIRCONIUM | 0.18 | 0.16 |
| ALUMINUM | BALANCE | BALANCE |

CLEANLINESS RATING OF BOTH HEATS — CLASSIFICATION "A" PER ASTM E-45-63, AS DETERMINED BY BOEING AEROSPACE COMPANY TESTS.

**TABLE 4: MECHANICAL PROPERTIES OF 6.35 mm (0.25 Inch) 2219-T851 ALUMINUM ALLOY**

| SPECIMEN NUMBER | MEASURED THICKNESS, mm (INCH) | GRAIN DIRECTION: L = LONGITUDINAL T = TRANSVERSE | TEST TEMPERATURE °K (°F) | ULTIMATE STRENGTH $MN/m^2$ (KSI) | YIELD STRENGTH $MN/m^2$ (KSI) | ELONGATION % IN 25.4 mm (1.0 INCH) | ELONGATION % IN 50.8 mm (2.0 INCH) | REDUCTION IN AREA, % | POISSON'S RATIO | YOUNG'S MODULUS $E \times 10^3$ $MN/m^2$ ($E \times 10^6$ PSI) |
|---|---|---|---|---|---|---|---|---|---|---|
| 851-L-1 | 6.34 (0.2497) | L | 144 (-200) | 502 (72.8) | 388 (56.3) | 16 | 11 | 35 | - | - |
| -2 | 6.36 (0.2502) | L | ↓ | 502 (72.8) | 388 (56.3) | 17 | 11 | 34 | 0.286 | 74.5 (10.8) |
| Avg. | | | | 502 (72.8) | 388 (56.3) | 16 | 11 | 34 | | |
| 851-T-1 | 6.32 (0.2487) | T | | 507 (73.5) | 377 (54.7) | 17 | 12 | 26 | - | - |
| -2 | 6.33 (0.2492) | T | | 508 (73.7) | 379 (55.0) | 16 | 11 | 25 | 0.297 | 81.4 (11.8) |
| Avg. | | | | 507 (73.6) | 378 (54.8) | 16 | 11 | 25 | | |
| 851-L-3 | 6.33 (0.2492) | L | 291 (65) | 452 (65.6) | 348 (50.4) | 17 | 12 | 34 | - | - |
| -4 | 6.33 (0.2494) | L | ↓ | 454 (65.8) | 348 (50.5) | 18 | 12 | 35 | 0.303 | 75.8 (11.0) |
| Avg. | | | | 453 (65.7) | 348 (50.4) | 17 | 12 | 34 | | |
| 851-T-3 | 6.30 (0.2480) | T | | 456 (66.1) | 336 (48.8) | 17 | 12 | 28 | - | - |
| -4 | 6.31 (0.2483) | T | | 456 (66.2) | 339 (49.2) | 14 | 11 | 28 | 0.317 | 82.7 (12.0) |
| Avg. | | | | 456 (66.1) | 337 (49.0) | 15 | 11 | 28 | | |
| 851-L-5 | 6.32 (0.2490) | L | 450 (350) | 328 (47.5) | 281 (40.7) | 27 | 17 | 58 | - | - |
| -6 | 6.33 (0.2494) | L | ↓ | 326 (47.3) | 277 (40.2) | 23 | 18 | 59 | 0.331 | 67.6 (9.8) |
| Avg. | | | | 327 (47.4) | 279 (40.4) | 25 | 17 | 58 | | |
| 851-T-5 | 6.32 (0.2488) | T | | 325 (47.1) | 270 (39.1) | 29 | 18 | 56 | - | - |
| -6 | 6.33 (0.2492) | T | | 325 (47.2) | 273 (39.6) | 26 | 18 | 58 | 0.332 | 64.8 (9.4) |
| Avg. | | | | 325 (47.1) | 271 (39.3) | 27 | 18 | 57 | | |

TABLE 5: MECHANICAL PROPERTIES OF 6.35 mm (0.25 Inch) 2219-T87 ALUMINUM ALLOY

| SPECIMEN NUMBER | MEASURED THICKNESS, mm (INCH) | GRAIN DIRECTION: L = LONGITUDINAL T = TRANSVERSE | TEST TEMPERATURE °K (°F) | ULTIMATE STRENGTH $MN/m^2$ (KSI) | YIELD STRENGTH $MN/m^2$ (KSI) | ELONGATION % IN 25.4 mm (1.0 INCH) | ELONGATION % IN 50.8 mm (2.0 INCH) | REDUCTION IN AREA, % | POISSON'S RATIO | YOUNG'S MODULUS E, $10^3$ $MN/m^2$ (E, $10^6$ psi) |
|---|---|---|---|---|---|---|---|---|---|---|
| 87-L-1 | 6.25 (0.2460) | L | 144 (-200) | 525 (76.1) | 425 (61.7) | 15 | 11 | 27 | - | - |
| -2 | 6.28 (0.2471) | L | ↓ | 525 (76.1) | 425 (61.6) | 12 | 11 | 31 | 0.290 | [illegible] (11.3) |
| Avg. | | | | 525 (76.1) | 425 (61.6) | 13 | 11 | 29 | | |
| 87-T-1 | 6.30 (0.2481) | T | | 536 (77.7) | 430 (62.3) | 14 | 10 | 18 | - | - |
| -2 | 6.26 (0.2465) | T | | 541 (78.5) | 427 (61.3) | 13 | 9 | 13 | 0.289 | 75.8 (11.0) |
| Avg. | | | | 538 (78.1) | 428 (62.1) | 13 | 9 | 15 | | |
| 87-L-3 | 6.28 (0.2474) | L | 291 (65) | 468 (67.9) | 381 (55.3) | 19 | 13 | 35 | - | - |
| -4 | 6.27 (0.2467) | L | ↓ | 469 (68.0) | 380 (55.1) | 16 | 12 | 33 | 0.311 | 73.1 (10.6) |
| Avg. | | | | 468 (67.9) | 380 (55.2) | 17 | 12 | 34 | | |
| 87-T-3 | 6.29 (0.2476) | T | | 476 (69.0) | 381 (55.3) | 12 | 10 | 20 | - | - |
| -4 | 6.32 (0.2488) | T | | 478 (69.3) | 381 (55.3) | 14 | 11 | 22 | 0.316 | 79.3 (11.5) |
| Avg. | | | | 477 (69.1) | 381 (55.3) | 13 | 10 | 21 | | |
| 87-L-5 | 6.30 (0.2482) | L | 450 (350) | 327 (47.4) | 293 (42.5) | 21 | 14 | 51 | - | - |
| -6 | 6.31 (0.2486) | L | ↓ | 327 (47.4) | 289 (41.9) | 20 | 14 | 53 | 0.316 | 66.2 (9.6) |
| Avg. | | | | 327 (47.4) | 291 (42.2) | 20 | 14 | 52 | | |
| 87-T-5 | 6.29 (0.2477) | T | | 334 (48.5) | 294 (42.6) | 23 | 15 | 48 | - | - |
| -6 | 6.28 (0.2473) | T | | 330 (47.9) | 296 (43.0) | 27 | 17 | 52 | 0.332 | 64.8 (9.4) |
| Avg. | | | | 332 (48.2) | 295 (42.8) | 25 | 16 | 50 | | |

TABLE 6: MECHANICAL PROPERTIES OF 3.18 mm (0.125 INCH) 2219-T87 ALUMINUM ALLOY

| SPECIMEN NUMBER | MEASURED THICKNESS, mm (INCH) | GRAIN DIRECTION: L = LONGITUDINAL T = TRANSVERSE | TEST TEMPERATURE °K (°F) | ULTIMATE STRENGTH $MN/m^2$ (KSI) | YIELD STRENGTH $MN/m^2$ (KSI) | ELONGATION % IN 25.4 mm (1.0 INCH) | ELONGATION % IN 50.8 mm (2.0 IN) | REDUCTION IN AREA, % | POISSON'S RATIO | YOUNG'S MODULUS $E \times 10^3$ $MN/m^2$ ($E \times 10^6$ PSI) |
|---|---|---|---|---|---|---|---|---|---|---|
| 87-L-7 | 3.17 (0.1248) | L | 144 (-200) | 516 (74.8) | 421 (61.0) | 13 | 9 | 33 | — | — |
| -8 | 3.22 (0.1267) | L | | 525 (76.1) | 424 (61.5) | 15 | 11 | 34 | 0.300 | 75.1 (10.9) |
| AVG. | — | — | | 520 (75.4) | 422 (61.2) | 14 | 10 | 33 | | |
| 87-T-7 | 3.23 (0.1273) | T | | 536 (77.8) | 427 (62.0) | 14 | 10 | 23 | — | — |
| -8 | 3.08 (0.1212) | T | | 533 (77.3) | 426 (61.8) | 10 | 8 | 20 | 0.318 | 77.2 (11.2) |
| AVG. | — | — | | 534 (77.5) | 426 (61.9) | 12 | 9 | 21 | | |
| 87-L-9 | 3.18 (0.1251) | L | 291 (65) | 467 (67.8) | 380 (55.1) | 16 | 11 | 38 | — | — |
| -10 | 3.24 (0.1274) | L | | 472 (68.4) | 382 (55.4) | 15 | 12 | 36 | 0.323 | 73.8 (10.7) |
| AVG. | — | — | | 469 (68.1) | 381 (55.2) | 15 | 11 | 37 | | |
| 87-T-9 | 3.10 (0.1220) | T | | 470 (68.2) | 382 (55.4) | 11 | 9 | 23 | — | — |
| -10 | 3.23 (0.1270) | T | | 475 (68.9) | 381 (55.3) | 12 | 8 | 25 | 0.316 | 71.0 (10.3) |
| AVG. | — | — | | 472 (68.5) | 381 (55.3) | 11 | 8 | 24 | | |
| 87-L-11 | 3.23 (0.1272) | L | 450 (350) | 328 (47.5) | 293 (42.5) | 18 | 12 | 55 | — | — |
| -12 | 3.24 (0.1275) | L | | 328 (47.5) | 285 (41.3) | 20 | 13 | 53 | 0.330 | 62.7 (9.1) |
| AVG. | — | — | | 328 (47.5) | 289 (41.9) | 19 | 12 | 54 | | |
| 87-T-11 | 3.22 (0.1269) | T | | 332 (48.2) | 299 (43.4) | 18 | 14 | 46 | — | — |
| -12 | 3.10 (0.1222) | T | | 329 (47.7) | 297 (43.1) | 13 | 9 | 40 | 0.340 | 65.5 (9.5) |
| AVG. | — | — | | 330 (47.9) | 298 (43.2) | 15 | 11 | 43 | | |

TABLE 7: STATIC FRACTURE DATA FROM SURFACE FLAW TESTS, TS PROPAGATION DIRECTION

| MATERIAL | TEST TEMPERATURE °K (°F) | SPECIMEN NUMBER | MEASURED THICKNESS, t mm (INCH) | MEASURED WIDTH, W mm (INCH) | FLAW DEPTH, a mm (INCH) | FLAW LENGTH, 2c mm (INCH) | FAILURE STRESS, $MN/m^2$ (KSI) | $\sigma/\sigma_{YS}$ | a/Q mm (INCH) |
|---|---|---|---|---|---|---|---|---|---|
| 2219 -T851 | 144 (-200) | 851-SF-1 | 6.35 (0.250) | 102 (4.00) | 2.51 (0.099) | 8.26 (0.325) | 382 ( 55.4) | 1.01 | 1.75 (.069) |
| | 291 ( 65) | -2 | 6.32 (0.249) | 102 (4.00) | 2.62 (0.103) | 8.36 (0.329) | 357 (51.8) | 1.06 | 1.78 (.070) |
| | 450 (350) | -3 | 6.32 (0.249) | 102 (4.00) | 2.82 (0.111) | 8.38 (0.330) | 289 (41.9) | 1.07 | 1.83 (.072) |
| 2219 -T87 | 144 (-200) | 87-SF-1 | 6.27 (0.247) | 102 (4.00) | 2.72 (0.107) | 8.51 (0.335) | 410 (59.4) | 0.96 | 1.80 (.071) |
| | 291 ( 65 ) | -2 | 6.27 (0.247) | 102 (4.00) | 2.84 (0.112) | 8.59 (0.338) | 390 (56.6) | 1.02 | 191 (.075) |
| | 450 (350) | -3 | 6.27 (0.247) | 102 (4.00) | 2.62 (0.103) | 8.46 (0.333) | 245 (35.6) | 0.83 | 1.73 (.068) |
| | 450 (350) | -7 | 6.30 (0.248) | 102 (4.01) | 2.74 (0.108) | 8.71 (0.343) | 305 (44.3) | 1.03 | 1.85 (.073) |
| | 144 (-200) | 87-SF-4 | 3.18 (0.125) | 76 (3.00) | 1.47 (0.058) | 4.39 (0.173) | 443 (64.2) | 1.04 | 0.95 (.0375) |
| | 291 ( 65 ) | -5 | 3.28 (0.129) | 76 (3.00) | 1.50 (0.059) | 4.32 (0.170) | 399 (57.8) | 1.05 | 0.94 (.0370) |
| | 450 (350) | -6 | 3.28 (0.129) | 76 (3.00) | 1.52 (0.060) | 4.45 (0.175) | 341 (49.4) | 1.15 | 0.97 (.0380) |

ALL SPECIMENS FRACTURED BEFORE LEAKING

TABLE 8: STATIC FRACTURE DATA FROM SINGLE EDGE NOTCH TENSION TESTS OF 6.35 mm (0.25 INCH) 2219-T851 ALUMINUM ALLOY, TL PROPAGATION DIRECTION

| TEST TEMPERATURE °K (°F) | SPECIMEN IDENTIFICATION | THICKNESS, t mm (INCH) | WIDTH, w mm (INCH) | INITIAL CRACK LENGTH, $a_i$ mm (INCH) | MAXIMUM GROSS AREA STRESS, $\sigma_{MAX}$ $MN/m^2$ (KSI) | STRESS INTENSITY CALCULATED FROM $a_i$ And $\sigma_{MAX}$, $K_{CN}$ $MN/m^{3/2}$ (KSI $\sqrt{IN}$) | $\sigma_{NET}/\sigma_{ys}$ @ $K_{CN}$ | CRITICAL CRACK LENGTH, $a_{cr}$, From CPC MEASUREMENTS mm (INCH) | CRITICAL GROSS AREA FAILURE STRESS, $\sigma_{cr}$ $MN/m^2$ (KSI) | CRITICAL STRESS INTENSITY, $K_{cr}$ $MN/m^2$ (KSI $\sqrt{IN}$) | $K_{cr}/K_{CN}$ @ KS |
|---|---|---|---|---|---|---|---|---|---|---|---|
| 144 (-200) | 851-1 | 6.35 (0.250) | 305 (11.99) | 89.7 (3.53) | 115.2 (16.71) | 100.8 (91.7) | 0.97 | 109.7 (4.32) | 115.2 (16.71) | 128.3 (116.7) | 1.28 |
| | 851-2 | 6.35 (0.250) | 305 (11.99) | 90.4 (3.56) | 112.0 (16.25) | 98.7 (89.8) | 0.96 | 112.8 (4.44) | 112.0 (16.25) | 129.8 (118.1). | 1.30 |
| 291 (65) | 851-3 | 6.35 (0.250) | 381 (14.99) | 123.2 (4.85) | 87.6 (12.70) | 95.3 (86.7) | 0.93 | 147.8 (5.82) | 87.6 (12.70) | 122.2 (111.2) | 1.23 |
| | 851-4 | 6.35 (0.250) | 380 (14.98) | 110.7 (4.36) | 96.1 (13.94) | 92.8 (84.4) | 0.89 | 1 | - | - | - |
| 450 (350) | 851-5 | 6.35 (0.250) | 508 (20.00) | 151.4 (5.96) | 105.7 (15.33) | 120.9 (110.0) | 1.26 | 218.2 (8.59) | 105.7 (15.33) | 200.0 (182.0) | 2.23 |
| | 851-6 | 6.32 (0.249) | 508 (20.00) | 151.9 (5.98) | 106.5 (15.45) | 122.1 (111.1) | 1.25 | 216 (8.5 2 | 106.5 (15.45) | 198 (180) | 2.2 |

ALL SPECIMENS EXHIBIT 100% SHEAR LIP

1 $a_{cr}$ COULD NOT BE DETERMINED FROM C.P.G. TRACE, LOAD RANGE NOT HIGH ENOUGH

2 $a_{cr}$ BEYOND RANGE OF SINGLE C.P.G. USED, $a_{cr}$ EXTRAPOLATED FROM COD VS. C.P.G. PLOT

TABLE 9: STATIC FRACTURE DATA FROM SINGLE EDGE NOTCH TENSION TESTS OF 6.35 mm (0.25 INCH) 2219-T87 ALUMINUM ALLOY, TL PROPAGATION DIRECTION

| TEST TEMPERATURE °K (°F) | SPECIMEN IDENTIFICATION | THICKNESS, t mm (INCH) | WIDTH, w mm (INCH) | INITIAL CRACK LENGTH, $a_i$ mm (INCH) | MAXIMUM GROSS AREA STRESS, $\sigma_{MAX}$ $MN/m^2$ (KSI) | STRESS INTENSITY CALCULATED FROM $a_i$ And $\sigma_{MAX}$, $K_{CN}$ $MN/m^{3/2}$ (KSI $\sqrt{IN}$) | $\sigma_{NET}/\sigma_{ys}$ @ $K_{CN}$ | CRITICAL CRACK LENGTH, $a_{cr}$, From CPG MEASUREMENTS mm (INCH) | CRITICAL GROSS AREA FAILURE STRESS, $\sigma_{cr}$ $MN/m^2$ (KSI) | CRITICAL STRESS INTENSITY, $K_{cr}$ $MN/m^2$ (KSI $\sqrt{IN}$) | $\sigma_{NET}/\sigma_{ys}$ @ $K_{cr}$ |
|---|---|---|---|---|---|---|---|---|---|---|---|
| 144 (-200) | 87-1 | 6.27 (0.247) | 305 (12.00) | 89.2 (3.51) | 93.3 (13.53) | 81.1 (73.8) | 0.69 | 105.7 (4.16) | 93.3 (13.53) | 98.6 (89.7) | 0.87 |
| | 87-[illegible] | 6.27 (0.247) | 305 (12.00) | 89.4 (3.52) | 99.0 (14.36) | 86.2 (78.4) | 0.74 | 108.0 (4.25) | 99.0 (14.36) | 107.4 (97.7) | 0.95 |
| 291 (65) | 87-3 | 6.30 (0.248) | 381 (14.99) | 113.5 (4.47) | 88.3 (12.80) | 87.5 (79.6) | 0.75 | 135.9 (5.35) | 88.3 (12.80) | 108.4 (98.6) | 0.96 |
| | 87-4 | 6.32 (0.249) | 380 (14.98) | 114.0 (4.49) | 81.5 (11.79) | 80.7 (73.4) | 0.70 | 136.1 (5.36) | 81.5 (11.82) | 100.4 (91.4) | 0.89 |
| 450 (350) | 87-5 | 6.27 (0.247) | 508 (20.00) | 151.9 (5.98) | 88.4 (12.82) | 101.3 (92.2) | 0.97 | 215.4 (8.48) | 88.4 (12.82) | 164.1 (149.3) | 1.68 |
| | 87-6 | 6.27 (0.247) | 508 (20.00) | 153.2 (6.03) | 97.3 (14.11) | 112.3 (102.2) | 1.08 | 224 (8.8) [1] | 97.3 (14.11) | 192 (175) | 2.0 |

ALL SPECIMENS EXHIBIT 100% SHEAR LIP

[1] $a_{cr}$ BEYOND RANGE OF SINGLE CPG USED, $a_{cr}$ EXTRAPOLATED FROM COD VS. CPG PLOT

TABLE 10: STATIC FRACTURE DATA FROM SINGLE EDGE NOTCH TENSION TESTS OF 3.18 mm (0.125 INCH) 2219-T87 ALUMINUM ALLOY, TL PROPAGATION DIRECTION

| TEST TEMPERATURE °K (°F) | SPECIMEN IDENTIFICATION | THICKNESS, t mm (INCH) | WIDTH, w mm (INCH) | INITIAL CRACK LENGTH, $a_i$ mm (INCH) | MAXIMUM GROSS AREA STRESS, $\sigma_{MAX}$ $MN/m^2$ (KSI) | STRESS INTENSITY CALCULATED FROM $a_i$ And $\sigma_{MAX}$, $K_{CN}$ $MN/m^{3/2}$ (KSI $\sqrt{IN}$) | $\sigma_{NET}/\sigma_{ys}$ @ $K_{CN}$ | CRITICAL CRACK LENGTH, $a_{cr}$, From CPG MEASUREMENTS mm (INCH) | CRITICAL GROSS AREA FAILURE STRESS, $\sigma_{cr}$ $MN/m^2$ (KSI) | CRITICAL STRESS INTENSITY, $K_{cr}$ $MN/m^2$ (KSI $\sqrt{IN}$) | $\sigma_{NET}/\sigma_{ys}$ @ $K_{cr}$ |
|---|---|---|---|---|---|---|---|---|---|---|---|
| 144 (-200) | 87-7 | 3.20 (0.126) | 305 (11.99) | 88.9 (3.50) | 102.9 (14.93) | 89.0 (81.0) | 0.76 | 104.9 (4.13) | 102.9 (14.93) | 108.4 (98.6) | 0.95 |
| | 87-8 | 3.38 (0.133) | 305 (11.99) | 92.2 (3.63) | 98.9 (14.35) | 89.2 (81.2) | 0.76 | 110.0 (4.33) | 98.9 (14.35) | 110.6 (100.6) | 0.98 |
| 291 (65) | 87-9 | 3.20 (0.126) | 381 (14.99) | 113.0 (4.45) | 92.4 (13.40) | 91.0 (82.8) | 0.78 | 135.1 (5.32) | 92.4 (13.40) | 112.4 (102.3) | 1.00 |
| | 87-10 | 3.20 (0.126) | 381 (14.99) | 114.6 (4.51) | 82.4 (11.95) | 82.3 (74.9) | 0.71 | 132.8 (5.23) | 82.4 (11.95) | 97.9 (89.1) | 0.87 |
| 450 (350) | 87-11 | 3.20 (0.126) | 508 (19.99) | 152.9 (6.02) | 104.0 (15.09) | 120.0 (109.2) | 1.15 | 222.0 (8.74) | 104.0 (15.09) | 203.4 (185.1) | 2.08 |
| | 87-12 | 3.20 (0.126) | 507 (19.98) | 151.4 (5.96) | 93.5 (13.56) | 106.8 (97.2) | 1.02 | 214.6 (8.45) | 93.5 (13.56) | 172.4 (156.9) | 1.75 |

ALL SPECIMENS EXHIBIT 100% SHEAR LIP

TABLE 11: CYCLIC CRACK GROWTH DATA, 6.35 mm (0.250 INCH) 2219-T851 SF SPECIMENS, FREQ = 1 Hz (60 CPM), TS PROPAGATION DIRECTION, CONSTANT TEMPERATURE

| TEST TEMPERATURE °K (°F) | SPECIMEN IDENTIFICATION | THICKNESS, t mm (INCH) | WIDTH, w mm (INCH) | MAX. GROSS AREA STRESS, $\sigma_{MAX.}$ MN/m² (KSI) | $\sigma/\sigma_y$ | R | TEST SEQUENCE | FLAW DEPTH, a mm (INCH) | FLAW LENGTH, 2c mm (INCH) | a/2c | a/t | MAX STRESS INTENSITY, K MN/m$^{3/2}$ (KSI$\sqrt{IN}$) | CYCLES | REMARKS |
|---|---|---|---|---|---|---|---|---|---|---|---|---|---|---|
| 291 (65) | 851-SF-C1 | 6.32 (0.249) | 102 (4.00) | 169 (24.5) | 0.50 | 0 | START | 1.78 (0.070) | 5.84 (0.230) | 0.304 | 0.28 | 11.4 (10.4) | 24,971 | |
| | | | | | | | STOP | t | 16.81 (0.662) | 0.376 | 1.00 | 24.8 (22.6) | | |
| | 851-SF-C2 | 6.32 (0.249) | 102 (4.00) | 288 (41.7) | 0.85 | | START | 0.79 (0.031) | 2.13 (0.084) | 0.369 | 0.12 | 12.0 (10.9) | 11,036 | |
| | | | | | | | STOP | t | 20.45 (0.805) | 0.309 | 1.00 | 48.5 (44.1) | | |
| 450 (350) | 851-SF-C3 | 6.32 (0.249) | 102 (4.01) | 136 (19.7) | 0.50 | 0.5 | START | 2.39 (0.094) | 8.20 (0.323) | 0.291 | 0.38 | 10.9 (9.9) | 24,825 | |
| | | | | | | | STOP | 2.64 (0.104) | 8.56 (0.337) | 0.309 | 0.42 | 11.3 (10.3) | | |
| | | | | | | | START | 3.15 (0.124) | 9.35 (0.368) | 0.337 | 0.50 | 12.1 (11.0) | 117,800 | |
| | | | | | | | STOP | t | 21.39 (0.842) | 0.296 | 1 00 | 22.7 (20.7) | | |
| | 851-SF-C4 | 6.30 (0.248) | 102 (4.00) | 230 (33.4) | 0.85 | | START | 0.99 (0.039) | 3.00 (0.118) | 0.331 | 0.16 | 11.3 (10.3) | 68,205 | |
| | | | | | | | STOP | t | 19.18 (0.755) | 0.328 | 1.00 | 37.6 (34.2) | | |

TABLE 12: CYCLIC CRACK GROWTH DATA, 6.35 mm (0.250 INCH) 2219-T87 SF SPECIMENS, FREQ = 1 Hz (60 CPM), TS PROPAGATION DIRECTION, CONSTANT TEMPERATURE

| TEST TEMPERATURE °K (°F) | SPECIMEN IDENTIFICATION | THICKNESS, t mm (INCH) | WIDTH, w mm (INCH) | MAX GROSS AREA STRESS, $\sigma_{MAX}$ MN/m² (KSI) | $\sigma/\sigma_y$ | R | TEST SEQUENCE | FLAW DEPTH, a mm (INCH) | FLAW LENGTH 2c mm (INCH) | a/2c | a/t | MAXIMUM STRESS INTENSITY, K MN/m$^{3/2}$ (KSI$\sqrt{IN}$) | CYCLES | REMARKS |
|---|---|---|---|---|---|---|---|---|---|---|---|---|---|---|
| 291 (65 | 87-SF-C1 | 6.27 (0.247) | 102 (4.01) | 191 (27.7) | 0.50 | 0 | START | 1.30 (0.051) | 4.57 (0.180) | 0.283 | 0.21 | 11.1 (10.1) | 22,550 | |
| | | | | | | | STOP | t | 20.57 (0.81) | 0.305 | 1.00 | 31.2 (28.4) | | |
| | 87-SF-C2 | 6.27 (0.247) | 102 (4.00) | 289 (41.9) | 0.76 | | START | 0.66 (0.026) | 1.98 (0.078) | 0.333 | 0.11 | 11.4 (10.4) | 4,650 | |
| | | | | | | | STOP | 1.02 (0.040) | 2.79 (0.110) | 0.364 | 0.16 | 13.7 (12.5) | | |
| | | | | 324 (47.0) | 0.85 | | START | 1.02 (0.040) | 2.79 (0.110) | 0.364 | 0.16 | 15.5 (14.1) | 8,137 | |
| | | | | | | | STOP | 2.79 (0.110) | 6.35 (0.250) | 0.440 | 0.45 | 23.7 (21.6) | | |
| 450 | 87-SF-C3 | 6.25 (0.246) | 102 (4.01) | 148 (21.5) | 0.50 | 0.5 | START | 2.21 (0.087) | 7.24 (0.285) | 0.305 | 0.35 | 11.2 (10.2) | 84,960 | |
| | | | | | | | STOP | t | 21.72 (0.855) | 0.288 | 1.00 | 25.2 (22.9) | | |
| | 87-SF-C4 | 6.27 (0.247) | 102 (4.00) | 252 (36.6) | 0.85 | | START | 0.79 (0.031) | 2.49 (0.098) | 0.316 | 0.13 | 11.2 (10.2) | 24,078 | |
| | | | | | | | STOP | 5.46 (0.215) | 18.03 (0.710) | 0.303 | 0.87 | 38.7 (35.2) | | |

TABLE 13: CYCLIC CRACK GROWTH DATA, 3.18 mm (0.125 INCH) 2219-T87 SF SPECIMENS. FREQ. = 1 Hz (60 CPM), TS PROPAGATION DIRECTION, CONSTANT TEMPERATURE

| TEST TEMPERATURE °K (°F) | SPECIMEN IDENTIFICATION | THICKNESS, t mm (INCH) | WIDTH, W mm (INCH) | MAX. GROSS AREA STRESS, σ MAX. MN/m² (KSI) | σ/σy | R | TEST SEQUENCE | FLAW DEPTH, a mm (INCH) | FLAW LENGTH, 2c mm (INCH) | a/2c | a/t | MAX. STRESS INTENSITY, K MN/m^3/2 (KSI √IN) | CYCLES | REMARKS |
|---|---|---|---|---|---|---|---|---|---|---|---|---|---|---|
| 291 (65) | 87-SF-C7 | 3.20 (0.126) | 76 (3.00) | 152 (22.0) | 0.40 | 0 | START | 1.07 (0.042) | 4.09 (0.161) | 0.261 | 0.33 | 8.4 (7.6) | 8,610 | SPECIMEN FAILED IN GRIP, WIDTH NECKED DOWN AND TEST CONTINUED |
| | | | | | | | STOP | 1.63 (0.064) | 4.32 (0.170) | 0.376 | 0.51 | 9.1 (8.3) | | |
| | | | 51 (2.00) | 191 (27.7) | 0.50 | | START | 1.63 (0.064) | 4.32 (0.170) | 0.376 | 0.51 | 11.5 (10.5) | 2,430 | |
| | | | | | | | STOP | t | 9.40 (0.370) | 0.341 | 1.00 | 21.1 (19.2) | | |
| | 87-SF-C8 | 3.23 (0.127) | 51 (2.00) | 324 (47.0) | 0.85 | | START | 0.79 (0.031) | 1.75 (0.069) | 0.449 | 0.25 | 12.4 (11.3) | 4,960 | |
| | | | | | | | STOP | t | 9.40 (0.370) | 0.342 | 1.00 | 36.9 (33.6) | | |
| 450 (350) | 87-SF-C9 | 3.23 (0.127) | 51 (2.00) | 148 (21.5) | 0.50 | 0.5 | START | 2.16 (0.085) | 6.30 (0.248) | 0.343 | 0.67 | 11.5 (10.5) | 24,202 | |
| | | | | | | | STOP | t | 11.05 (0.435) | 0.292 | 1.00 | 17.8 (16.2) | | |
| | 87-SF-C10 | 3.20 (0.126) | 51 (2.00) | 252 (36.6) | 0.85 | | START | 0.95 (0.0375) | 2.67 (0.105) | 0.357 | 0.30 | 12.1 (11.0) | 1,041 | SPECIMEN DELAMINATED |
| | | | | | | | STOP | 0.97 (0.038) | 2.67 (0.105) | 0.362 | 0.30 | 12.1 (11.0) | | |

TABLE 14: CYCLIC CRACK GROWTH DATA, 6.35 mm (0.250 INCH) 2219-T851 SENT SPECIMENS, FREQ = 1 Hz (60 CPM), TL PROPAGATION DIRECTION, CONSTANT TEMPERATURE.

| TEST TEMPERATURE °K (°F) | SPECIMEN IDENTI-FICATION | THICKNESS, t mm (INCH) | WIDTH, w mm (INCH) | MAXIMUM GROSS AREA STRESS, $\sigma_{MAX}$ MN/m² (KSI) | R | TEST SEQUENCE | FLAW LENGTH, a mm (INCH) | MAXIMUM STRESS INTENSITY, K MN/m$^{3/2}$ (KSI$\sqrt{IN}$) | CYCLES | REMARKS |
|---|---|---|---|---|---|---|---|---|---|---|
| 291 (65) | 851-C1 | 6.32 (0.249) | 76.2 (3.00) | 38.6 (5.6) | 0 | START | 14.0 (0.55) | 10.8 (9.8) | 41,560 | |
| | | | | | | STOP | 35.1 (1.38) | 32.1 (29.2) | | |
| | 851-C2 | 6.32 (0.249) | 76.2 (3.00) | 77.2 (11.2) | | START | 13.0 (0.51) | 20.3 (18.5) | 5,371 | |
| | | | | | | STOP | 24.1 (0.95) | 36.7 (33.4) | | |
| | 851-C3 | 6.35 (0.250) | 305.1 (12.01) | 38.6 (5.6) | | START | 76.7 (3.02) | 28.6 (26.0) | 7,592 | |
| | | | | | | STOP | 142.7 (5.62) | 66.4 (60.4) | | |
| | 851-C4 | 6.35 (0.250) | 305.3 (12.02) | 77.2 (11.2) | | START | 19.8 (0.78) | 22.4 (20.4) | 12,112 | |
| | | | | | | STOP | 102.1 (4.02) | 78.2 (71.2) | | |
| 450 (350) | 851-C5 | 6.32 (0.249) | 76.2 (3.00) | 31.0 (4.5) | 0.5 | START | 22.4 (0.88) | 13.5 (12.3) | 63,124 | |
| | | | | | | STOP | 25.4 (1.00) | 15.6 (14.2) | | |
| | | | | | | START | 26.4 (1.040) | 16.5 (15.0) | 30 | Suslic test, held max load for 2 min on each cycle |
| | | | | | | STOP | 26.6 (1.047) | 16.6 (15.1) | | |
| | | | | | | START | 27.9 (1.10) | 17.9 (16.3) | 38,929 | |
| | | | | | | STOP | 35.6 (1.40) | 26.6 (24.2) | | |
| | 851-C6 | 6.32 (0.249) | 76.2 (3.00) | 62.0 (9.0) | | START | 13.2 (0.52) | 16.6 (15.1) | 25,770 | |
| | | | | | | STOP | 23.1 (0.91) | 28.0 (25.5) | | |
| | 851-C7 | 6.35 (0.250) | 305.3 (12.02) | 31.0 (4.5) | | START | 76.5 (3.01) | 22.9 (20.8) | 48,600 | |
| | | | | | | STOP | 114.3 (4.50) | 36.7 (33.4) | | |
| | | | | | | START | 116.8 (4.60) | 37.9 (34.5) | 30 | Suslic test, held at max load for 2 min on each cycle |
| | | | | | | STOP | 117.9 (4.64) | 38.4 (34.9) | | |
| | | | | | | START | 122.2 (4.81) | 40.6 (36.9) | 5,600 | |
| | | | | | | STOP | 142.5 (5.61) | 53.2 (48.4) | | |
| | 851-C8 | 6.35 (0.250) | 305.1 (12.01) | 62.0 (9.0) | | START | 19.1 (0.75) | 17.6 (16.0) | 69,876 | |
| | | | | | | STOP | 95.0 (3.74) | 57.8 (52.6) | | |
| | 851-C12 | 6.35 (0.250) | 305.1 (12.01) | 62.0 (9.0) | 0 | START | 20.6 (0.81) | 18.4 (16.7) | 12,520 | |
| | | | | | | STOP | 95.5 (3.76) | 58.1 (52.9) | | |

TABLE 15: CYCLIC CRACK GROWTH DATA, 6.35 mm (0.250 INCH) 2219-T87 SENT SPECIMENS, FREQ = 1 Hz (60 CPM), TL PROPAGATION DIRECTION, CONSTANT TEMPERATURE.

| TEST TEMPERATURE °K (°F) | SPECIMEN IDENTI-FICATION | THICKNESS, t mm (INCH) | WIDTH, w mm (INCH) | MAXIMUM GROSS AREA STRESS, $\sigma_{MAX}$ MN/m² (KSI) | R | TEST SEQUENCE | FLAW LENGTH, a mm (INCH) | MAXIMUM STRESS INTENSITY, K MN/m^3/2 (KSI√IN) | CYCLES | REMARKS |
|---|---|---|---|---|---|---|---|---|---|---|
| 291 (65) | 87-C1 | 6.25 (0.246) | 76.5 (3.01) | 40.0 (5.8) | 0 | START | 13.0 (0.51) | 10.6 (9.6) | 49,564 | |
| | | | | | | STOP | 37.3 (1.47) | 37.4 (34.0) | | |
| | 87-C2 | 6.27 (0.247) | 76.5 (3.01 | 80.0 (11.6) | | START | 12.7 (0.50) | 20.7 (18.8) | 4,485 | |
| | | | | | | STOP | 25.9 (1.02) | 41.2 (37.5) | | |
| | 87-C3 | 6.27 (0.247) | 305.1 (12.01) | 40.0 (5.8) | | START | 76.2 (3.00) | 29.5 (26.8) | 5,070 | |
| | | | | | | STOP | 149.6 (5.89) | 75.4 (68.6) | | |
| | 87-C4 | 6.27 (0.247) | 305.3 (12.02) | 80.0 (11.6) | | START | 19.3 (0.76) | 22.9 (20.8) | 8 721 | |
| | | | | | | STOP | 105.7 (4.16) | 84.5 (76.9) | | |
| | 87-C12 | 6.30 (0.248) | 305.1 (12.01) | 80.0 (11.6) | 0.5 | START | 20.1 (0.79) | 23.3 (21.2) | 31,137 | |
| | | | | | | STOP | 105.4 (4.15) | 84.4 (76.8) | | |
| 450 (350) | 87-C5 | 6.27 (0.247) | 76.5 (3.01) | 31.0 (4.5) | 0.5 | START | 18.4 (0.725) | 11.0 (10.0) | 84,365 | |
| | | | | | | STOP | 36.6 (1.44) | 27.8 (25.3) | | |
| | 87-C6 | 6.27 (0.247) | 76.5 (3.01) | 62.0 (9.0) | | START | 13.0 (0.51) | 16.3 (14.8) | 19,082 | |
| | | | | | | STOP | 25.4 (1.00) | 31.2 (28.4) | | |
| | 87-C7 | 6.30 (0.248) | 305.1 (12.01) | 31.0 (4.5) | | START | 76.2 (3.00) | 22.9 (20.8) | 15,824 | |
| | | | | | | STOP | 114.6 (4.51) | 36.7 (33.4) | | |
| | | | | | | START | 119.6 (4.71) | 39.2 (35.7) | 30 | Sustic test held max load for 2 min on each cycle |
| | | | | | | STOP | 122.4 (4.82) | 40.7 (37.0) | | |
| | | | | | | START | 132.1 (5.20) | 46.3 (42.1) | 1 199 | |
| | | | | | | STOP | 149.1 (5.87) | 58.2 (53.0) | | |
| | 87-C8 | 6.30 (0.248) | 305.1 (12.01) | 62.0 (9.0) | | START | 19.3 (0.76) | 17.8 (16.2) | 35,340 | |
| | | | | | | STOP | 103.1 (4.06) | 63.5 (57.8) | | |

TABLE 16: CYCLIC CRACK GROWTH DATA, 3.18 mm (0.125 INCH) 2219-T87 SENT SPECIMENS, FREQ = 1 Hz (60 CPM), TL PROPAGATION DIRECTION, CONSTANT TEMPERATURE.

| TEST TEMPERATURE °K (°F) | SPECIMEN IDENTI-FICATION | THICKNESS, t mm (INCH) | WIDTH, w mm (INCH) | MAXIMUM GROSS AREA STRESS, $\sigma_{MAX}$ MN/m² (KSI) | R | TEST SEQUENCE | FLAW LENGTH, a mm (INCH) | MAXIMUM STRESS INTENSITY, K MN/m$^{3/2}$ (KSI$\sqrt{IN}$) | CYCLES | REMARKS |
|---|---|---|---|---|---|---|---|---|---|---|
| 291 (65) | 87-C13 | 3.33 (0.131) | 76.5 (3.01) | 40.0 (5.8) | 0 | START | 12.7 (0.50) | 10.3 (9.4) | 47,259 | |
| | | | | | | STOP | 36.6 (1.44) | 35.9 (32.7) | | |
| | 87-C14 | 3.20 (0.126) | 76.5 (3.01) | 80.0 (11.6) | | START | 12.7 (0.50) | 20.7 (18.8) | 5,583 | |
| | | | | | | STOP | 25.7 (1.01) | 40.7 (37.0) | | |
| | 87-C15 | 3.10 (0.122) | 305.1 (12.01) | 40.0 (5.8) | | START | 76.2 (3.00) | 29.5 (26.8) | 5,835 | |
| | | | | | | STOP | 149.9 (5.90) | 75.7 (68.9) | | |
| | 87-C16 | 3.23 (0.127 | 304.8 (12.00 | 80.0 (11.6) | | START | 19.1 (0.75) | 22.7 (20.7) | 13,405 | |
| | | | | | | STOP | 102.9 (4.05) | 81.9 (74.5) | | |
| 450 (350) | 87-C17 | 3.12 (0.123) | 76.5 (3.01) | 31.0 (4.5) | 0.5 | START | 17.8 (0.70) | 10.8 (9.8) | 145,730 | |
| | | | | | | STOP | 36.8 (1.45 | 28.2 (25.7) | | |
| | 87-C18 | 3.25 (0.128) | 76.5 (3.01) | 62.0 (9.0) | | START | 13.0 (0.51) | 16.3 (14.8) | 21,864 | |
| | | | | | | STOP | 24.9 (0.98) | 30.6 (27.8) | | |
| | 87-C19 | 3.12 (0.123) | 305.1 (12.01) | 31.0 (4.5) | | START | 76.2 (3.00) | 22.9 (20.8) | 16,763 | |
| | | | | | | STOP | 149.6 (5.89) | 58.[illegible] (53.2) | | |
| | 87-C20 | 3.20 (0.126) | 305.1 (12.01) | 62.0 (9.0) | | START | 19.1 (0.75) | 17.6 (16.0) | 41,627 | |
| | | | | | | STOP | 101.1 (3.98) | 62.0 (56.4) | | |

TABLE 17: THERMAL PROFILE CYCLIC CRACK GROWTH DATA, 6.35mm (0.025 INCH) 2219-T851 SF SPECIMENS, TS PROPAGATION DIRECTION

| SPECIMEN IDENTIFICATION | THICKNESS, t mm (INCH) | WIDTH, w mm (INCH) | MAXIMUM GROSS AREA STRESS @ RT, $\sigma_{RT}$ $MN/m^2$ (KSI) | MAXIMUM GROSS AREA STRESS @ ET, $\sigma_{ET}$ $MN/m^2$ (KSI) | $\sigma/\sigma_{ys}$ @ TEMP. | TEST SEQUENCE | FLAW DEPTH, a mm (INCH) | FLAW LENGTH, 2c mm (INCH) | a/2c | a/t | $\sigma_{NET}/\sigma_{ys}$ @ TEMP | MAXIMUM STRESS INTENSITY @ RT, $K_{I_{RT}}$ $MN/m^{3/2}$ (KSI $\sqrt{IN}$) | MAXIMUM STRESS INTENSITY @ ET, $K_{I_{ET}}$ $MN/m^{3/2}$ (KSI $\sqrt{IN}$) | FLIGHTS | REMARKS |
|---|---|---|---|---|---|---|---|---|---|---|---|---|---|---|---|
| 851-SF-C5 | 6.32 (0.249) | 102 (4.01) | 169 (24.5) | 136 (19.7) | 0.5 | START | 3.66 (0.144) | 12.70 (0.500) | 0.288 | 0.58 | 0.53 | 18.1 (16.5) | 14.6 (13.3) | 53 | FULL SPECTRUM |
| | | | | | | STOP | ↑ | 18.54 (0.730) | 0.341 | 1.00 | 0.58 | 26.3 (23.9) | 21.1 (19.2) | | |
| 851-SF-C6 | 6.25 (0.246) | 102 (4.01) | 288 (41.7) | 230 (33.4) | 0.85 | START | 3.78 (0.149) | 12.70 (0.500) | 0.298 | 0.61 | 0.90 | 32.4 (29.5) | 26.4 (24.0) | 5 | FULL SPECTRUM |
| | | | | | | STOP | 5.44 (0.214) | 18.67 (0.735) | 0.291 | 0.87 | 0.97 | 46.7 (42.5) | 36.3 (33.0) | | |

RT = ROOM TEMPERATURE

ET = ELEVATED TEMPERATURE (450K (350°F))

ORIGINAL PAGE IS OF POOR QUALITY

ORIGINAL PAGE IS
OF POOR QUALITY

TABLE 18: THERMAL PROFILE CYCLIC CRACK GROWTH DATA, 6.35mm (0.250 INCH) AND 3.18mm (0.125 INCH) 2219-T87 SF SPECIMENS, TS PROPAGATION DIRECTION.

| SPECIMEN IDENTIFICATION | THICKNESS, t mm (INCH) | WIDTH, w mm (INCH) | MAXIMUM GROSS AREA STRESS @ RT, $\sigma_{RT}$ MN/m$^2$ (KSI) | MAXIMUM GROSS AREA STRESS @ ET, $\sigma_{ET}$ MN/m$^2$ (KSI) | $\sigma/\sigma_{ys}$ @ TEMP. | TEST SEQUENCE | FLAW DEPTH, a mm (INCH) | FLAW LENGTH, a mm (INCH) | $\sigma_{NET}/\sigma_{ys}$ @ TEMP | a/2c | a/t | MAXIMUM STRESS INTENSITY @ RT, $K_{IRT}$ MN/m$^{3/2}$ (KSI $\sqrt{IN}$) | MAXIMUM STRESS INTENSITY @ ET, $K_{IET}$ MN/m$^{3/2}$ (KSI $\sqrt{IN}$) | FLIGHTS | REMARKS |
|---|---|---|---|---|---|---|---|---|---|---|---|---|---|---|---|
| 87-SF-C5 | 6.30 (0.248) | 102 (4.01) | 324 (47.0) | 252 (36.6) | 0.85 | START | 1.78 (0.070) | 5.89 (0.232) | 0.86 | 0.302 | 0.28 | 22.9 (20.8) | 17.8 (16.2) | 15 | FULL SPECTRUM |
| | | | | | | STOP | 3.00 (0.118) | 8.89 (0.350) | 0.88 | 0.337 | 0.48 | 29.0 (26.4) | 22.6 (20.6) | | |
| 87-SF-C6 | 6.25 (0.246) | 102 (4.01) | 191 (27.7) | 148 (21.5) | 0.50 | START | 3.53 (0.139) | 12.01 (0.473) | 0.53 | 0.294 | 0.57 | 19.8 (18.0) | 15.4 (14.0) | 40 | FULL SPECTRUM |
| | | | | | | STOP | 5.64 (0.222) | 17.40 (0.685) | 0.57 | 0.324 | 0.90 | 27.9 (25.4) | 21.7 (19.7) | | |
| 87-SF-C11 | 3.20 (0.126) | 51 (2.00) | 324 (47.0) | 252 (36.6) | 0.85 | START | 1.83 (0.072) | 5.94 (0.234) | 0.90 | 0.308 | 0.57 | 24.5 (22.3) | 19.1 (17.4) | 3 | FULL SPECTRUM |
| | | | | | | STOP | 2.16 (0.085) | 7.11 (0.280) | 0.92 | 0.304 | 0.67 | 28.2 (25.7) | 22.0 (20.0) | | |
| 87-SF-C12 | 3.18 (0.125) | 51 (2.00) | 191 (27.7) | 148 (21.5) | 0.50 | START | – | – | – | – | – | – | – | – | FAILED ON LOADING |
| | | | | | | STOP | – | – | – | – | – | – | – | | TEST MACHINE MALFUNCTION |

RT = ROOM TEMPERATURE
ET = ELEVATED TEMPERATURE (450K [350F])

TABLE 19: THERMAL PROFILE CYCLIC CRACK GROWTH DATA, 6.35 mm (0.250 INCH) 2219-T87 SENT SPECIMENS, TL PROPAGATION DIRECTION

| SPECIMEN IDENTIFICATION | THICKNESS, t mm (INCH) | WIDTH, w mm (INCH) | MAX GROSS AREA STRESS @ RT, $\sigma_{RT}$ $MN/m^2$ (KSI) | MAX GROSS AREA STRESS @ ET, $\sigma_{ET}$ $MN/m^2$ (KSI) | $\sigma/\sigma_{ys}$ @ TEMP. | TEST SEQUENCE | FLAW LENGTH, a mm (INCH) | $\sigma_{NET}/\sigma_{ys}$ @ TEMP | MAX STRESS INTENSITY @ RT, $K_{RT}$ $MN/m^{3/2}$ (KSI $\sqrt{IN}$) | MAX STRESS INTENSITY @ ET, $K_{ET}$ $MN/m^{3/2}$ (KSI $\sqrt{IN}$) | FLIGHTS | REMARKS |
|---|---|---|---|---|---|---|---|---|---|---|---|---|
| 851- | 6.32 | 76 | 77.2 | 62.0 | 0.23 | START | 17.8 (0.70) | 0.56 | 26.7 (24.3) | 20.8 (18.9) | 23 | FULL SPECTRUM TEST |
| C9 | (0.249) | (3.00) | (11.2) | (9.0) | | STOP | 25.1 (0.99) | 0.84 | 38.5 (35.0) | 29.9 (27.2) | | |
| 851- | 6.32 | 76 | 77.2 | 62.0 | 0.23 | START | 13.0 (0.51) | 0.44 | 20.3 (18.5) | 15.8 (14.4) | 46 | MODIFIED FULL SPECTRUM TEST R = 0 @ ELEVATED TEMPERATURE |
| C10 | (0.249) | (3.00) | (11.2) | (9.0) | | STOP | 17.3 (0.68) | 0.56 | 25.9 (23.6) | 20.1 (18.3) | | |
| 851- | 6.32 | 305 | 38.6 | 31.0 | 0.11 | START | 76.2 (3.00) | 0.29 | 28.5 (25.9) | 22.1 (20.1) | 73 | FULL SPECTRUM TEST |
| C11 | (0.249) | (12.01) | (5.6) | (4.5) | | STOP | 80.8 (3.18) | 0.31 | 30.2 (27.5) | 23.4 (21.3) | | |
| | | | 38.6 | – | 0.11 | START | 80.8 (3.18) | 0.31 | 30.2 (27.5) | -- | — | CONSTANT AMPLITUDE CYCLIC TEST @ RT, R = 0 |
| | | | (5.6) | | | STOP | 95.8 (3.77) | 0.40 | 36.3 (33.1) | -- | | DURATION = 17,325 CYCLES |

RT = ROOM TEMPERATURE
ET = ELEVATED TEMPERATURE (450K (350°F))

ORIGINAL PAGE IS OF POOR QUALITY

TABLE 20 : THERMAL PROFILE CYCLIC CRACK GROWTH DATA, 6.35 mm (0.250 INCH) 2219-T851 SENT SPECIMENS, TL PROPAGATION DIRECTION

| SPECIMEN IDENTIFICATION | THICKNESS, t mm (INCH) | WIDTH, w mm (INCH) | MAX GROSS AREA STRESS @ RT, $\sigma_{RT}$ $MN/m^2$ (KSI) | MAX GROSS AREA STRESS @ ET, $\sigma_{ET}$ $MN/m^2$ (KSI) | $\sigma/\sigma_{ys}$ @ TEMP. | TEST SEQUENCE | FLAW LENGTH, a mm (INCH) | $\sigma_{NET}/\sigma_{ys}$ @ TEMP | MAXIMUM STRESS INTENSITY @ RT, $K_{RT}$ $MN/m^{3/2}$ (KSI$\sqrt{IN}$) | MAXIMUM STRESS INTENSITY @ ET, $K_{ET}$ $MN/m^{3/2}$ (KSI$\sqrt{IN}$) | FLIGHTS | REMARKS |
|---|---|---|---|---|---|---|---|---|---|---|---|---|
| 87- C9 | 6.27 (0.247) | 76 (3.01) | 80 (11.6) | 62 (9.0) | 0.21 | START | 17.8 (0.70) | 0.52 | 27.6 (25.1) | 21.4 (19.5) | 19 | MODIFIED FULL SPECTRUM TEST, ELEVATED TEMPERATURE = 394K (250°F) |
| | | | | | | STOP | 25.9 (1.02) | 0.80 | 41.2 (37.5) | 32.0 (29.1) | | |
| 87- C10 | 6.30 (0.248) | 76 (3.01) | 80 (11.6) | 62 (9.0) | 0.21 | START | 13.7 (0.54) | 0.42 | 21.9 (19.9) | 16.9 (15.4) | 50 | FULL SPECTRUM TEST |
| | | | | | | STOP | 24.6 (0.97) | 0.75 | 38.8 (35.3) | 30.1 (27.4) | | |
| 87- C11 | 6.30 (0.248) | 305 (12.0) | 40 (5.8) | 31 (4.5) | 0.10 | START | 76.5 (3.01) | 0.28 | 29.6 (26.9) | 23.0 (20.9) | 58 | FULL SPECTRUM TEST |
| | | | | | | STOP | 82.6 (3.25) | 0.30 | 32.0 (29.1) | 24.8 (22.6) | | |
| | | | 40 (5.8) | — | 0.10 | START | 82.6 (3.25) | 0.30 | 32.0 (29.1) | — | -- | CONSTANT AMPLITUDE CYCLIC TEST @ RT, R = 0 |
| | | | | | | STOP | 97.8 (3.85) | 0.37 | 38.6 (35.1) | — | | DURATION = 19,380 CYCLES |

RT = ROOM TEMPERATURE
ET = ELEVATED TEMPERATURE (450K (350°F) Unless noted in Remarks)

ORIGINAL PAGE IS OF POOR QUALITY

TABLE 21: THERMAL PROFILE CYCLIC CRACK GROWTH DATA, 3.18 mm (0.125 INCH) 2219-T87 SENT SPECIMENS, TL PROPAGATION DIRECTION

| SPECIMEN IDENTIFICATION | THICKNESS, t mm (INCH) | WIDTH, w mm (INCH) | MAX GROSS AREA STRESS @ RT, $\sigma_{RT}$ $MN/m^2$ (KSI) | MAX GROSS AREA STRESS @ ET, $\sigma_{ET}$ $MN/m^2$ (KSI) | $\sigma/\sigma_{ys}$ @TEMP. | TEST SEQUENCE | FLAW LENGTH, a mm (INCH) | $\sigma_{NET}/\sigma_{ys}$ @ TEMP | MAXIMUM STRESS INTENSITY @RT, $K_{RT}$ $MN/m^{3/2}$ (KSI$\sqrt{IN}$) | MAXIMUM STRESS INTENSITY @ ET $K_{ET}$ $MN/m^{3/2}$ (KSI $\sqrt{IN}$) | FLIGHTS | REMARKS |
|---|---|---|---|---|---|---|---|---|---|---|---|---|
| 87-C21 | 3.25 (0.128) | 76 (3.01) | 80 (11.6) | 62 (9.0) | 0.21 | START | 17.8 (0.70) | 0.52 | 27.4 (24.9) | 21.2 (19.3) | 28 | MODIFIED FULL SPECTRUM TEST, ELEVATED TEMPERATURE = 422K (300°F) |
| | | | | | | STOP | 25.7 (1.01) | 0.80 | 40.7 (37.0) | 31.5 (28.7) | | |
| 87-C23 | 3.38 (0.133) | 305 (12.00) | 40 (5.8) | 31 (4.5) | 0.10 | START | 77.0 (3.03) | 0.28 | 29.8 (27.1) | 23.1 (21.0) | 46 | FULL SPECTRUM TEST |
| | | | | | | STOP | 82.8 (3.26) | 0.31 | 32.1 (29.2) | 24.9 (22.7) | | |
| | | | -- | 31 (4.5) | 0.10 | START | 82.8 (3.26) | 0.31 | -- | 24.9 (22.7) | — | CONSTANT AMPLITUDE CYCLIC TEST @ ET, R = 0.5 |
| | | | | | | STOP | 99.1 (3.90) | 0.38 | -- | 30.3 (27.6) | | DURATION = 10,550 CYCLES |
| 87-C24 | 3.23 (0.127) | 305 (12.00) | 80 (11.6) | 31 (4.5) | 0.21 @ RT | START | 20.3 (0.80) | ▷1 | 23.5 (21.4) | 9.1 (8.3) | 50 | MODIFIED FULL SPECTRUM TEST, NO SUSTAINED LOAD AT ET, $\sigma_{ET}/\sigma_{RT} = 0.5 \frac{\sigma_{ys} @ ET}{\sigma_{ys} @ RT}$ |
| | | | | | 0.10 @ET | STOP | 22.9 (0.90) | ▷2 | 25.1 (22.8) | 9.7 (8.8) | | |

RT = ROOM TEMPERATURE
ET = ELEVATED TEMPERATURE (450K (350°F) (Unless Noted in Remarks)
▷1 = $\sigma_{NET}/\sigma_{ys}$ = 0.27 - RT, 0.13 @ ET
▷2 = $\sigma_{NET}/\sigma_{ys}$ = 0.28 - RT, 0.14 @ ET

TABLE 22: THERMAL PROFILE CYCLIC CRACK GROWTH DATA, SUSTAIN LOAD AT ET FOLLOWED BY CONSTANT AMPLITUDE CYCLIC TEST AT RT, 3.18 mm (0.125 INCH) SENT SPECIMEN, TL PROPAGATION DIRECTION

| SPECIMEN IDENTIFICATION | THICKNESS, t mm (INCH) | WIDTH, w mm (INCH) | MAXIMUM GROSS AREA STRESS @ RT, $\sigma_{RT}$ $MN/m^2$ (KSI) | MAXIMUM GROSS AREA STRESS @ ET, $\sigma_{ET}$ $MN/m^2$ (KSI) | $\sigma/\sigma_{ys}$ @ TEMP. | TEST SEQUENCE | FLAW LENGTH, a mm (INCH) | $\sigma_{NET}/\sigma_{ys}$ @ TEMP | MAXIMUM STRESS INTENSITY @ RT, $K_{RT}$ $MN/m^{3/2}$ (KSI $\sqrt{IN}$) | MAXIMUM STRESS INTENSITY @ ET, $K_{ET}$ $MN/m^{3/2}$ (KSI $\sqrt{IN}$) | REMARKS |
|---|---|---|---|---|---|---|---|---|---|---|---|
| 87-C22 | 3.20 (0.126) | 76 (3.01) | — | 62 (9.0) | 0.21 | START | 13.0 (0.51) | 0.40 | — | 16.3 (148) | SUSTAINED LOAD AT ET FOR 2 HOURS |
| | | | | | | STOP | 15.7 (0.62) | 0.47 | — | 19.1 (17.4) | |
| | | | 80 (11.6) | — | 0.21 | START | 15.7 (0.62) | 0.47 | 24.6 (22.4) | — | CONSTANT AMPLITUDE CYCLIC TEST @ RT, R = 0 DURATION = 6032 CYCLES |
| | | | | | | STOP | 26.2 (1.03) | 0.82 | 41.7 (37.9) | — | |

RT = ROOM TEMPERATURE
ET = ELEVATED TEMPERATURE (450K (350° F))